Chapter 1

INTRODUCTION

The electro-oxidation of organic compounds at noble metal electrodes has been studied extensively for possible applications in electrochemical power sources (Parsons and VanderNoot, 1988) and electrochemical wastewater treatment (Comninellis, 1994). Gold is the noblest and most inert of all metals. It also possesses weak chemisorbing properties due to the absence of vacancies in its d-bands. Surprisingly, it still displays a wide range of electro-oxidation activity – especially in alkaline solutions (Burke and Nugent, 1998).

It is known that a bimetallic electrode is usually more active for the electro-oxidation of organics than the respective pure metals (Parsons and VanderNoot, 1988). The gold alloy containing 40% platinum has been identified (Stelmach et al., 1994) as being the most active for the oxidation of various organics in base. However, the effect of the microstructure of gold-platinum alloys on their electrochemical properties has largely been ignored in the past.

The Gold 990 alloy (Au-1wt% Ti) was developed originally for the jewellery industry (Gafner, 1989). The electrochemical properties of this alloy have not been investigated before. It is possible to heat treat Gold 990 to obtain two different heat treatment conditions: (a) with titanium in solid solution with the gold and (b) the precipitation-hardened condition, with small Au_4Ti precipitates.

This study has been subdivided into three main parts:

- In the first part, the heat treatments of the Au-Pt and the Au-Ti alloys are investigated. By employing different heat treatment temperatures and times, different microstructures are produced.
- In the second part, the electrochemical properties of the heat treated electrodes are studied in acid and alkaline solutions without an organic compound in the solution.
- In the third part, the electro-oxidation of ethylene glycol at Au-Pt and Gold 990 electrodes in different heat treatment conditions is investigated. Ethylene glycol was selected as a model organic compound due to the fact that its oxidation at noble metal electrodes has been studied extensively (Kadirgan et al., 1990; Hahn et al., 1987).

Chapter 2

THEORETICAL BACKGROUND

2. Electrochemical behaviour of pure gold in aqueous media

2.1. Gold in acidic media

A typical cyclic voltammogram recorded for a polycrystalline gold disc electrode in acid is shown in Figure 2.1 (Burke and Nugent, 1997). During the positive sweep, monolayer oxide (α-oxide) formation results in an increase in anodic current at 1.35 V versus the reversible hydrogen electrode (RHE). The charge associated with further monolayer oxidation for gold in acid tends to be distributed along a plateau with no major change until oxygen gas evolution commences at 2.0 V_{RHE} (not shown in Figure 2.1). During the negative sweep, the monolayer oxide reduction peak is observed at 1.1 V_{RHE}.

Birss and Xia (2001) formed α-oxide films at sputtered polycrystalline gold electrodes in 0.1 M H_2SO_4 solutions. The composition and properties of the film were established using potentiostatic, cyclic voltammmetry, ellipsometric and in-situ mass measurement techniques. The α-oxide is proposed to be AuO at potentials below 1.5 V_{RHE}, and a mixture of AuO and Au_2O_3 above this, likely becoming primarily Au_2O_3 at still higher potentials. This is based on ellipsometric evidence and the measured mass to charge ratio of 8 g/mol electrons at all potentials.

2.2. Gold in alkaline media

Examples of cyclic voltammograms recorded for gold in base are shown in Figure 2.2 (Burke and Nugent, 1997). Monolayer oxide growth commences at 1.25 V_{RHE}. At more positive potentials, oxygen gas evolution occurs. Over the range of 1.6 to 2.0 V_{RHE} oxygen gas evolution is believed to be catalysed in a transient manner by some type of nascent hydrous gold oxide species formed at the monolayer oxide/aqueous solution interface (Burke and Nugent, 1997). Regular oxygen gas evolution on gold in base (as in acid) occurs only above 2.0 V_{RHE}.

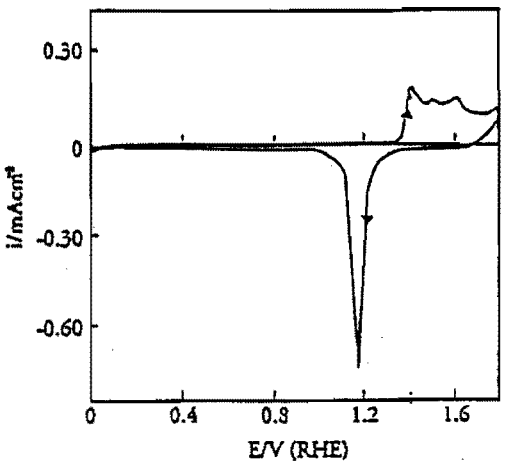

Figure 2.1. Typical cyclic voltammogram (0.0 to 1.80 V_{RHE}, 50mV/s, 25℃) recorded for a polycrystalline gold disc electrode in 1.0 mol/dm^3 H_2SO_4 (Burke and Nugent, 1997).

An interesting feature of the negative sweep in Figure 2.2(b) is the appearance of a second cathodic peak at 0.85 V_{RHE}. The monolayer oxide reduction peak was observed in this case at 1.1 V_{RHE} and the subsequent peak is assumed to be due to the reduction of hydrous gold oxide species formed on the gold surface at the upper end of the cycle (Burke and Nugent, 1997).

2.3. Premonolayer oxidation of gold

Gold is frequently regarded as the ideal solid electrode system for fundamental investigations in electrochemistry. This is due to the fact that in the absence of redox active species in the aqueous phase, the system apparently exhibits only double layer (non-Faradaic) behaviour over the range of 0 to 1.3 V_{RHE} in acid and 0 to 1.2 V_{RHE} in base. However, there have been assertions that Faradaic behaviour due to the formation of oxy-species at the gold surface occurs within the double layer region. However, the extent of premonolayer oxidation (the coverage involved) is small. This makes it difficult to detect these species and the responses associated with them.

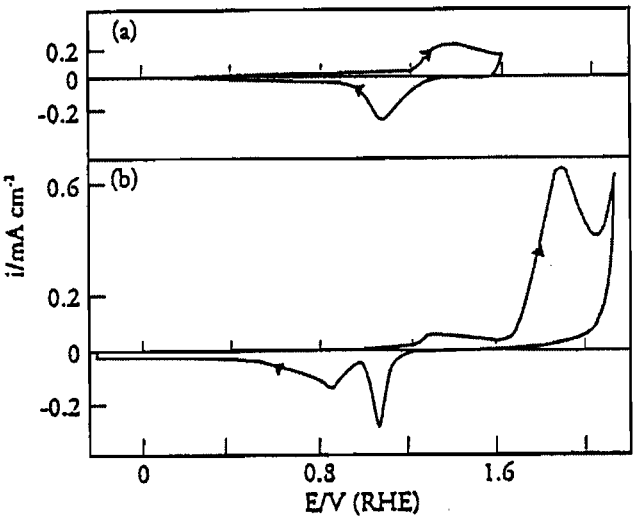

Figure 2.2. Typical cyclic voltammogram for a polycrystalline gold electrode in 1.0 mol/dm^3 NaOH at 25 ℃: (a) 0.0 to 1.60 V_{RHE} at 50 mV/s; (b) -0.2 to 2.1 V_{RHE} at 10 mV/s (Burke and Nugent, 1997).

2.3.1. Premonolayer oxidation of gold in acid

Watanabe and Gerischer (1981) postulated on the basis of photoelectrochemical data that gold exhibited premonolayer oxidation extending over the potential range 0.85 to 1.35 V_{RHE}. They postulated that this incipient oxidation represented the formation of chemisorbed species (Au-OH and/or Au-O) with surface coverages up to 20%.

Hutton and Williams (1994), using Scanning Laser Microscopy, found that gold oxidised in the premonolayer region. They found that this incipient oxide was stable, only being removed by prolonged evolution of hydrogen gas.

Gordon and Johnson (1994) investigated gold electrodes in acid solution by means of an Electrochemical Quartz Crystal Microbalance (EQCM). They proposed that the species formed during premonolayer oxidation corresponded to adsorbed hydroxyl radicals, designated as AuOH. Figure 2.3(a) (Gordon and Johnson, 1994) shows a typical current-potential (I-E) curve obtained at a gold film electrode in 0.10 M $HClO_4$. The very small anodic current observed during the positive potential scan in region A corresponds to charging of the electrical double layer. Region B during the positive scan corresponds to the premonolayer region and the slight increase in anodic current is concluded to result primarily from the formation of the submonolayer of hydrous oxide, designated as AuOH. The large wave in region C corresponds to the formation of the monolayer oxide. An electrochemical quartz crystal microbalance (EQCM) was

used to detect small surface mass changes during cyclic voltammetry. A decrease in frequency indicates an increase in mass. Figure 2.3(b) (Gordon and Johnson, 1994) shows the frequency-potential (f-E) curve recorded simultaneously with the I-E curve in Figure 2.3(a). During the positive scan there is no detectable change in frequency corresponding to double layer charging (region A). However, a rapid decrease in frequency (mass increase) by the amount Δf_B is observed in region B concomitantly with the formation of AuOH. Continuation of the positive scan through region C results in a further decrease in frequency by an amount Δf_C concomitantly with the formation of the monolayer oxide. Following scan reversal, the frequency remains constant until it increases very rapidly in the region corresponding to cathodic reduction of the monolayer oxide. Continuation of the negative scan back through the premonolayer region B results in further increase of frequency until the original value of f is attained in the double-layer region A.

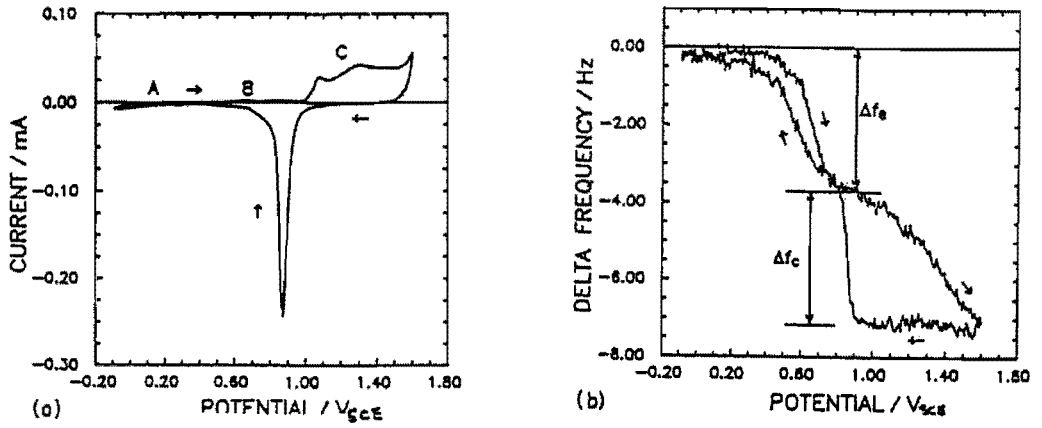

Figure 2.3. (a) Current-potential curve for Au EQCM film in 0.1 M $HClO_4$: scan rate 75 mV/s; no convective mixing. (b) Frequency-potential curve for Au EQCM film in 0.1 M $HClO_4$: scan rate 75 mV/s; no convective mixing. Obtained concomitant with I-E curve (Gordon and Johnson, 1994).

Gordon and Johnson (1994) proposed that the large values obtained for Δf_B and Δf_C in regions B and C respectively are the result of increased surface hydration as a consequence of the formation of AuOH (region B) and the monolayer oxide (region C). The magnitude of the increase was found to be independent of the nature of the acid. The mass increase in region B is consistent with an increase in surface hydration by about 32 H_2O molecules per AuOH site.

2.3.2. Premonolayer oxidation of gold in base

The electrochemical response due to premonolayer oxidation of gold in alkaline solutions tends to be of higher magnitude than in acid; the hydroxy species involved is more stable in solutions of high OH^- ion activity. Small peaks have been observed in the double layer region of cyclic voltammograms for gold in base (Burke and O'Leary, 1989).

Desilvestro and Weaver (1986) established, using Surface Enhanced Raman Spectroscopy (SERS), that the product of premonolayer oxidation was a hydroxy species, one that was of different character to the species involved in the regular monolayer oxidation reaction.

2.4.The electro-oxidation of chemical compounds at gold electrodes in aqueous media

Gold is the noblest and most inert of all metals. It is also a very weak chemisorber due to the absence of vacancies in its d-bands. It does, however, display a very wide range of electro-oxidation activity - especially in base (Vitt et al., 1990; Burke and Nugent, 1998).

Typical cyclic voltammograms for the electro-oxidation of formaldehyde, hydrazine, and ethylene glycol are shown in Figure 2.4 (Burke and Nugent, 1998). The following can be deduced from these cyclic voltammograms:

i. The electro-oxidation of chemical compounds commences in the premonolayer region during the positive sweep. As soon as monolayer oxidation starts, oxidation of the compound is inhibited.
ii. During the negative sweep, oxidation of the compound starts again as soon as the monolayer oxide has been reduced.
iii. In general, chemical compounds are oxidised at gold before the formation of a surface oxide layer, while oxygen is evolved at a gold surface after the formation of the oxide layer.

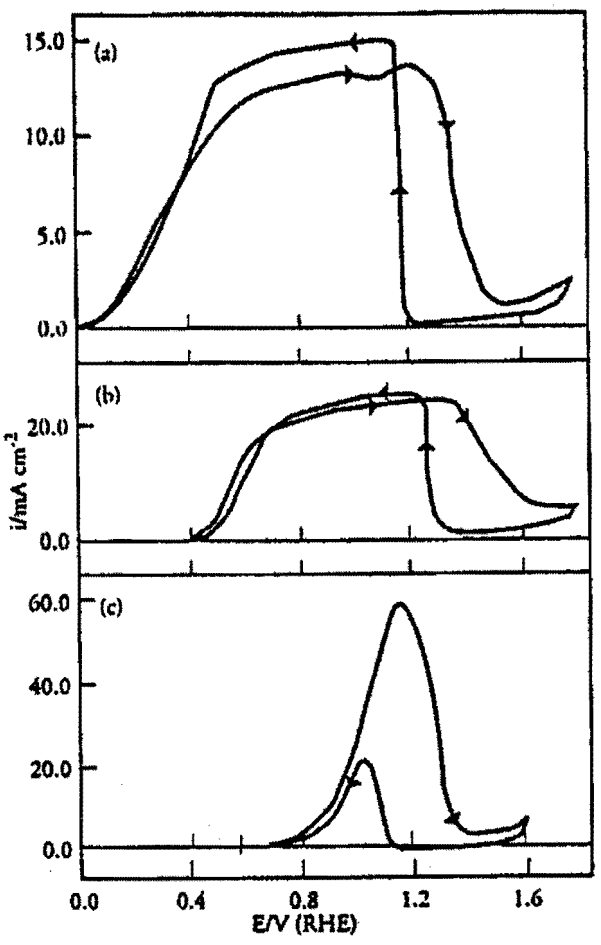

Figure 2.4. (a) Typical cyclic voltammogram (0 - 1.8 V, 5 mV/s) for a gold wire electrode in 1 mol/dm^3 NaOH with HCHO, to a level of 0.1 mol/dm^3, T = 25 ℃; (b) Typical cyclic voltammogram (0 - 1.8 V, 50 mV/s) for a smooth gold electrode in N_2-stirred 1 mol/dm^3 NaOH with N_2H_4, to a level of 0.1 mol/dm^3, T = 25 ℃; (c) Typical cyclic voltammogram (0 - 1.6 V, 50 mV/s) for a gold wire electrode in 1 mol/dm^3 NaOH with 0.1 mol/dm^3 ethylene glycol $(CH_2OH)_2$, T= 25 ℃ (Burke and Nugent, 1998).

2.4.1 Electro-oxidation by means of a submonolayer of adsorbed hydroxyl radicals

Electro-oxidation mechanisms have been proposed for oxidation at gold electrodes in acidic and alkaline solutions that involve adsorbed hydroxyl radicals (AuOH) (Vitt et al., 1990; Wen and Li, 1997). The adsorbed hydroxyl radicals are produced by means of the anodic discharge of H_2O in the premonolayer region (Vitt and Johnson, 1992).

$$H_2O \rightarrow {}^{\bullet}OH_{ads} + H^+ + e^- \qquad (1)$$

The formation of the submonolayer of hydroxyl radicals is favoured in alkaline solutions, which explains the rather poor electro-oxidation properties of gold in acidic solutions. A mechanism has been proposed in which the adsorbed hydroxyl radicals participate in the oxygen-transfer step (Vitt et al., 1990). It has also been speculated that the AuOH species formed in the premonolayer region can assist in the adsorption of polar organic molecules. Oriented H_2O dipoles centred at catalytic AuOH sites may also influence the orientation of electro-active functional groups in reactants that must diffuse to these catalytic sites (Gordon and Johnson, 1994).

Vitt and co-workers (1990) proposed that adsorption is necessary for all compounds whose oxidation is accompanied by the transfer of oxygen via the electrode surface. A mechanism that involve three fundamental processes for the various adsorbed species has been devised for these anodic reactions:

(1) oxygen transfer between the electrolyte and adsorbed hydroxyl radical (AuOH)

(2) deprotonation and

(3) electron transfer.

The mechanisms for various compounds seem to differ only in the order of these three reactions. For organic compounds (alcohols and aldehydes), deprotonation precedes electron transfer.

2.5. Alloys of gold

Noble metal alloys have been studied for the electro-oxidation of organic compounds, and some alloys display better activity than the pure metals. Most of the alloys that

have been studied are based on platinum (Parsons and VanderNoot, 1988; Stelmach et al., 1994).

2.5.1. Electrochemical behaviour of pure platinum

2.5.1.1. Mechanism of oxide formation

The early modelling of the initial stages of surface oxidation on platinum (Kozlowska et al., 1973) lead to the conclusion that two distinguishable and successive stages were involved:

$Pt + H_2O \rightarrow Pt/OH + H^+ + e^-$ (I)

followed by:

$Pt/OH \rightarrow Pt/O + H^+ + e$ (II)

(potential range 1.1 to 1.4 V_{RHE}) also coupled with place-exchange, schematically represented by:

$Pt/O \rightarrow O/Pt.$ (III)

By using the electrochemical quartz-crystal nanobalance (EQCN) technique, Birss et al (1993) showed that the above two-step mechanism is inapplicable. The two-step mechanism would require a mass change of 17 g/mol electrons in step I and -1 g/mol electrons in step II. However, the anodic mass-response profile involves a continuous mass increase, contrary to the expectations according to mechanism I, II. It actually corresponds to the first stage (to 1.1 V_{RHE}) of oxide film development being formed as Pt/O, first to half-coverage by O-species up to 1.1 V_{RHE}. This is followed by completion of coverage by O-species up to 1.4 V_{RHE} coupled with place exchange between O and Pt (step III).

Thus, platinum surface oxide formation is believed to preferably involve discharge of water molecules directly forming 'PtO' species, process IV:

$Pt + H_2O \rightarrow Pt/O + 2H^+ + 2e^-$ (IV)

where the H_2O reagent is initially present at a platinum site in the inner region of the double-layer, i.e. residing at the metal surface. As the electrosorption of O species in process IV progresses, water molecules consumed in (IV) are replaced from the double-layer and appear on the surface of the developing oxide film, probably H-bonded to it.

The mechanism of platinum oxide formation is shown schematically in Figure 3.1 (Zolfaghari et al., 2002). The above mechanism has to include the anticipated participation of adsorbed H_2O molecules which, initially, are presumed to fully cover Pt sites (Fig. 2.5a). It is believed that the H_2O molecules are bridge-coordinated to two adjacent Pt atoms. The second step in the diagram (Fig. 2.5b) shows half coverage by O at 1.1 V_{RHE}. The third step in the diagram (Fig. 2.5c and 2.5d) illustrates how a nominally complete O monolayer on platinum eventually becomes developed through place-exchange between O and Pt over the two outer layers of the original platinum structure.

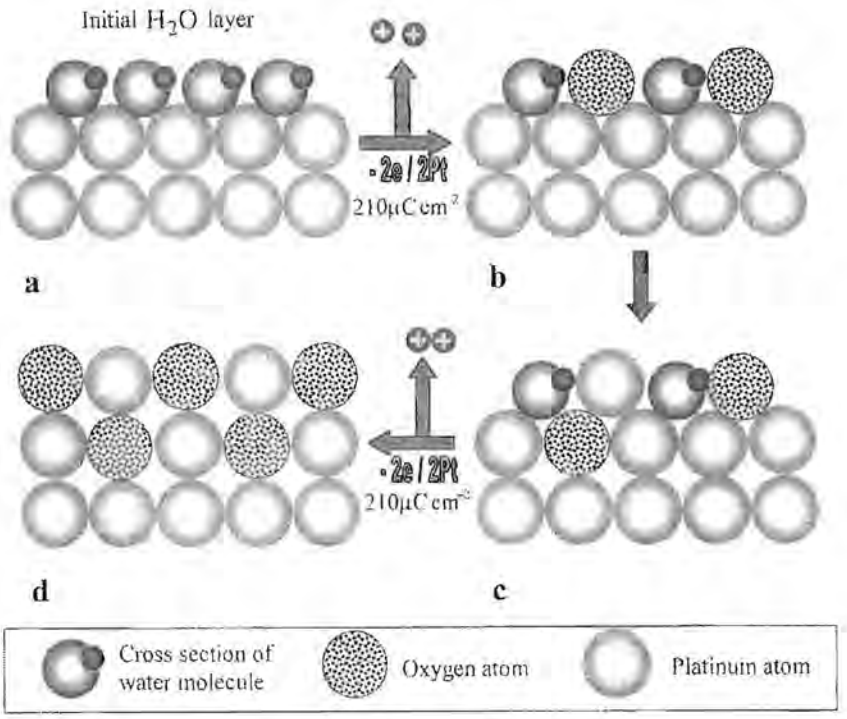

Figure 2.5. Cross-section of (a) initial water layer; (b) adsorbed O and H_2O; (c) adsorbed H_2O and place-exchanged O; (d) surface oxide (Zolfaghari et al., 2002).

A similar model of initial, two-electron oxidation of the platinum surface has also been proposed by Harrington and co-workers (1997) in their simulation of ac voltammetry behaviour over the region of Pt oxide-film formation. It was found that the shape of the ac voltammograms does not change much with frequency, suggesting a single time constant for oxide growth. No features were seen in the early stages of growth that can be assigned to the fast OH electrosorption, suggested previously to be the first step in oxide growth.

It was also suggested that although this mechanism is ruled out, some types of fast OH adsorption are still possible. Adsorption without charge transfer could be occurring. If OH electrosorption occurs in parallel with the slow oxide growth process, it might not be detectable by ac impedance. The admittances of the two processes would then be additive and a small admittance for OH electrosorption might contribute little to the total.

2.5.1.2. Electrochemical behaviour of platinum in alkaline solutions

Figure 2.6 (solid line) (Xia and Birss, 2000) shows a typical cyclic voltammogram of a Pt-coated quartz crystal in 0.1 M NaOH, as well as the associated frequency change (dashed line, inverse of mass change), measured during an oxidation/reduction scan between 0 and 1.6 V_{RHE}. In this range of potential the compact α-oxide film is formed (at ca. 0.6 V_{RHE}) and reduced, in peak C_1. The adsorption/desorption of a monolayer of hydrogen atoms is seen between 0.1 V and 0.4 V_{RHE}.

In Figure 2.6, a mass increase is seen, as expected, during Pt oxide formation, while oxide reduction is accompanied by an equivalent mass loss. From the integrated charge density during oxide reduction and the associated change in mass over the potential range of the cathodic peak, a ratio of 8.3g/mol e^- passed is obtained. A ratio of 8 g/mol electrons would be predicted for the formation of an anhydrous Pt oxide film, either PtO or PtO_2.

In the potential range of the hydrogen adsorption-desorption reaction it can be seen that as the potential is made more negative and hydrogen begins to adsorb, the electrode mass decreases, rather than increases, and vice versa during the positive scan. When hydrogen evolution commences in the negative scan, i.e. at 0.1 V_{RHE}, the frequency drops somewhat and then increases again in the positive scan. It is likely that the mass change between 0.15 and 0.4 V is due to the desorption of OH^- in the cathodic scan and its readsorption during the positive scan. The results of Figure 2.6 suggest that, during hydrogen atom adsorption on Pt (0.4-0.15 V_{RHE}), adsorbed hydroxide is concurrently being desorbed, then readsorbing again in the anodic sweep.

QCMB experiments involving α-oxide growth in 0.1 M NaOH with time at constant potentials were carried out by Xia and Birss (2000). Figure 2.7(a, b) (Xia and Birss, 2000) show both the oxide reduction charge density (per apparent area) and its g/mol e^-

ratio as a function of anodising time at two potentials: 1.3 and 1.6 V_{RHE} respectively. In both cases, the oxide reduction charge increases logarithmically with anodising time, reaching a near steady-state value after ca. 6 min (Fig. 2.7a) and 4 min (Fig. 2.8b).

Figure 2.7a shows that the mass to charge ratio for the oxide formed after very short times of anodising at 1.3 V_{RHE} is almost 9 g/mol electrons. While a ratio of 8 is expected for either PtO or PtO_2, this slightly higher value may indicate that the initial layer may have included some adsorbed OH^-, or the formation of a small amount of PtOH or $Pt(OH)_2$ (expected ratio for both is 17g/mol e^-). After 1 min of anodising at either 1.3 or 1.6 V, Figure 2.7(a,b) show similar ratios for the oxide film of 7.9 to 8.1 g/mol e^-, the expected values for PtO or PtO_2. Unfortunately, the form of Pt oxide cannot be distinguished from the QCMB data.

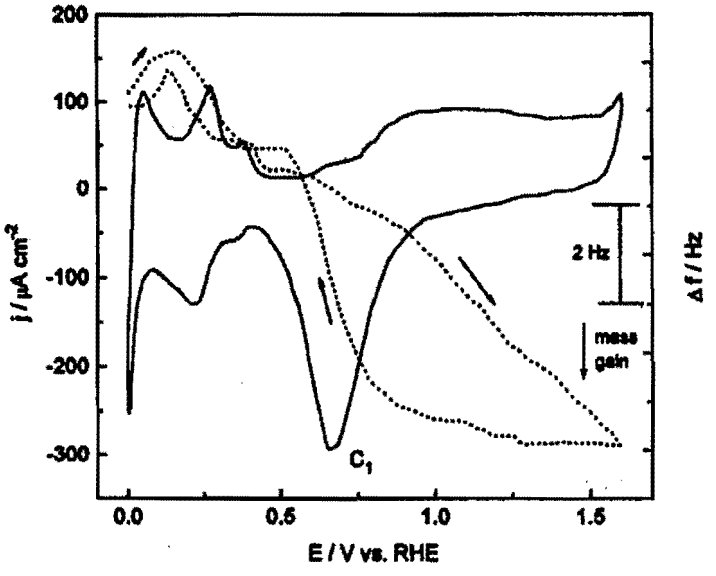

Figure 2.6. Cyclic voltammogram (solid line) and associated frequency change (dotted line) of a Pt-coated quartz crystal in 0.1 M NaOH between 0 and 1.6 V_{RHE} at 50mV/s (Xia and Birss, 2000).

Figure 2.8 (Xia and Birss, 2000) shows a plot of both the oxide reduction charge and the g/mol e^- ratios, monitored after 5 min at each of the anodising potentials between 1.2 and 1.9 V_{RHE}. The plot of the reduction charges appears to have two apparently linear segments, one for potentials less than 1.6 V, and one for potentials above this.

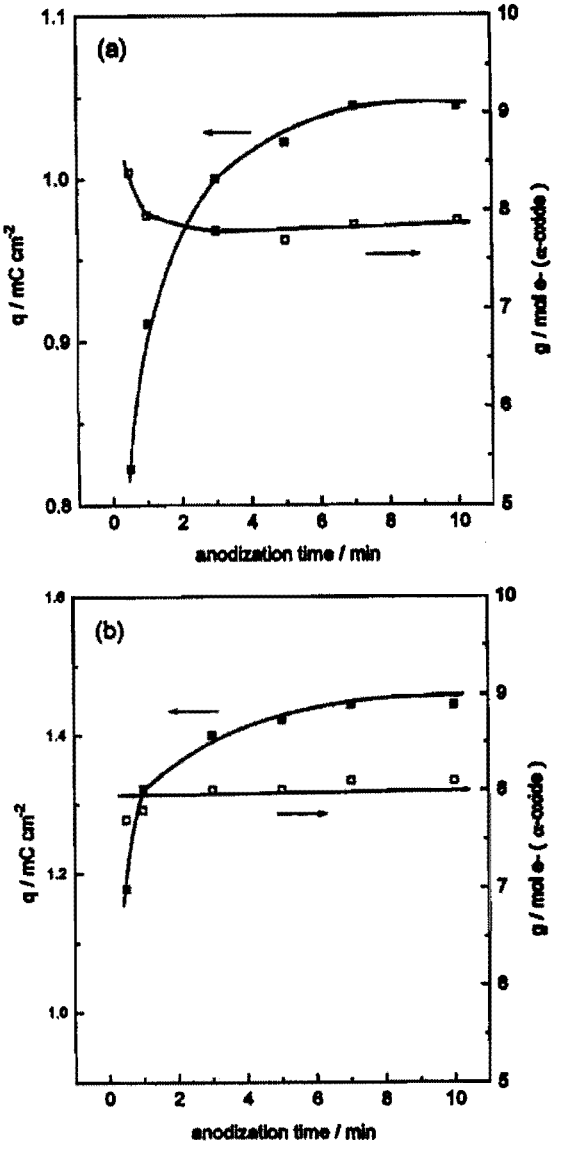

Figure 2.7: α-oxide reduction charge density (solid symbols) at 10 mV/s and its g/mol e$^-$ ratio (open symbols) as a function of anodisation time of Pt-coated quartz crystal at (a) 1.3 V_{RHE} and (b) 1.6 V_{RHE} in 0.1 M NaOH (Xia and Birss, 2000).

Ellipsometric data (Xia and Birss, 2000) also indicates that the platinum oxide films, formed using potentials below 1.6 V_{RHE}, have different optical properties from those formed at potentials above 1.6 V_{RHE}. However, for all upper potential limits, except 1.2 V_{RHE}, the g/mol e^- ratio remains 8. These results has been interpreted as indicating that the oxide formed over the range 1.3 to 1.6 V_{RHE} is PtO, then changing to PtO_2 when the applied potential becomes higher than 1.6 V_{RHE}.

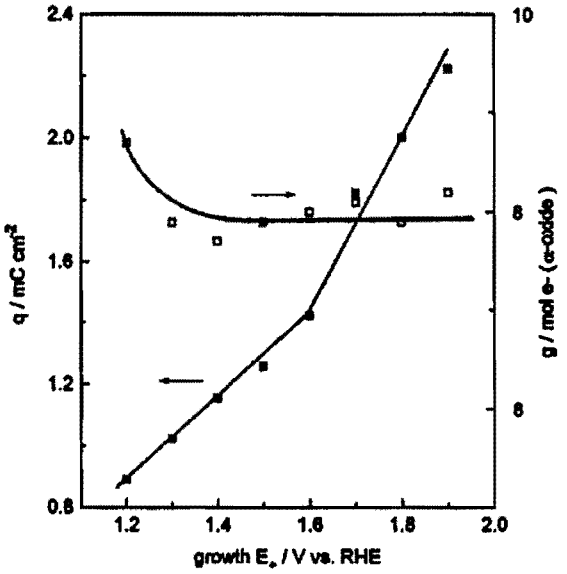

Figure 2.8. α-oxide reduction charge density (solid symbols) at 10 mV/s and its g/mol e^- ratio (open symbols) as a function of applied potential, after 5 minutes of anodisation of Pt-coated quartz crystal in 0.1 M NaOH (Xia and Birss, 2000).

2.5.1.3. Electrochemical behaviour of platinum in acid solutions

Figure 2.9 (solid curve) (Birss et al., 1993) shows a typical cyclic voltammogram of a Pt-coated quartz crystal in 0.1 M H_2SO_4, as well as the associated mass changes (broken curve) measured during the experiment. A mass increase is seen, as expected, during Pt-oxide formation, while oxide reduction is marked by mass loss. From the integrated charge density during α-oxide reduction and the associated change in frequency over the potential range of the cathodic peak, a ratio of ca. 8 g/mol of electrons passed is obtained. This is similar to what was found for the oxide formed in alkaline solutions and suggests again that the α-oxide is anhydrous in nature (either PtO or PtO_2). However, ellipsometric data indicates that the platinum oxide film formed potentiostatically and by multicycling in 0.1 M H_2SO_4 has different optical properties than either of the two α-oxide films formed in base.

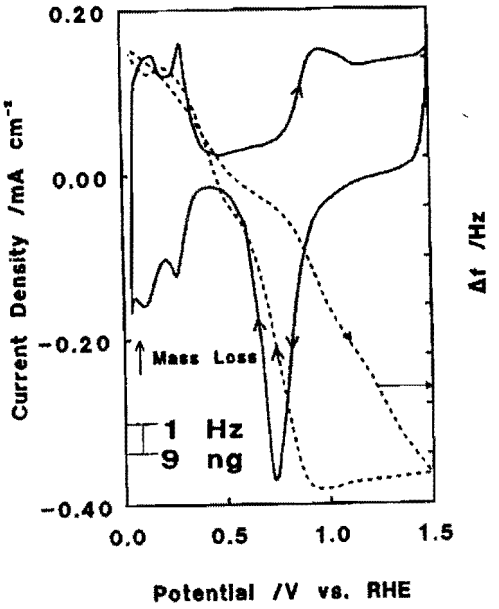

Figure 2.9. Cyclic voltammogram (solid line) and associated frequency change (dotted line) of a Pt coated quartz crystal in 0.1 M H_2SO_4; scanning rate 50 mV/s (Birss et al., 1993)

2.6. Gold-platinum alloys

The gold-platinum system has a miscibility gap (Figure 2.10) in the solid solution field (ASM Handbook, Volume 3: Alloy Phase Diagrams, 1992). The Pt-rich phase is frequently denoted as the α_1 phase and the Au-rich phase as α_2.

There was interest in gold-platinum alloys during the 1950's and 1960's when they were used as spinning jets in the viscose rayon process (Darling, 1962).

2.6.1. Cold rolling of Au-Pt alloys

The whole range of alloys can be cold worked after quenching from temperatures not higher than 1000°C. The most ductile material is achieved by annealing at 1000°C, after which the temperature can be slowly dropped before water-quenching from 850°C (Darling, 1962).

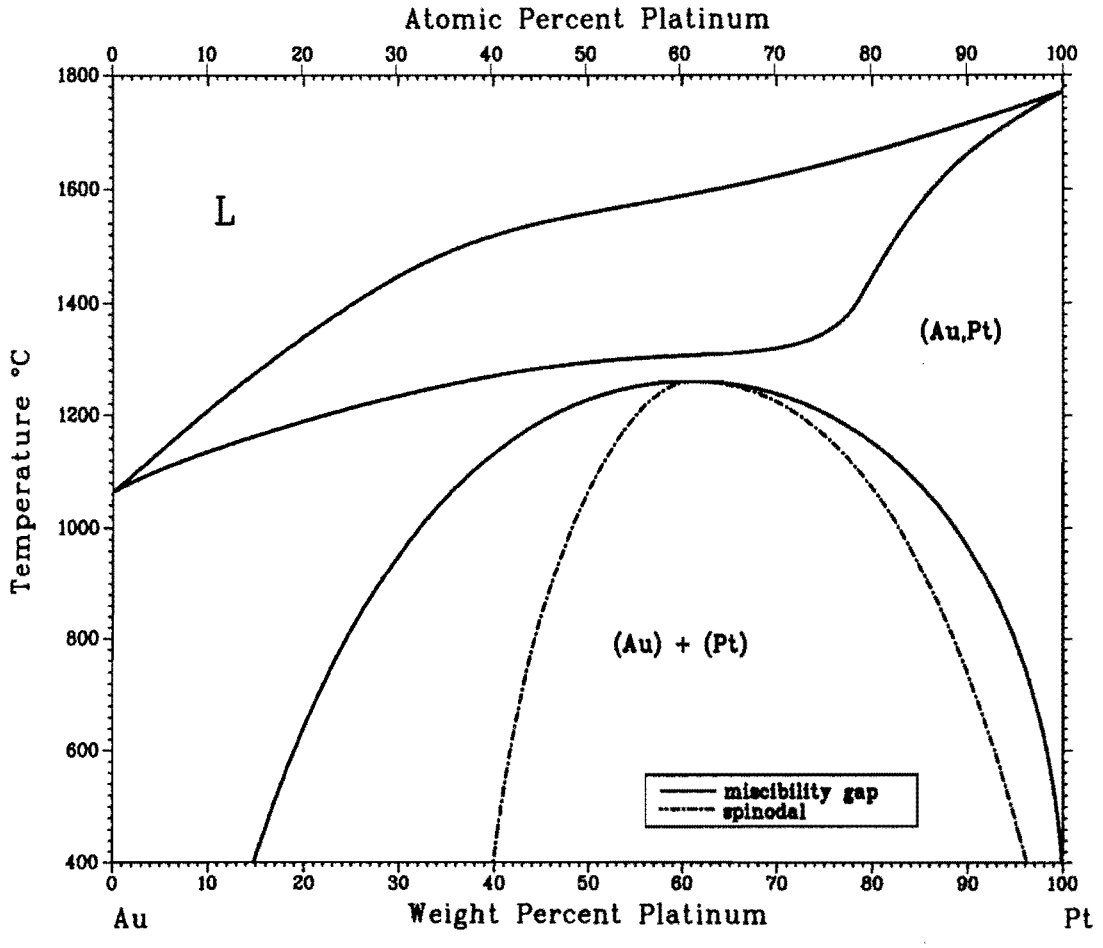

Figure 2.10. The Au-Pt phase diagram (ASM Handbook, Volume 3: Alloy Phase Diagrams, 1992)

2.6.2. Precipitation in Au-Pt alloys

The rate of precipitation depends upon the curvature of the free energy composition curves. The spinodal (Figure 2.10), being the locus of the inflexion points of the isothermal free energy composition curves, forms a lower limit of metastable equilibrium. Between the spinodal and the two-phase field exists a thermodynamic potential barrier that must be overcome before nucleation can occur, with the result that precipitation is retarded in this area (Darling, 1962).

2.6.3. Electrochemical behaviour of Au-Pt alloys

2.6.3.1. Homogeneous alloys

Woods (1971) studied the surface composition of Pt-Au alloys quenched from the region of continuous solid solution. Even though x-ray diffraction indicated that the alloys were homogeneous, the alloy electrodes gave current-potential curves (1 M H_2SO_4) that were equivalent to the sum of a pure platinum and a pure gold surface (Figure 2.11 (Woods. 1971)). It was suggested that this result can be explained if either:

1. Platinum and gold atoms in a homogeneous alloy have hydrogen and oxygen electrosorption properties equal to that of platinum and gold atoms in the pure metals or
2. The surface of platinum/gold alloys always consists of the equilibrium phases even though the bulk is homogeneous.

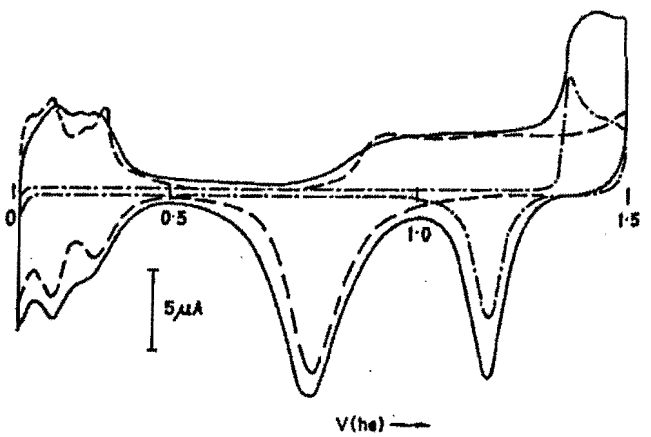

Figure 2.11. Current-potential curves showing hydrogen and oxygen adsorption in 1 M H_2SO_4 for a linear potential sweep of 40 mV/s. (-----) Pt; (-.-.-) Au and (____) homogeneous 65%Pt-35%Au alloy (Woods, 1971).

2.6.3.2. Heterogeneous alloys

Breiter (1965) studied the anodic formation and cathodic reduction of oxygen layers on Au-Pt alloys in acid solutions. Platinum-gold alloys with gold contents ranging from 5 to 70 at% were studied. The alloys had to be annealed at 875°C before wires of 0.3 mm

diameter could be drawn. Heterogeneous (two-phased) Au-Pt alloys were produced with this heat treatment (Fig. 2.10). Current-potential curves were measured in 1 N H_2SO_4 at a sweep rate of 30 mV/s. The current-potential curves of the 20, 40 and 60at% Au alloys are shown in Figure 2.12 (Breiter, 1965). The most notable feature of Figure 2.12 is the fact that the alloys have two reduction waves. The first wave between 1.4 and 1.0 V_{SHE} is attributed to the reduction of the oxygen layer on "gold" and the second one between 1.0 V and 0.6 V_{SHE} to that of the layer on "platinum". "Gold" is designated as being either gold atoms or the gold-rich phase of the heterogeneous alloys, while "platinum" is designated as being either platinum atoms or the platinum-rich phase of the alloys. The first reduction wave increased in height with increasing gold content while the second decreased (Fig. 2.12). The peaks of the two reduction waves appeared at slightly less anodic potentials on the alloys than on the respective pure metals. This indicates that the reduction of the oxygen layer on the two phases occurs with slightly larger hindrance than on the pure metals.

2.6.4. Electro-oxidation of chemical compounds at Au-Pt alloy electrodes

In alkaline media, the electro-oxidation activity of Au-Pt alloy electrodes is enhanced when compared with the respective metals (Stelmach et al., 1994; Beden et al., 1982). There are a few possible explanations for this synergistic effect of gold-platinum alloys.

2.6.5. Possible explanations for synergism on Au-Pt alloys

2.6.5.1. The bifunctional theory

The idea is that surface gold atoms adsorb oxygen-containing species, while surface platinum atoms adsorb the organic compound. The two different species interact leading to a final product. The two sites together give the complete reaction unit (Parsons and VanderNoot, 1988).

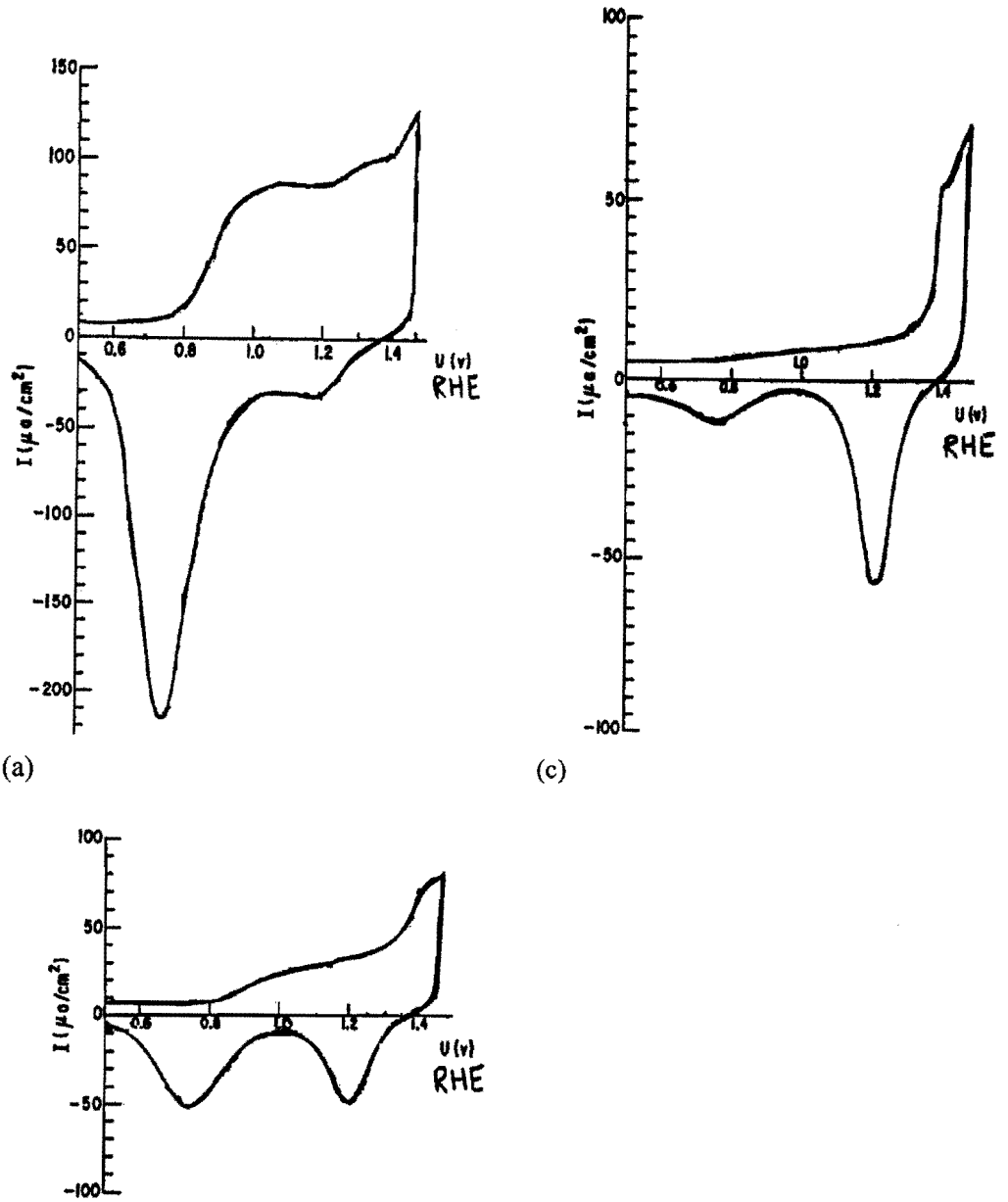

Figure 2.12. Current-potential curves for heterogeneous Au-Pt alloys containing (a) 20%, (b) 40% and (c) 60% Au in 1 N H_2SO_4. Sweep rate 30 mV/s (Breiter, 1965).

2.6.5.2. Changes in adsorption features

Stelmach and co-workers (1994) found an increased rate of electro-oxidation of formaldehyde at alloy electrodes in comparison with the respective pure metals. They proposed that the energy of adsorption for the various forms of the substrate molecule is decreased sufficiently in order to facilitate further oxidative desorption of

intermediates and to suppress the adsorption of strongly bound intermediates. The adsorptivity of the surface remains high enough to support electro-oxidation.

2.6.5.3. The Third-Body effect

The formation of poisonous species adsorbed on more than one surface site is suppressed. For the electro-oxidation of formic acid, it was found that a platinum atom that is surrounded by gold atoms has the highest activity. A single platinum atom cannot be "poisoned" by the strongly bound intermediate since it needs adsorption sites that are only available on larger platinum clusters (Rach and Heitbaum, 1987).

2.6.5.4. The creation of Lewis acid surface sites on alloy electrodes

It is thought that the introduction of an alloying element that has a d-orbital occupancy less than that of the matrix will result in surface states at the alloy that function as Lewis acid sites. Furthermore, it is speculated that these surface sites enable adsorption of reactant species that are Lewis bases because of the existence of non-bonded electron pairs in these compounds e.g. the O-atoms in hydroxyl moieties of alcohols and carbohydrates, and N-atoms in amino acids (Mho and Johnson, 2001). This speculation is supported by successful modelling of the variations in the half-wave potential of the anodic voltammetric wave for dimethyl sulfoxide at β-PbO_2 film electrodes as a function of the variation in the level of doping by Bi (Popovic et al., 1998). The electrocatalytic benefit of reactant adsorption is explained on the basis of increase in residence time for the reactant species within the applied electric field at the electrode/solution interface.

Mho and Johnson (2001) studied the electrocatalytic response of carbohydrates at Cu-Mn alloy electrodes. The occupancy of the outermost d-orbital is lower for Mn ($3d^5$) than that of Cu ($3d^{10}$). The alloy composition of Cu:Mn = 95:5 was chosen to correspond to a homogeneous solid solution. The voltammetric responses observed for carbohydrates in 0.10 M NaOH were significantly larger at the preanodised CuMn electrodes as compared to preanodised pure Cu electrodes. It is speculated that the observed electrocatalytic effect comes as a beneficial consequence of the preadsorption of the carbohydrates at Mn sites (Lewis acid) in the preanodised CuMn surface.

Lewis acid surface sites will also be formed at gold-platinum alloys. The electron configuration of gold is $[Xe]4f^{14}5d^{10}6s^{1}$ and the electron configuration for platinum is $[Xe]4f^{14}5d^{9}6s^{1}$.

2.7. The 60Au-40Pt alloy electrode

The Au-Pt alloy containing 60wt% Au has been identified previously (Stelmach et al., 1994) as the most active for the oxidation of aliphatic alcohols (Beltowska-Brzezinska, 1979), ethylene glycol (Eggert (Stelmach, 1994)) and formaldehyde (Beltowska-Brezezinska and Heitbaum, 1985) in alkaline media.

However, from the Au-Pt phase diagram (Fig. 2.10), it can be seen that different heat treatment temperatures can be used to produce different amounts of the α_1 and α_2 phases. The compositions of the two phases can also be changed by employing different heat treatment temperatures.

For the 60Au-40Pt alloy, annealing at 1100-1260°C will produce a homogeneous solid solution. Heat treatments at temperatures lower than 1100°C will produce a heterogeneous two-phased microstructure (Fig. 2.10). The different weight fractions of α_1 and α_2, and their composition as a function of heat treatment temperature are shown in Table 2.1 for the 60Au-40Pt alloy. The lever rule was applied in order to calculate the various weight fractions.

Table 2.1: Equilibrium weight fractions and composition of phases in a 60wt% Au-40wt% Pt alloy as functions of temperature.

Temp. (°C)	Weight fraction of α_1	Composition of α_1		Weight fraction α_2	Composition of α_2	
		Wt% Au	Wt% Pt		Wt% Au	Wt% Pt
1000	0.13	12	88	0.87	68	32
800	0.21	5	95	0.79	75	25
600	0.26	2	98	0.74	81	19
400	0.30	0	100	0.70	85	15

It will be interesting to study the electrochemical behaviour of the 60Au-40Pt alloy in different heat treatment conditions. The electro-oxidation of an organic compound, such as ethylene glycol, can be used to determine the effect of microstructure on the electrochemical properties of the alloy.

2.8. The electro-oxidation of ethylene glycol at noble metal electrodes

Ethylene glycol, $(CH_2OH)_2$, is a non-toxic diol-alcohol. It has the advantage of involving a large number of electrons per molecule in its oxidation (the oxidation reaction needs 8 electrons per molecule when the final product is oxalate (Hauffe and Heitbaum, 1978)). The electro-oxidation of ethylene glycol at noble metal electrodes has been studied extensively, due to the interest of using it as a fuel for alcohol fuel cells (Christensen and Hamnett, 1989; Kadirgan et al., 1990; Beden et al., 1982, Hahn et al., 1987).

2.8.1. The electro-oxidation of ethylene glycol at gold electrodes in acid

The cyclic voltammogram for the electro-oxidation of ethylene glycol at a gold electrode in acid is show in Figure 2.13 (Beden et al., 1987). It can clearly be seen from Figure 2.13 that nearly no oxidation of ethylene glycol occurs at gold in acid.

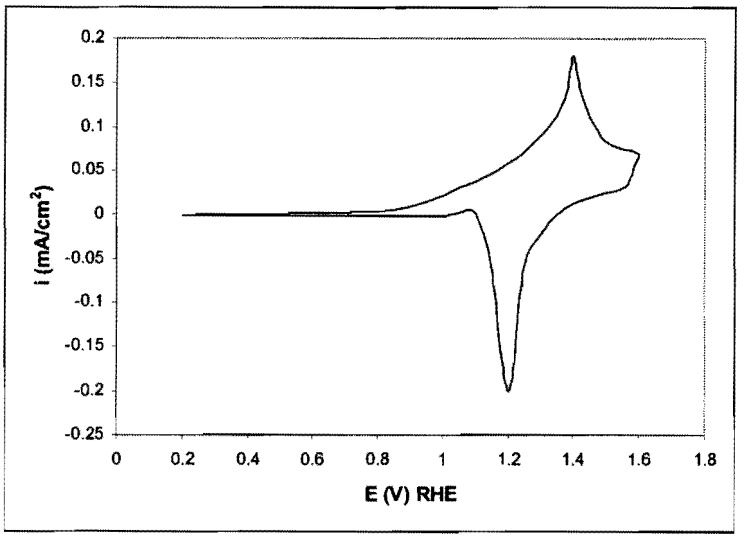

Figure 2.13. Oxidation of ethylene glycol at a gold electrode in acid medium. Conditions: 0.1 M $HClO_4$, 0.1 M ethylene glycol, 25°C, 50 mV/s (After Beden et al., 1987).

2.8.2. The electro-oxidation of ethylene glycol at gold electrodes in base

A cyclic voltammogram for the electro-oxidation of ethylene glycol at a gold electrode in base is show in Figure 2.14, together with the voltammogram of gold in the supporting electrolyte alone (Kadirgan et al., 1990). Ethylene glycol oxidation starts at 0.8 V_{RHE} during the positive sweep, giving a peak of 12 mA/cm^2 at approximately 1.2 V_{RHE} (peak A). The electro-oxidation of ethylene glycol is inhibited by the formation of the surface oxide on the gold electrode. During the negative sweep, oxidation of ethylene glycol commences only after the surface gold oxide has been reduced, reaching a current maximum of about 4 mA/cm^2 at 1 V_{RHE} (peak B). The positive and negative potential scans are almost superimposed in the potential range from 0.8 to 1 V_{RHE}. Hauffe and Heitbaum (1978) found that the peak currents (peaks A and B) are somewhat smaller when the solution is stirred with argon gas. This can be explained by an accelerated transportation of intermediates into the solution.

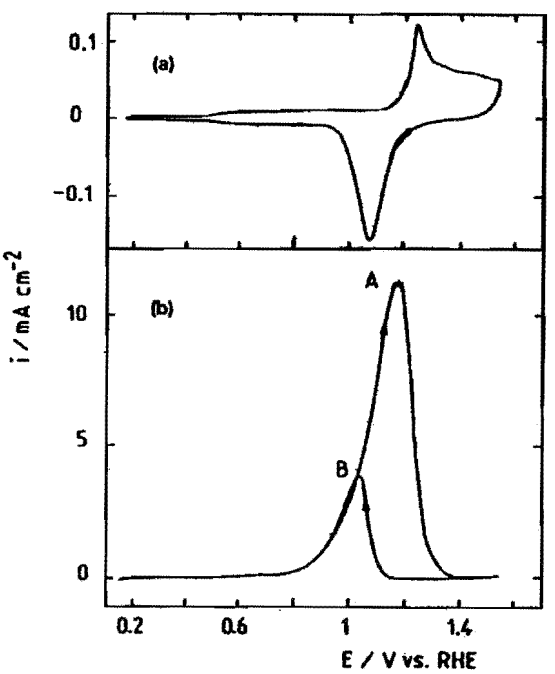

Figure 2.14. Cyclic voltammograms of a gold bead electrode (0.1 M NaOH, 25°C, 50 mV/s. (a) Without ethylene glycol; (b) with 0.1 M ethylene glycol (Kadirgan et al., 1990).

It is not possible to sustain long electrolysis of ethylene glycol at a fixed potential, because of poisoning phenomena that occurs at the electrode surface (Kadirgan et al., 1990). A cleaning procedure has to be used for sustainable electrolysis. The simplest technique is to use potential programs with potential plateaux separated repeatedly by a single cleaning potential sweep. The electrode surface and the poisons are oxidised at the upper potential limit. The surface oxides are reduced at the lower potential limit, before returning to the potential plateaux. The major product of electrolysis at 1.13 V_{RHE} is glycolate. Small quantities of oxalate, carbonate and formate are also formed (Kadirgan et al., 1990).

Kadirgan and co-workers (1990) used electromodulated infrared reflectance spectroscopy (EMIRS) to check for the presence of adsorbed CO-type poisons. These CO poisons would be formed by the rupture of the C-C bond during chemisorption at negative potentials. It was found the CO band is not present initially and that it grows during spectral accumulation performed to improve signal to noise ratio. However, the CO band is far from being the main infrared band observed. This implies that ethylene glycol does not dissociate immediately on gold at low potentials and that the CO poisoning species are formed only progressively. Glycolaldehyde and glyoxalate were found to be the main adsorbed species.

2.8.3. The electro-oxidation of ethylene glycol at platinum electrodes in acid

A cyclic voltammogram for the electro-oxidation of 0.1 M ethylene glycol in 0.1 M $HClO_4$ is shown in Figure 2.15 (Hahn et al., 1987). Several peaks and shoulders, labelled A to D are found.

Inhibition of hydrogen adsorption in the hydrogen region occurs due to adsorption of ethylene glycol. Electrochemically Modulated Infrared Reflectance Spectroscopy (EMIRS) was used by Hahn et al (1987) to study the adsorption of ethylene glycol. It was found that the adsorption is dissociative, leading to the formation of a poisoning linearly bonded CO species. Oxidation of the CO starts at 0.6 V_{RHE}, at the same potential where the overall oxidation process of ethylene glycol begins (Fig. 2.15).

By using in situ FTIR spectroscopy, Christensen and Hamnett (1989) identified the main products of ethylene glycol oxidation in acid as glycolic acid and CO_2.

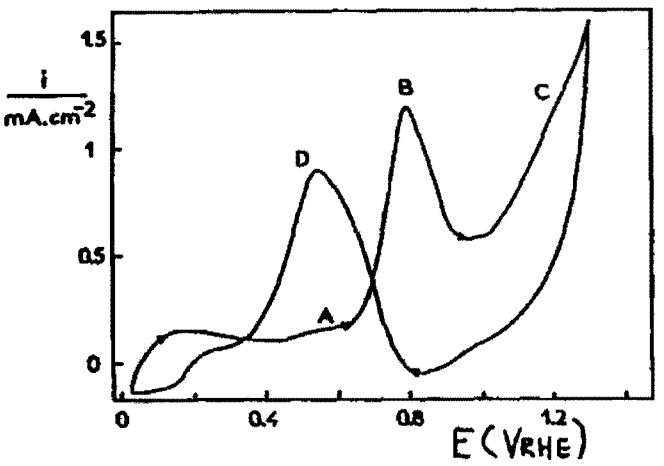

Figure 2.15. Cyclic voltammogram for the oxidation of 0.1 M ethylene glycol in 0.1 M $HClO_4$, on platinum. Conditions: 100 mV/s, 25°C (Hahn et al., 1987).

2.8.4. The electro-oxidation of ethylene glycol at platinum electrodes in base

Cyclic voltammograms of a platinum electrode in 1 M NaOH in the absence and in the presence of 0.1 M ethylene glycol are shown in Figure 2.16 (Kadirgan et al., 1983). Ethylene glycol oxidation begins at 0.35 V_{RHE} during the positive sweep, giving a steep rise A at 0.65 V_{RHE}, then a peak B of 6.6 mA/cm^2 at 0.73 V_{RHE} and a small peak C at 1.05 V_{RHE}. The decrease of current after peak B is related to the formation of surface oxides on the platinum electrode. Ethylene glycol oxidation takes place during the negative sweep after the reduction of the surface oxides, reaching a maximum rate of 2 mA/cm^2 at 0.63 V_{RHE} (peak D). The current densities obtained in alkaline solution are much higher than in acid solution (Figure 2.15). The oxidation process also appears to be less irreversible in alkaline than in acid medium, in which the main oxidation peaks of ethylene glycol are separated by more than 250 mV during the positive and negative sweeps (Fig. 2.15).

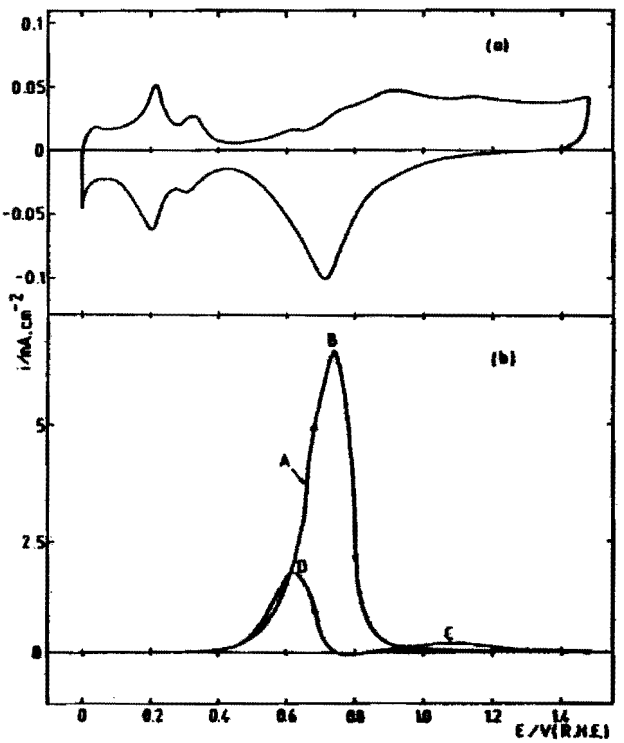

Figure 2.16. Cyclic voltammograms of a Pt bead electrode (1 M NaOH, 25°C, 50 mV/s): (a) without ethylene glycol; (b) with 0.1 M ethylene glycol (Kadirgan et al., 1983).

Electrochemically Modulated Infrared Reflectance Spectroscopy (EMIRS) was used by Hahn et al (1987) to study the adsorption of ethylene glycol at platinum in alkaline solutions. The adsorption was found to be dissociative. However, almost equal amounts of bridge-bonded and linearly bonded CO species were found in alkaline solutions. This is in contrast to acidic solutions, where only linearly bonded CO species were found (Hahn et al., 1987). An important shift towards lower wavenumbers of the linearly-bonded CO band centre was observed when the pH was increased. This might be due to interactions with the solvent or with adsorbed OH species, and a decrease of the CO coverage. The adsorption of molecular ethylene glycol may also play a role. The drastic change in the CO coverage as a function of pH is most probably related to a change in the electrocatalytic activity of platinum towards the oxidation of ethylene glycol when changing from acid to alkaline solutions.

The main products of ethylene glycol oxidation in base at platinum are glycolate, oxalate and CO_3^{2-}, determined by in situ FTIR (Christensen and Hamnett, 1989).

2.8.5. The electro-oxidation of ethylene glycol at Au-Pt electrodes in base

The cyclic voltammograms for ethylene glycol oxidation in base at Au, Pt and a 50Au-50Pt alloy electrode are shown in Figure 2.17 (Beden et al., 1982). The Au-Pt alloy electrode was prepared by electrolytic codeposition of the two metals on a platinum bead. The alloy electrode was then annealed by warming it to red heat in a hydrogen flame. For the alloy electrode it can be seen that during the positive sweep, electro-oxidation of ethylene glycol occurs in two main peaks. The first peak is in the same potential range as pure platinum and the second peak corresponds to oxidation on pure gold. However, the current densities obtained with the alloy electrode are much higher than those on the pure metals. At the Pt-region, the electro-oxidation activity is enhanced eight times and at the Au-region two times.

The 60Au-40Pt alloy electrode has been found to be the most active for ethylene glycol oxidation (Eggert (Stelmach, 1994)). However, the effect of the heat treatment condition of this alloy (Table 3.1) on the electro-oxidation of ethylene glycol needs to be considered.

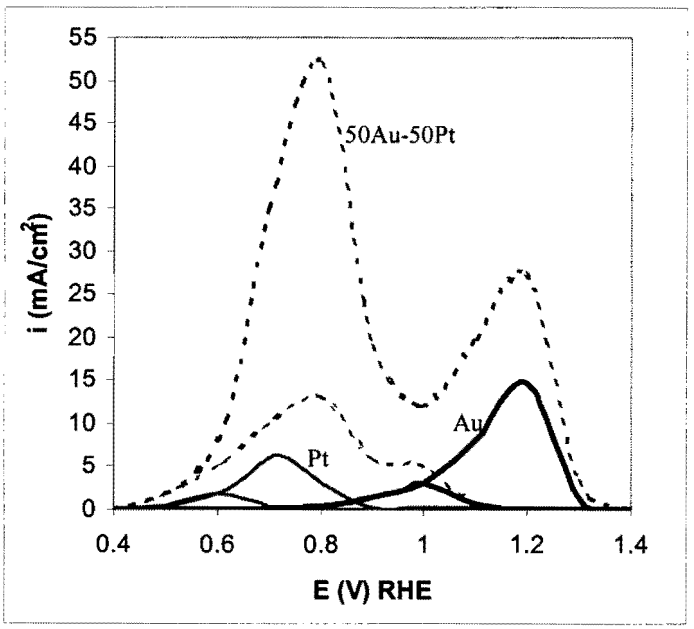

Figure 2.17. Cyclic voltammograms for ethylene glycol electro-oxidation in 1 M NaOH (0.1 M ethylene glycol, 25℃, 50 mV/s) on a platinum bead electrode, a gold bead electrode and a 50Au-50Pt alloy electrode (After Beden et al., 1982).

2.9. The Au-1wt% Ti alloy (Gold 990)

The Au-1wt% Ti alloy was originally developed to produce an alloy with at least 990 fineness, with colour close to that of pure gold and with durability as good as that of standard jewellery alloys (Gafner, 1989).

The addition of 1 wt% (4 at%) of titanium to gold substantially hardens the precious metal and enhances its wear resistance. The enhanced hardening is due to the formation of fine Au_4Ti precipitates under the appropriate thermo-mechanical treatments (The Au-Ti phase diagram (ASM Handbook, Volume 3: Alloy Phase Diagrams, 1992) is shown in Figure. 2.18). The addition of titanium to gold satisfies two important criteria for achieving optimum precipitation hardening:

1) It has a high solubility in gold at elevated temperature, which maximises its dissolution into gold.
2) The gold-titanium system has a shallow solvus curve towards pure gold, which enables a significant proportion of titanium to be retained in supersaturated solid solution on quenching. The Au_4Ti compound, which constitutes the strengthening precipitate, is substantially harder than the gold matrix and so gives rise to a substantial reinforcement.

2.9.1. Preparation of Gold 990

The alloy is prepared (Gafner, 1989) by melting together the constituents in a vacuum induction furnace, and casting the alloy into a suitable ingot. It is then precipitation hardened in two stages by first carrying out a solution heat-treatment, involving a heating stage at 800°C in air, or a vacuum or inert atmosphere, followed by quenching the ingot in water. Tests have shown that no significant loss of titanium occurs when solutionising is in air, because a protective surface layer forms. This brown layer can subsequently be removed mechanically or by dipping the alloy in a 10% $K_2S_2O_7$ solution in water. Precipitation hardening is accomplished by heating the alloy at a lower temperature, typically at 400-500°C, with or without an intermediate cold working stage.

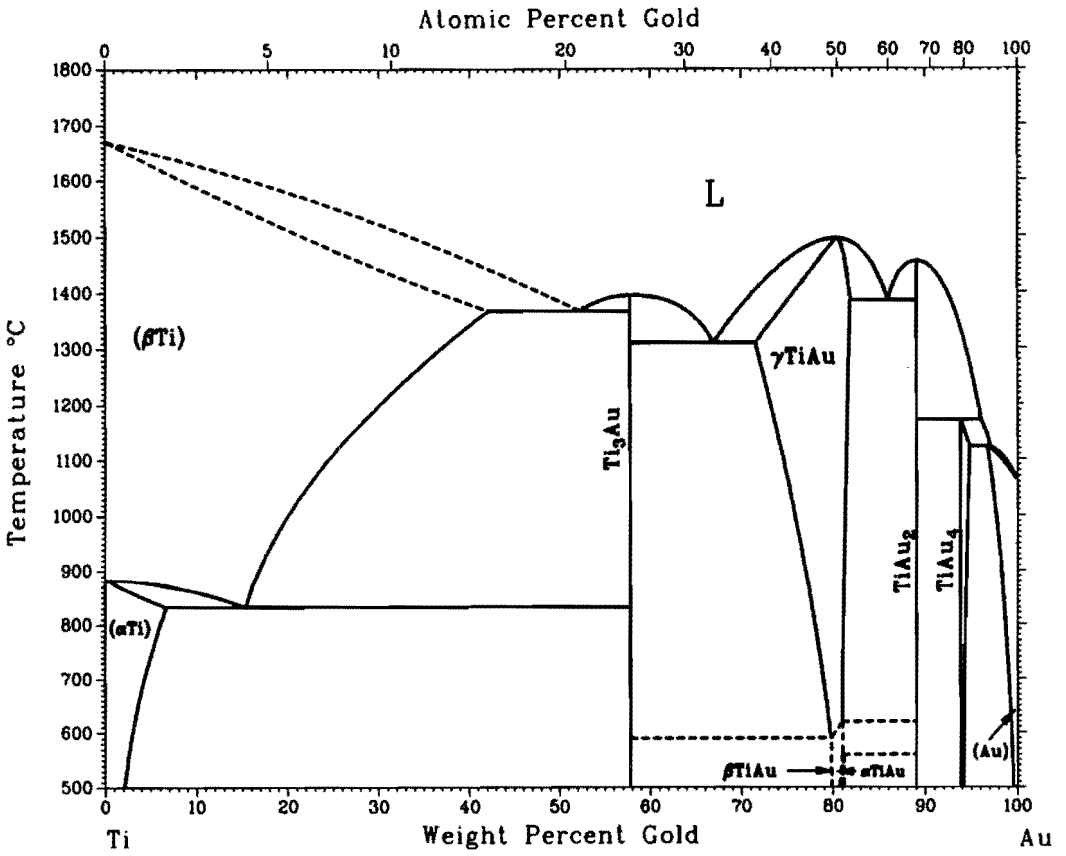

Figure 2.18. The Au-Ti phase diagram (ASM Handbook, Volume 3: Alloy Phase Diagrams, 1992).

It would be of interest to investigate the electrochemical properties of the alloy in two different heat treatment conditions (Fig. 2.18):

1) With titanium in solid solution.
2) In the precipitation-hardened condition (with Au_4Ti precipitates).

2.9.2. The electrochemical behaviour of pure titanium

Potentiodynamic polarisation curves for titanium in 0.5 M H_2SO_4 were measured at 303, 313 and 323 K by Shibata and Zhu (1995) and are shown in Figure 2.19.

An active-passive transition is found at around -0.49 $V_{Ag/AgCl}$. The critical current for passivation and the passive current increase with temperature. It is interesting that a second peak appears around 2.1 $V_{Ag/AgCl}$, which decreases with increase in temperature. The origin of this peak is still uncertain. According to Armstrong (1977) it could be due to a phase transformation of the originally formed oxide. The steady passive current was again reached beyond this second peak. A rapid current increase then

follows due to oxygen evolution. The oxygen evolution potential shifted in the negative direction with increase in temperature.

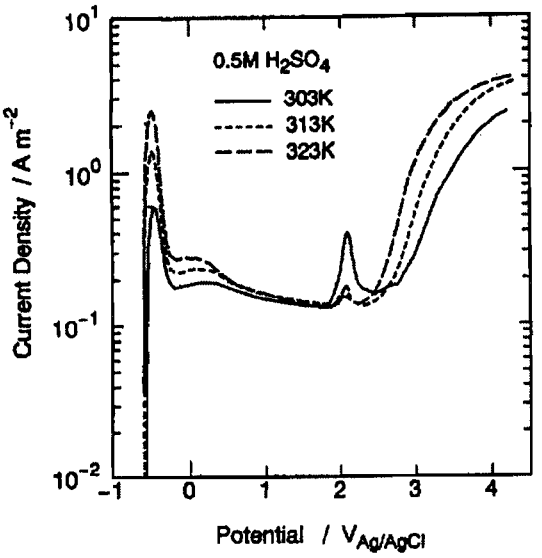

Figure 2.19. Anodic polarisation curves of Ti in 0.5 M H_2SO_4 solution at 303, 313 and 323 K (Shibata and Zhu, 1995).

The frequency and current responses as a function of the potential for titanium in 5 M H_2SO_4 are shown in Figure 2.20 (Herranen and Carlsson, 2001). As expected, the anodic current corresponding to dissolution of titanium is first accompanied by an increase in frequency (this corresponds to a decrease in mass). After reaching the passivation potential at –470 mV_{SCE}, with the corresponding critical current density (i_c), the current decreases as a result of oxide formation. However, the mass continues to decrease in the active-passive region. This indicates that the passive layer is not intact until a passive potential of about –150 mV_{SCE} is reached. An increase in mass is observed in the passive region. A second current density peak at 1.72 V_{SCE} was only found in 0.1 M H_2SO_4 - proposed to be due to a phase transformation of the oxide (Armstrong, 1977).

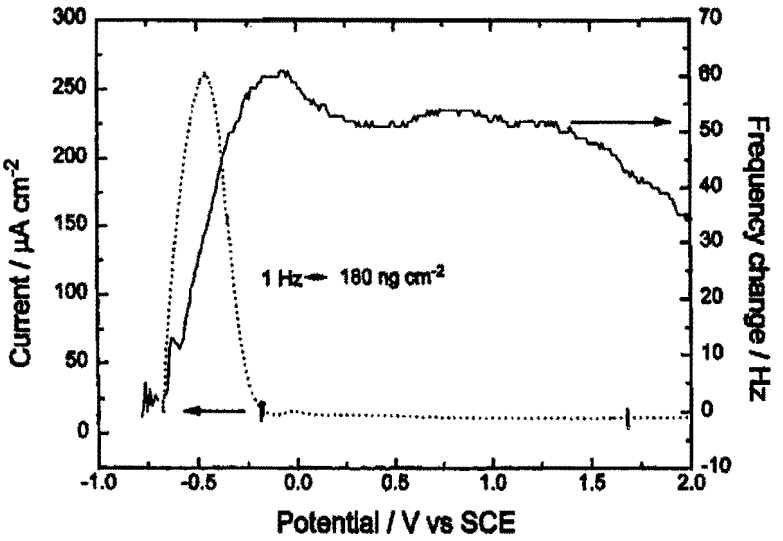

Figure 2.20. Current and frequency changes as functions of the potential of Ti in 5 M H_2SO_4 (Herranen and Carlsson, 2001).

A number of studies of the structure and composition of passive films on titanium have been reported. Armstrong (1977) studied the electrochemical behaviour of titanium films in 1 M $HClO_4$ and 0.5 M H_2SO_4 and characterised the surface oxide by XPS and AES. This indicated a mixture of metal oxides (TiO_2, Ti_2O_3 and TiO). Electrodes prepared at a larger anodic charge (potentials up to 2 V_{SCE}) showed more TiO_2 character.

Pure titanium is expected to be in the passive condition at the potentials applied for cyclic voltammetry of gold electrodes (0 – 1.8 V_{RHE} in acid and 0 – 1.6 V_{RHE} in base, Figures 2.1 and 2.2). This fact is also supported by the Pourbaix diagram for titanium shown in Figure 2.21 (Pourbaix, 1974).

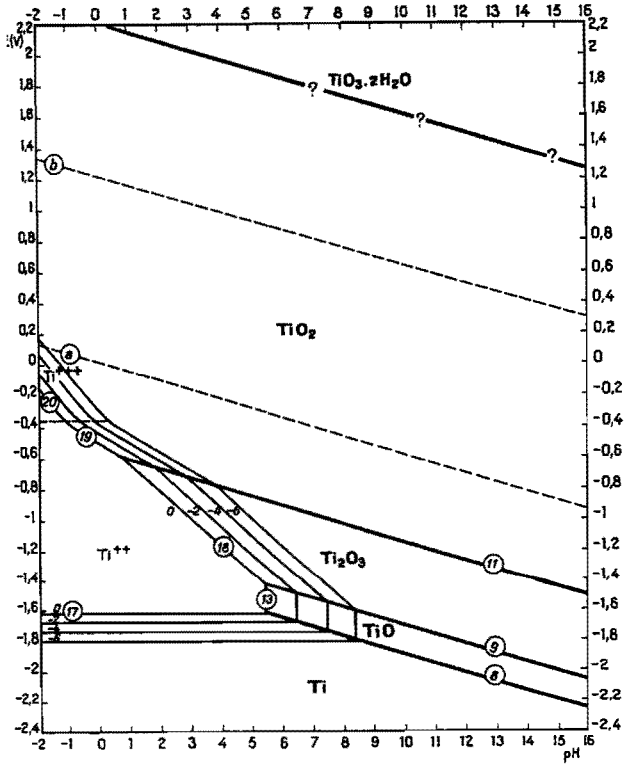

Figure 2.21: Potential – pH equilibrium diagram for the system titanium – water, at 25°C (Pourbaix, 1974).

2.10. Conclusions

- Even though gold is a weak chemisorber, it displays a wide range of electro-oxidation activity, especially in alkaline solutions.
- It is believed that organic compounds are oxidised at gold anodes in the presence of a submonolayer of adsorbed hydroxyl radicals (AuOH) before monolayer oxide formation.
- A bimetallic electrode is usually more active for the electro-oxidation of organics than the respective pure metals.
- The 60Au-40Pt alloy electrode has been identified in the literature as being the most active for the electro-oxidation of various organics in base. However, the effect of the microstructure of the alloy on its electrochemical properties has largely been ignored in the past.
- The electro-oxidation of ethylene glycol at noble metal electrodes has been studied extensively. This organic compound can therefore be used as a model compound to study the effect of heat treatment condition on the electrochemical properties of the gold alloys.

- The Gold 990 alloy was developed originally for the jewellery industry. The electrochemical properties of this alloy have not been studied before.

Chapter 3

THE HEAT TREATMENT OF Au-Pt ALLOYS AND THE GOLD 990 ALLOY

3.1. Introduction

The gold alloy containing 40% platinum has been identified (Stelmach et al., 1994) as being the most active for the oxidation of various organic compounds in alkaline solutions. However, the effect of the microstructure of gold-platinum alloys on their electrochemical properties has largely been ignored in the past. The purpose of this chapter is to discuss the microstructures of the 60Au-40Pt alloy obtained after different heat treatments. The spinodal decomposition reaction in the 50Au-50Pt alloy is also discussed.

The Gold 990 alloy (Au-1wt%Ti) is a precipitation-hardenable alloy. The different heat treatments of the Gold 990 alloy will also be reviewed in this chapter.

3.2. The 60Au-40Pt alloy

Gold and platinum (both 99.99%) were melted together (in the required ratio) in an arc-furnace with a water-cooled copper hearth under a protective argon atmosphere. The sample (approximately 10 g) was turned around after each melt and re-melted three times to ensure homogeneity.

3.2.1. The 60Au-40Pt alloy heat treated at 1300°C

The 1300°C heat treatment of the 60Au-40Pt alloy is shown schematically in Figure 3.1. Partial melting of the sample will occur at 1300°C. The liquid phase will be gold-rich with a composition of approximately 85Au-15Pt. The solid phase will be platinum-rich. The composition of this phase is difficult to estimate, due to the fact that the solidus line is almost horizontal at these temperatures. A small deviation from 1300°C will result in

large deviations in the composition of this phase. For the same reason, the lever rule cannot be used to accurately predict the amount of each phase that will be formed. However, the Pt-rich phase obtained by this heat treatment will have a higher gold content than the Pt-rich phases formed in the miscibility gap (Figure 3.1).

The sample was kept at 1300°C for 1 hour before quenching in water. After quenching, the sample was cold-rolled to a thickness of approximately 2 mm. A disk with a diameter of 6 mm was subsequently punched. The sample was mounted in a resin by using a black phenolic thermosetting powder. It was polished using diamond paste (6, 5 and finally 1 μm). The microstructure was studied by means of optical microscopy and scanning electron microscopy (SEM).

The microstructure of the 60Au-40Pt alloy after the 1300°C heat treatment is shown in Figure 3.2. Etching was not required to produce the microstructure shown in Figure 3.2. It can be seen that the Pt-rich areas formed by this heat treatment are relatively large, with typical diameters of 30 –50 μm (Figure 3.2).

Back-scattered electron imaging cannot be used to study the Au-rich and Pt-rich areas, because the atomic weights of gold and platinum are similar (196.97 and 195.08 g/mol respectively). However, the Au-rich and Pt-rich phases can be distinguished by elemental mapping using energy dispersive X-ray analysis in a scanning electron microscope.

An elemental map (using energy-dispersive X-ray analysis based on the L lines of the two metals) of the 60Au-40Pt alloy heat treated at 1300°C is shown in Figure 3.3. The elemental map confirms that optical microscopy without etching of the sample can be employed to study the microstructures of Au-Pt alloys (Compare Figures 3.2 and 3.3).

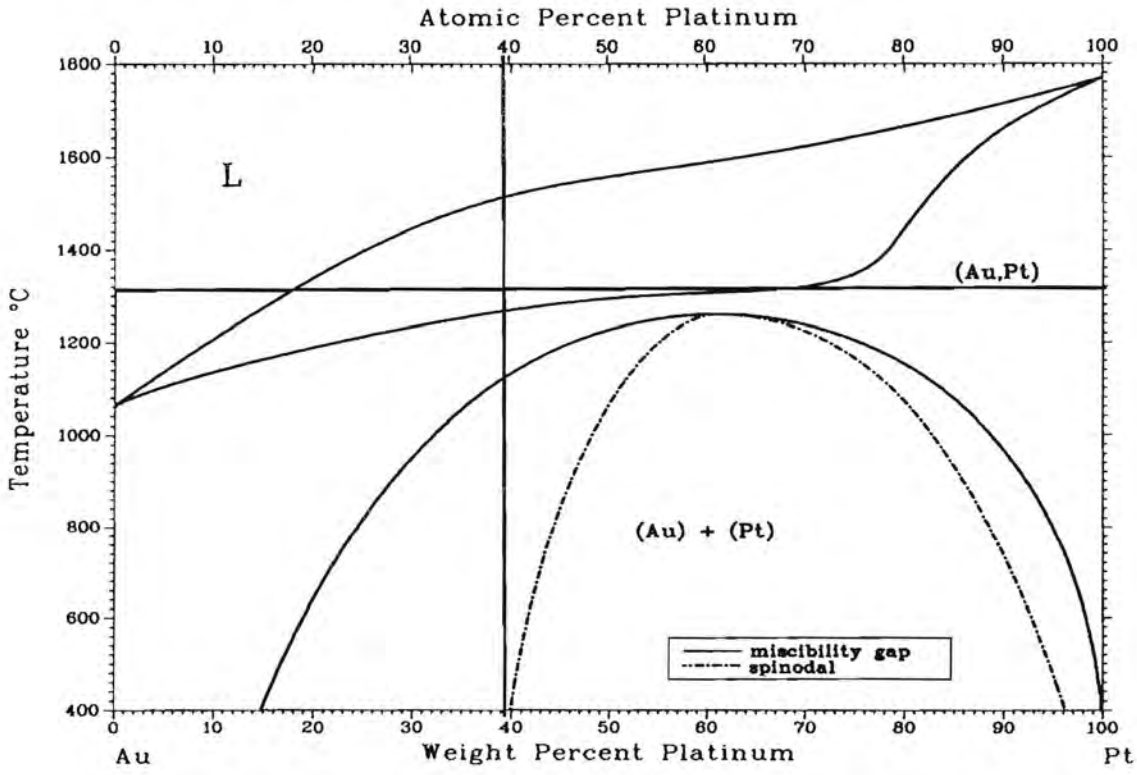

Figure 3.1. The 1300°C heat treatment of the 60Au-40Pt alloy (ASM Handbook, Volume 3: Alloy Phase Diagrams, 1992)

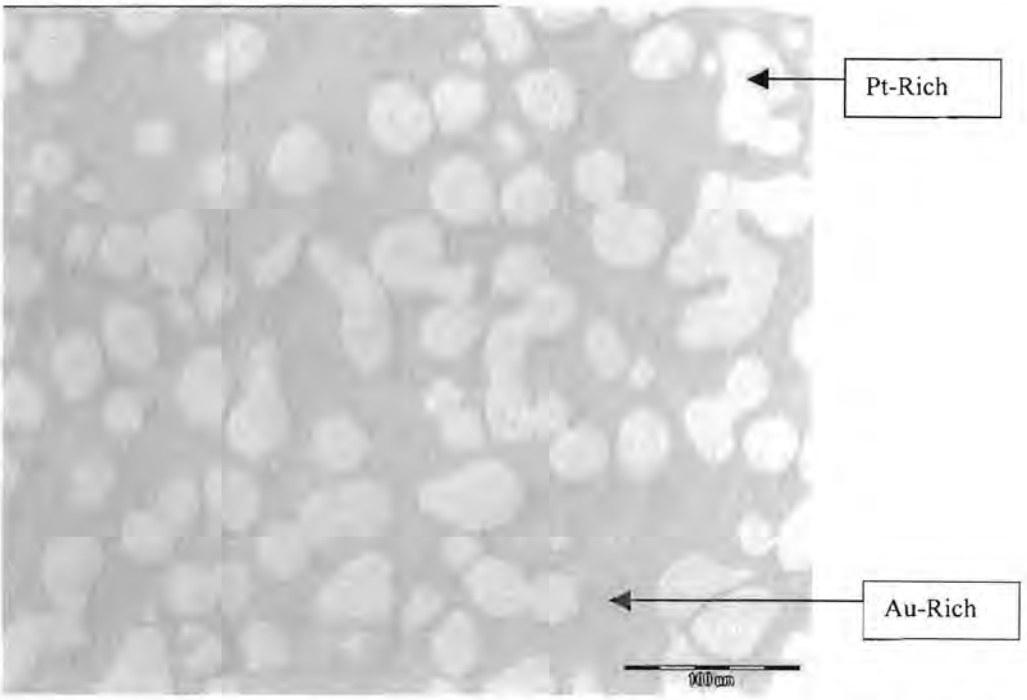

Figure 3.2. Optical photomicrograph of the 60Au-40Pt alloy after heat treatment at 1300°C for 1 hour (No etching).

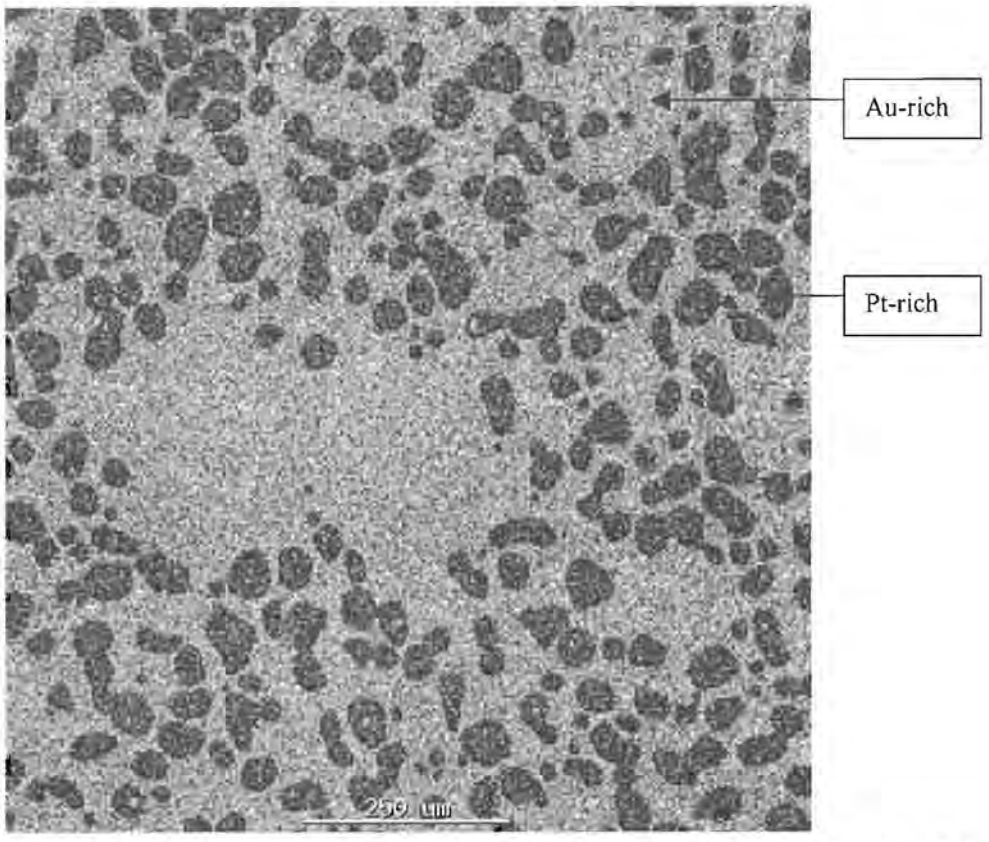

Figure 3.3: Elemental map (based on L lines of energy-dispersive X-ray analysis) of the 60Au-40Pt alloy heat treated at 1300°C.

3.2.2. The 60Au-40Pt alloy heat treated at 1200°C

Samples of the 60Au-40Pt alloy in the 1300°C heat treatment condition were heat treated at 1200°C, followed by water quenching. The 1200°C heat treatment of the 60Au-40Pt alloy is shown schematically in Figure 3.4. This heat treatment is designed to produce a homogeneous solid solution of platinum in gold. Due to the fact that the Pt-rich areas are relatively large in the 1300°C condition (Fig. 3.2), the influence of time at 1200°C was investigated by heat treating two samples for different times. The first sample was treated at 1200°C for 24 hours and the second sample for 168 hours (1 week).

The samples were polished using diamond paste (6, 5 and finally 1 µm). The microstructures were studied by means of optical microscopy and scanning electron microscopy (SEM). X-ray diffraction (XRD) was used to confirm whether a solid solution was produced after the solutionising heat treatment.

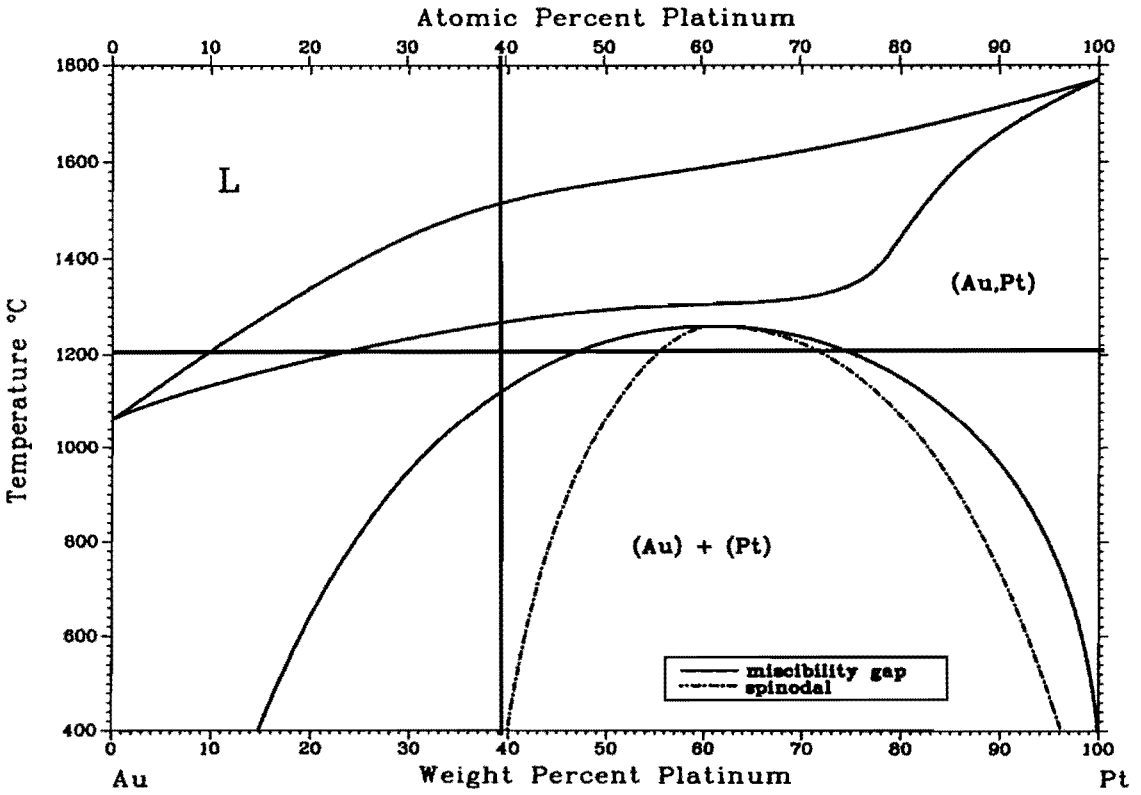

Figure 3.4. The 1200°C heat treatment of the 60Au-40Pt alloy (ASM Handbook, Volume 3: Alloy Phase Diagrams, 1992)

3.2.2.1. The 60Au-40Pt alloy heat treated at 1200°C for 24 hours

The X-ray diffraction patterns for the 1300°C and the 1200°C heat treated samples are shown in Figure 3.5. The 1300°C treated sample has two peaks, corresponding to the Au-rich and Pt-rich phases. Two peaks are observed because of the difference in lattice parameters of the two phases. Both phases are face-centered cubic (fcc). The 1200°C treated sample only has one peak, showing that the solutionising heat treatment was successful. The "prestik" peaks in Figure 3.5 are due to the sample holder that was used during XRD.

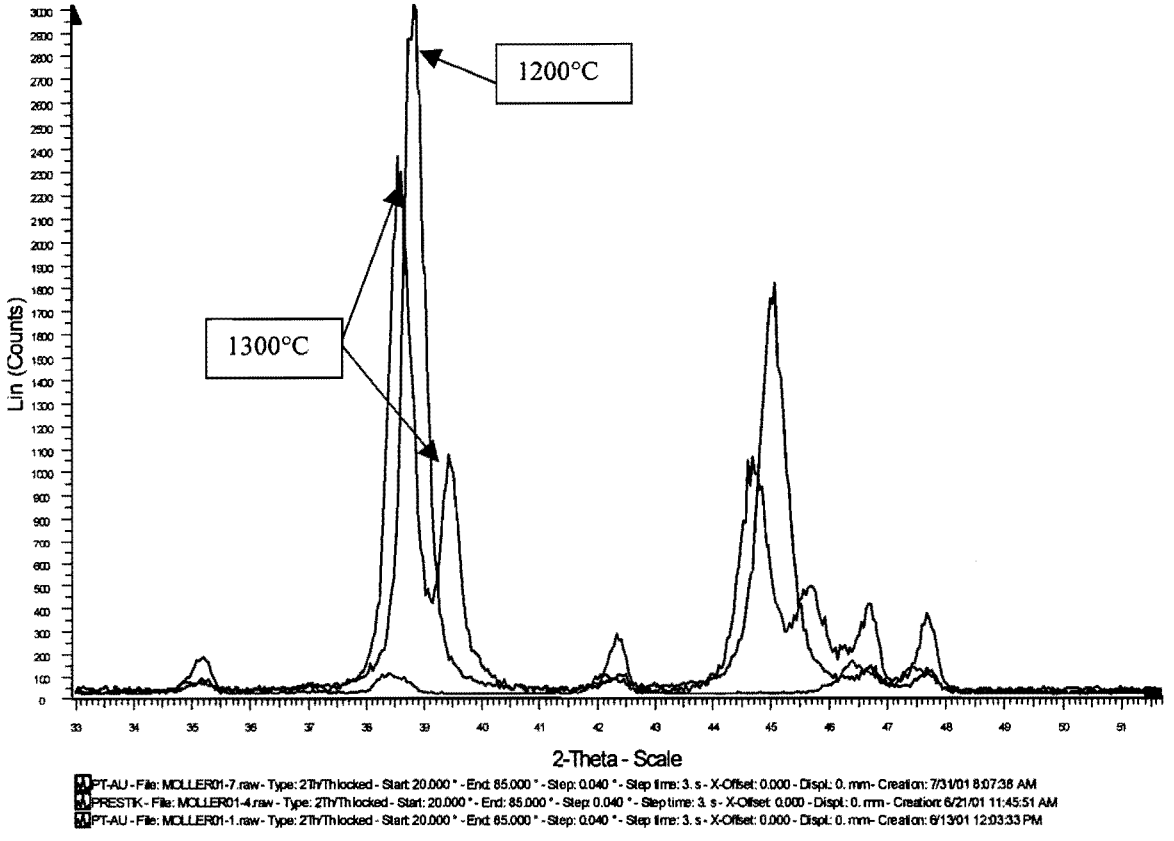

Figure 3.5. X-ray diffraction patterns of the samples heat treated at 1300°C and at 1200°C.

The microstructure of the 60Au-40Pt alloy after heat treatment at 1200°C for 24 hours is shown in Figure 3.6. The microstructure confirms that a single-phase solid solution was produced. However, it can be seen that porosity resulted during this heat treatment.

The porosity is not due to shrinkage during solidification, because at 1200°C no liquid is formed. It can, however, be explained by the Kirkendall effect.

UNIVERSITEIT VAN PRETORIA
UNIVERSITY OF PRETORIA
YUNIBESITHI YA PRETORIA

Electrochemistry of gold-based alloys

By

Heinrich Möller

A dissertation submitted in partial fulfillment of the requirements for the degree of

Master of Engineering

in the Department of Materials Science and Metallurgical Engineering,
Faculty of Engineering, Built Environment and Information Technology,
University of Pretoria

2002

Electrochemistry of gold-based alloys

by

Heinrich Möller

Supervisor: Prof. P.C. Pistorius

Department of Materials Science and Metallurgical Engineering

Degree: Master of Engineering

ABSTRACT

The electro-oxidation of organic compounds at noble metal electrodes has been widely studied in the past. A bimetallic electrode is often more active than the respective pure metals. However, the effect of the microstructure of the alloys on their electrochemical properties has largely been ignored in the past.

The electro-oxidation of ethylene glycol at gold-platinum and gold-titanium electrodes in different heat treatment conditions was studied to determine how the different microstructures would influence the electrochemistry of these alloys.

Kirkendall porosity was produced by the solid solution heat treatment of the two-phased 60Au-40Pt electrodes. The extra surface area due to the porosity resulted in high apparent current densities at the porous electrodes in both acid and alkaline solutions without ethylene glycol. Only slightly higher apparent current densities were obtained at the porous gold-platinum electrodes compared to the non-porous electrodes when ethylene glycol was present in the solution. Kirkendall porosity was not produced by the solid solution heat treatment of the two-phased 50Au-50Pt electrodes.

The gold-platinum electrodes were more active for the electro-oxidation of ethylene glycol than both pure gold and platinum. The electrodes in the solid solution heat treatment condition were more active than the two-phased electrodes. This can be explained by the Third-body effect, which means that platinum atoms that are surrounded by gold atoms are less likely to become poisoned by intermediates than platinum atoms

that are surrounded by other platinum atoms. Poisoning of all the electrodes occurred during electrolysis of ethylene glycol at a fixed potential. The poisoning species at pure gold and pure platinum could be removed by potential pulsing and sustainable electrolysis of ethylene glycol was possible at these electrodes. Unfortunately, the same technique was not as successful with the gold-platinum alloys and their activities declined during the long-term electrolysis of ethylene glycol.

The electrochemical behaviour of the Gold 990 (Au-1wt% Ti) electrodes is similar to pure gold in acid and alkaline solutions. It is possible that the titanium content is too low to have a significant influence on the electrochemical behaviour of gold. The titanium may also be in the passive condition or it may have dissolved selectively from the Gold 990 alloy resulting in a pure gold surface.

Keywords: Gold, platinum, gold-platinum alloys, gold-titanium alloys, Gold 990, Kirkendall porosity, electrochemistry, electro-oxidation, ethylene glycol, cyclic voltammetry.

ACKNOWLEDGEMENTS

I would like to thank and herewith express my sincere appreciation to the following:

- Professor Chris Pistorius, my supervisor, for guidance and continuous support.
- Mintek for financial assistance.
- Doctor Elma van der Lingen and Stephen Roberts from Mintek for guidance and sample preparation.
- The Department of Materials Science and Metallurgical Engineering and IMMRI for facilities.
- Lida Roos, my fiancée, for her love, continuos support and patience.
- My father, mother, Robert, Danie and Johan for their prayers and support.
- The Roose: Lida's parents, Hannes and Marileen for their continuous support.
- Carel Coetzee for assistance with the SEM.
- Doctor Sabine Verryn of the Geology department for assistance with XRD.
- Sarah Havenga and Johann Borman for their assistance.
- My friend Heinrich Hutchison for his valuable contribution.
- The personnel and specially my fellow graduate students for their support and advice.
- The Lord, for the abilities He gave me and the opportunity to develop them.

CONTENTS

Chapter 1

INTRODUCTION

The electro-oxidation of organic compounds at noble metal electrodes has been studied extensively for possible applications in electrochemical power sources (Parsons and VanderNoot, 1988) and electrochemical wastewater treatment (Comninellis, 1994). Gold is the noblest and most inert of all metals. It also possesses weak chemisorbing properties due to the absence of vacancies in its d-bands. Surprisingly, it still displays a wide range of electro-oxidation activity – especially in alkaline solutions (Burke and Nugent, 1998).

It is known that a bimetallic electrode is usually more active for the electro-oxidation of organics than the respective pure metals (Parsons and VanderNoot, 1988). The gold alloy containing 40% platinum has been identified (Stelmach et al., 1994) as being the most active for the oxidation of various organics in base. However, the effect of the microstructure of gold-platinum alloys on their electrochemical properties has largely been ignored in the past.

The Gold 990 alloy (Au-1wt% Ti) was developed originally for the jewellery industry (Gafner, 1989). The electrochemical properties of this alloy have not been investigated before. It is possible to heat treat Gold 990 to obtain two different heat treatment conditions: (a) with titanium in solid solution with the gold and (b) the precipitation-hardened condition, with small Au_4Ti precipitates.

This study has been subdivided into three main parts:

- In the first part, the heat treatments of the Au-Pt and the Au-Ti alloys are investigated. By employing different heat treatment temperatures and times, different microstructures are produced.
- In the second part, the electrochemical properties of the heat treated electrodes are studied in acid and alkaline solutions without an organic compound in the solution.
- In the third part, the electro-oxidation of ethylene glycol at Au-Pt and Gold 990 electrodes in different heat treatment conditions is investigated. Ethylene glycol was selected as a model organic compound due to the fact that its oxidation at noble metal electrodes has been studied extensively (Kadirgan et al., 1990; Hahn et al., 1987).

Chapter 2

THEORETICAL BACKGROUND

2. Electrochemical behaviour of pure gold in aqueous media

2.1. Gold in acidic media

A typical cyclic voltammogram recorded for a polycrystalline gold disc electrode in acid is shown in Figure 2.1 (Burke and Nugent, 1997). During the positive sweep, monolayer oxide (α-oxide) formation results in an increase in anodic current at 1.35 V versus the reversible hydrogen electrode (RHE). The charge associated with further monolayer oxidation for gold in acid tends to be distributed along a plateau with no major change until oxygen gas evolution commences at 2.0 V_{RHE} (not shown in Figure 2.1). During the negative sweep, the monolayer oxide reduction peak is observed at 1.1 V_{RHE}.

Birss and Xia (2001) formed α-oxide films at sputtered polycrystalline gold electrodes in 0.1 M H_2SO_4 solutions. The composition and properties of the film were established using potentiostatic, cyclic voltammmetry, ellipsometric and in-situ mass measurement techniques. The α-oxide is proposed to be AuO at potentials below 1.5 V_{RHE}, and a mixture of AuO and Au_2O_3 above this, likely becoming primarily Au_2O_3 at still higher potentials. This is based on ellipsometric evidence and the measured mass to charge ratio of 8 g/mol electrons at all potentials.

2.2. Gold in alkaline media

Examples of cyclic voltammograms recorded for gold in base are shown in Figure 2.2 (Burke and Nugent, 1997). Monolayer oxide growth commences at 1.25 V_{RHE}. At more positive potentials, oxygen gas evolution occurs. Over the range of 1.6 to 2.0 V_{RHE} oxygen gas evolution is believed to be catalysed in a transient manner by some type of nascent hydrous gold oxide species formed at the monolayer oxide/aqueous solution interface (Burke and Nugent, 1997). Regular oxygen gas evolution on gold in base (as in acid) occurs only above 2.0 V_{RHE}.

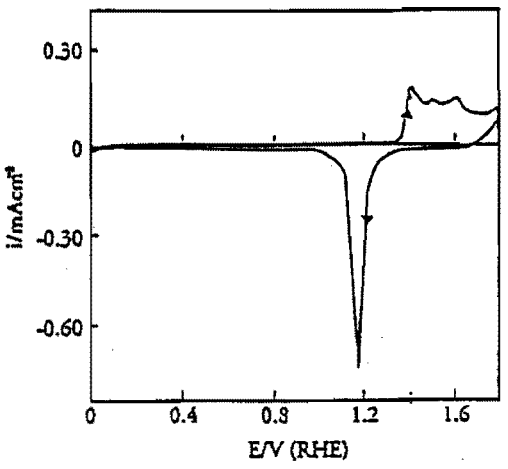

Figure 2.1. Typical cyclic voltammogram (0.0 to 1.80 V_{RHE}, 50mV/s, 25℃) recorded for a polycrystalline gold disc electrode in 1.0 mol/dm^3 H_2SO_4 (Burke and Nugent, 1997).

An interesting feature of the negative sweep in Figure 2.2(b) is the appearance of a second cathodic peak at 0.85 V_{RHE}. The monolayer oxide reduction peak was observed in this case at 1.1 V_{RHE} and the subsequent peak is assumed to be due to the reduction of hydrous gold oxide species formed on the gold surface at the upper end of the cycle (Burke and Nugent, 1997).

2.3. Premonolayer oxidation of gold

Gold is frequently regarded as the ideal solid electrode system for fundamental investigations in electrochemistry. This is due to the fact that in the absence of redox active species in the aqueous phase, the system apparently exhibits only double layer (non-Faradaic) behaviour over the range of 0 to 1.3 V_{RHE} in acid and 0 to 1.2 V_{RHE} in base. However, there have been assertions that Faradaic behaviour due to the formation of oxy-species at the gold surface occurs within the double layer region. However, the extent of premonolayer oxidation (the coverage involved) is small. This makes it difficult to detect these species and the responses associated with them.

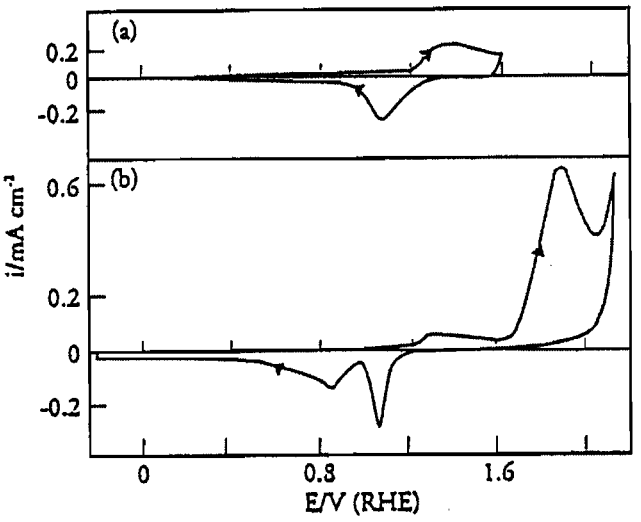

Figure 2.2. Typical cyclic voltammogram for a polycrystalline gold electrode in 1.0 mol/dm^3 NaOH at 25 ℃: (a) 0.0 to 1.60 V_{RHE} at 50 mV/s; (b) -0.2 to 2.1 V_{RHE} at 10 mV/s (Burke and Nugent, 1997).

2.3.1. Premonolayer oxidation of gold in acid

Watanabe and Gerischer (1981) postulated on the basis of photoelectrochemical data that gold exhibited premonolayer oxidation extending over the potential range 0.85 to 1.35 V_{RHE}. They postulated that this incipient oxidation represented the formation of chemisorbed species (Au-OH and/or Au-O) with surface coverages up to 20%.

Hutton and Williams (1994), using Scanning Laser Microscopy, found that gold oxidised in the premonolayer region. They found that this incipient oxide was stable, only being removed by prolonged evolution of hydrogen gas.

Gordon and Johnson (1994) investigated gold electrodes in acid solution by means of an Electrochemical Quartz Crystal Microbalance (EQCM). They proposed that the species formed during premonolayer oxidation corresponded to adsorbed hydroxyl radicals, designated as AuOH. Figure 2.3(a) (Gordon and Johnson, 1994) shows a typical current-potential (I-E) curve obtained at a gold film electrode in 0.10 M $HClO_4$. The very small anodic current observed during the positive potential scan in region A corresponds to charging of the electrical double layer. Region B during the positive scan corresponds to the premonolayer region and the slight increase in anodic current is concluded to result primarily from the formation of the submonolayer of hydrous oxide, designated as AuOH. The large wave in region C corresponds to the formation of the monolayer oxide. An electrochemical quartz crystal microbalance (EQCM) was

used to detect small surface mass changes during cyclic voltammetry. A decrease in frequency indicates an increase in mass. Figure 2.3(b) (Gordon and Johnson, 1994) shows the frequency-potential (f-E) curve recorded simultaneously with the I-E curve in Figure 2.3(a). During the positive scan there is no detectable change in frequency corresponding to double layer charging (region A). However, a rapid decrease in frequency (mass increase) by the amount Δf_B is observed in region B concomitantly with the formation of AuOH. Continuation of the positive scan through region C results in a further decrease in frequency by an amount Δf_C concomitantly with the formation of the monolayer oxide. Following scan reversal, the frequency remains constant until it increases very rapidly in the region corresponding to cathodic reduction of the monolayer oxide. Continuation of the negative scan back through the premonolayer region B results in further increase of frequency until the original value of f is attained in the double-layer region A.

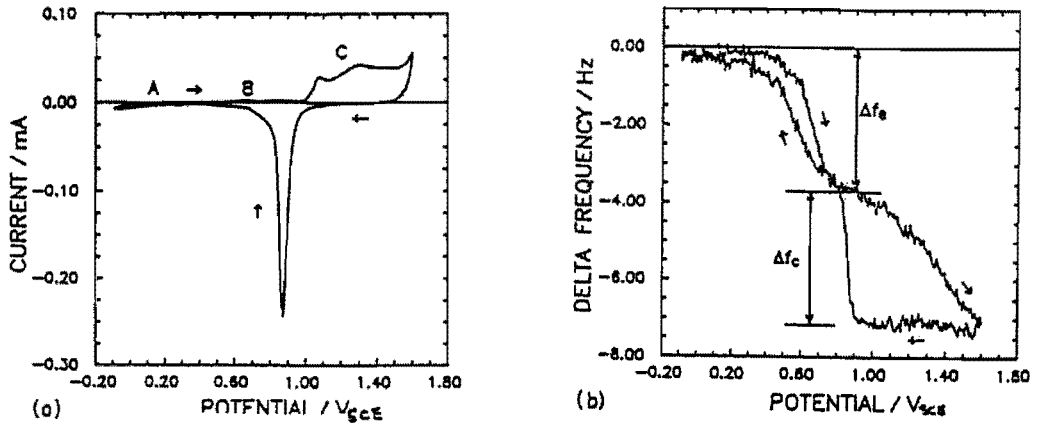

Figure 2.3. (a) Current-potential curve for Au EQCM film in 0.1 M $HClO_4$: scan rate 75 mV/s; no convective mixing. (b) Frequency-potential curve for Au EQCM film in 0.1 M $HClO_4$: scan rate 75 mV/s; no convective mixing. Obtained concomitant with I-E curve (Gordon and Johnson, 1994).

Gordon and Johnson (1994) proposed that the large values obtained for Δf_B and Δf_C in regions B and C respectively are the result of increased surface hydration as a consequence of the formation of AuOH (region B) and the monolayer oxide (region C). The magnitude of the increase was found to be independent of the nature of the acid. The mass increase in region B is consistent with an increase in surface hydration by about 32 H_2O molecules per AuOH site.

2.3.2. Premonolayer oxidation of gold in base

The electrochemical response due to premonolayer oxidation of gold in alkaline solutions tends to be of higher magnitude than in acid; the hydroxy species involved is more stable in solutions of high OH^- ion activity. Small peaks have been observed in the double layer region of cyclic voltammograms for gold in base (Burke and O'Leary, 1989).

Desilvestro and Weaver (1986) established, using Surface Enhanced Raman Spectroscopy (SERS), that the product of premonolayer oxidation was a hydroxy species, one that was of different character to the species involved in the regular monolayer oxidation reaction.

2.4.The electro-oxidation of chemical compounds at gold electrodes in aqueous media

Gold is the noblest and most inert of all metals. It is also a very weak chemisorber due to the absence of vacancies in its d-bands. It does, however, display a very wide range of electro-oxidation activity - especially in base (Vitt et al., 1990; Burke and Nugent, 1998).

Typical cyclic voltammograms for the electro-oxidation of formaldehyde, hydrazine, and ethylene glycol are shown in Figure 2.4 (Burke and Nugent, 1998). The following can be deduced from these cyclic voltammograms:

i. The electro-oxidation of chemical compounds commences in the premonolayer region during the positive sweep. As soon as monolayer oxidation starts, oxidation of the compound is inhibited.
ii. During the negative sweep, oxidation of the compound starts again as soon as the monolayer oxide has been reduced.
iii. In general, chemical compounds are oxidised at gold before the formation of a surface oxide layer, while oxygen is evolved at a gold surface after the formation of the oxide layer.

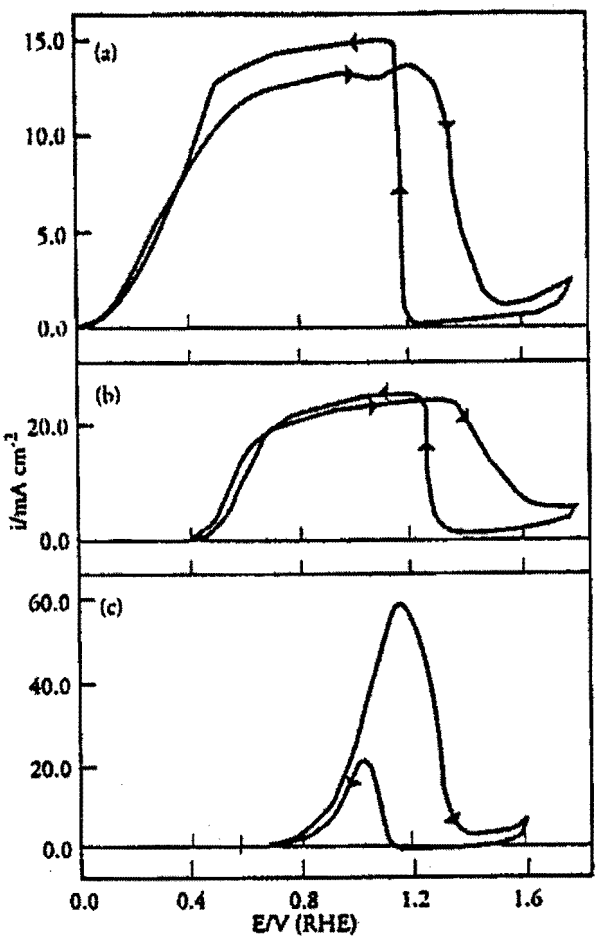

Figure 2.4. (a) Typical cyclic voltammogram (0 - 1.8 V, 5 mV/s) for a gold wire electrode in 1 mol/dm^3 NaOH with HCHO, to a level of 0.1 mol/dm^3, T = 25 ℃; (b) Typical cyclic voltammogram (0 - 1.8 V, 50 mV/s) for a smooth gold electrode in N_2-stirred 1 mol/dm^3 NaOH with N_2H_4, to a level of 0.1 mol/dm^3, T = 25 ℃; (c) Typical cyclic voltammogram (0 - 1.6 V, 50 mV/s) for a gold wire electrode in 1 mol/dm^3 NaOH with 0.1 mol/dm^3 ethylene glycol $(CH_2OH)_2$, T= 25 ℃ (Burke and Nugent, 1998).

2.4.1 Electro-oxidation by means of a submonolayer of adsorbed hydroxyl radicals

Electro-oxidation mechanisms have been proposed for oxidation at gold electrodes in acidic and alkaline solutions that involve adsorbed hydroxyl radicals (AuOH) (Vitt et al., 1990; Wen and Li, 1997). The adsorbed hydroxyl radicals are produced by means of the anodic discharge of H_2O in the premonolayer region (Vitt and Johnson, 1992).

$$H_2O \rightarrow {}^{\bullet}OH_{ads} + H^+ + e^- \qquad (1)$$

The formation of the submonolayer of hydroxyl radicals is favoured in alkaline solutions, which explains the rather poor electro-oxidation properties of gold in acidic solutions. A mechanism has been proposed in which the adsorbed hydroxyl radicals participate in the oxygen-transfer step (Vitt et al., 1990). It has also been speculated that the AuOH species formed in the premonolayer region can assist in the adsorption of polar organic molecules. Oriented H_2O dipoles centred at catalytic AuOH sites may also influence the orientation of electro-active functional groups in reactants that must diffuse to these catalytic sites (Gordon and Johnson, 1994).

Vitt and co-workers (1990) proposed that adsorption is necessary for all compounds whose oxidation is accompanied by the transfer of oxygen via the electrode surface. A mechanism that involve three fundamental processes for the various adsorbed species has been devised for these anodic reactions:

(1) oxygen transfer between the electrolyte and adsorbed hydroxyl radical (AuOH)

(2) deprotonation and

(3) electron transfer.

The mechanisms for various compounds seem to differ only in the order of these three reactions. For organic compounds (alcohols and aldehydes), deprotonation precedes electron transfer.

2.5. Alloys of gold

Noble metal alloys have been studied for the electro-oxidation of organic compounds, and some alloys display better activity than the pure metals. Most of the alloys that

have been studied are based on platinum (Parsons and VanderNoot, 1988; Stelmach et al., 1994).

2.5.1. Electrochemical behaviour of pure platinum

2.5.1.1. Mechanism of oxide formation

The early modelling of the initial stages of surface oxidation on platinum (Kozlowska et al., 1973) lead to the conclusion that two distinguishable and successive stages were involved:

$Pt + H_2O \rightarrow Pt/OH + H^+ + e^-$ (I)

followed by:

$Pt/OH \rightarrow Pt/O + H^+ + e$ (II)

(potential range 1.1 to 1.4 V_{RHE}) also coupled with place-exchange, schematically represented by:

$Pt/O \rightarrow O/Pt.$ (III)

By using the electrochemical quartz-crystal nanobalance (EQCN) technique, Birss et al (1993) showed that the above two-step mechanism is inapplicable. The two-step mechanism would require a mass change of 17 g/mol electrons in step I and -1 g/mol electrons in step II. However, the anodic mass-response profile involves a continuous mass increase, contrary to the expectations according to mechanism I, II. It actually corresponds to the first stage (to 1.1 V_{RHE}) of oxide film development being formed as Pt/O, first to half-coverage by O-species up to 1.1 V_{RHE}. This is followed by completion of coverage by O-species up to 1.4 V_{RHE} coupled with place exchange between O and Pt (step III).

Thus, platinum surface oxide formation is believed to preferably involve discharge of water molecules directly forming 'PtO' species, process IV:

$Pt + H_2O \rightarrow Pt/O + 2H^+ + 2e^-$ (IV)

where the H_2O reagent is initially present at a platinum site in the inner region of the double-layer, i.e. residing at the metal surface. As the electrosorption of O species in process IV progresses, water molecules consumed in (IV) are replaced from the double-layer and appear on the surface of the developing oxide film, probably H-bonded to it.

The mechanism of platinum oxide formation is shown schematically in Figure 3.1 (Zolfaghari et al., 2002). The above mechanism has to include the anticipated participation of adsorbed H_2O molecules which, initially, are presumed to fully cover Pt sites (Fig. 2.5a). It is believed that the H_2O molecules are bridge-coordinated to two adjacent Pt atoms. The second step in the diagram (Fig. 2.5b) shows half coverage by O at 1.1 V_{RHE}. The third step in the diagram (Fig. 2.5c and 2.5d) illustrates how a nominally complete O monolayer on platinum eventually becomes developed through place-exchange between O and Pt over the two outer layers of the original platinum structure.

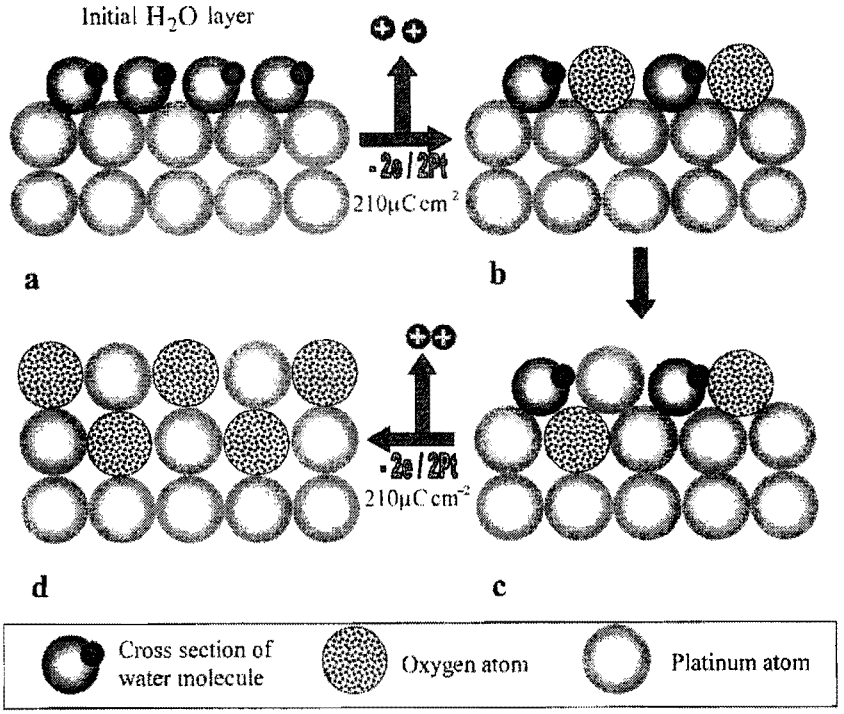

Figure 2.5. Cross-section of (a) initial water layer; (b) adsorbed O and H_2O; (c) adsorbed H_2O and place-exchanged O; (d) surface oxide (Zolfaghari et al., 2002).

A similar model of initial, two-electron oxidation of the platinum surface has also been proposed by Harrington and co-workers (1997) in their simulation of ac voltammetry behaviour over the region of Pt oxide-film formation. It was found that the shape of the ac voltammograms does not change much with frequency, suggesting a single time constant for oxide growth. No features were seen in the early stages of growth that can be assigned to the fast OH electrosorption, suggested previously to be the first step in oxide growth.

It was also suggested that although this mechanism is ruled out, some types of fast OH adsorption are still possible. Adsorption without charge transfer could be occurring. If OH electrosorption occurs in parallel with the slow oxide growth process, it might not be detectable by ac impedance. The admittances of the two processes would then be additive and a small admittance for OH electrosorption might contribute little to the total.

2.5.1.2. Electrochemical behaviour of platinum in alkaline solutions

Figure 2.6 (solid line) (Xia and Birss, 2000) shows a typical cyclic voltammogram of a Pt-coated quartz crystal in 0.1 M NaOH, as well as the associated frequency change (dashed line, inverse of mass change), measured during an oxidation/reduction scan between 0 and 1.6 V_{RHE}. In this range of potential the compact α-oxide film is formed (at ca. 0.6 V_{RHE}) and reduced, in peak C_1. The adsorption/desorption of a monolayer of hydrogen atoms is seen between 0.1 V and 0.4 V_{RHE}.

In Figure 2.6, a mass increase is seen, as expected, during Pt oxide formation, while oxide reduction is accompanied by an equivalent mass loss. From the integrated charge density during oxide reduction and the associated change in mass over the potential range of the cathodic peak, a ratio of 8.3g/mol e^- passed is obtained. A ratio of 8 g/mol electrons would be predicted for the formation of an anhydrous Pt oxide film, either PtO or PtO_2.

In the potential range of the hydrogen adsorption-desorption reaction it can be seen that as the potential is made more negative and hydrogen begins to adsorb, the electrode mass decreases, rather than increases, and vice versa during the positive scan. When hydrogen evolution commences in the negative scan, i.e. at 0.1 V_{RHE}, the frequency drops somewhat and then increases again in the positive scan. It is likely that the mass change between 0.15 and 0.4 V is due to the desorption of OH^- in the cathodic scan and its readsorption during the positive scan. The results of Figure 2.6 suggest that, during hydrogen atom adsorption on Pt (0.4-0.15 V_{RHE}), adsorbed hydroxide is concurrently being desorbed, then readsorbing again in the anodic sweep.

QCMB experiments involving α-oxide growth in 0.1 M NaOH with time at constant potentials were carried out by Xia and Birss (2000). Figure 2.7(a, b) (Xia and Birss, 2000) show both the oxide reduction charge density (per apparent area) and its g/mol e^-

ratio as a function of anodising time at two potentials: 1.3 and 1.6 V_{RHE} respectively. In both cases, the oxide reduction charge increases logarithmically with anodising time, reaching a near steady-state value after ca. 6 min (Fig. 2.7a) and 4 min (Fig. 2.8b).

Figure 2.7a shows that the mass to charge ratio for the oxide formed after very short times of anodising at 1.3 V_{RHE} is almost 9 g/mol electrons. While a ratio of 8 is expected for either PtO or PtO_2, this slightly higher value may indicate that the initial layer may have included some adsorbed OH^-, or the formation of a small amount of PtOH or $Pt(OH)_2$ (expected ratio for both is 17g/mol e^-). After 1 min of anodising at either 1.3 or 1.6 V, Figure 2.7(a,b) show similar ratios for the oxide film of 7.9 to 8.1 g/mol e^-, the expected values for PtO or PtO_2. Unfortunately, the form of Pt oxide cannot be distinguished from the QCMB data.

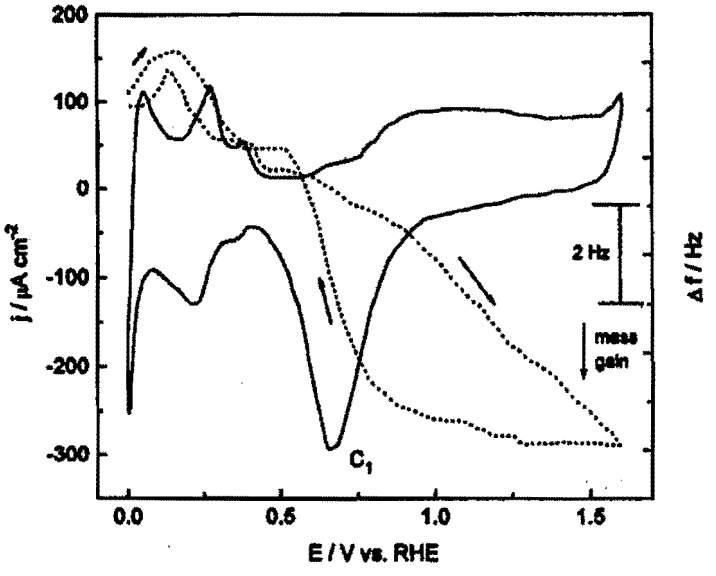

Figure 2.6. Cyclic voltammogram (solid line) and associated frequency change (dotted line) of a Pt-coated quartz crystal in 0.1 M NaOH between 0 and 1.6 V_{RHE} at 50mV/s (Xia and Birss, 2000).

Figure 2.8 (Xia and Birss, 2000) shows a plot of both the oxide reduction charge and the g/mol e^- ratios, monitored after 5 min at each of the anodising potentials between 1.2 and 1.9 V_{RHE}. The plot of the reduction charges appears to have two apparently linear segments, one for potentials less than 1.6 V, and one for potentials above this.

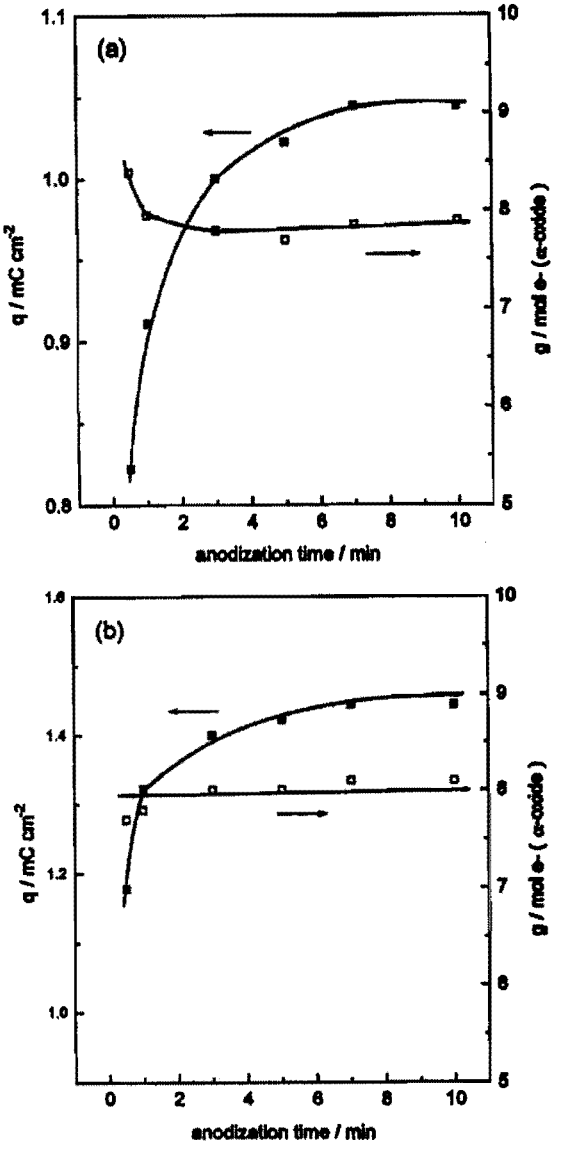

Figure 2.7: α-oxide reduction charge density (solid symbols) at 10 mV/s and its g/mol e$^-$ ratio (open symbols) as a function of anodisation time of Pt-coated quartz crystal at (a) 1.3 V_{RHE} and (b) 1.6 V_{RHE} in 0.1 M NaOH (Xia and Birss, 2000).

Ellipsometric data (Xia and Birss, 2000) also indicates that the platinum oxide films, formed using potentials below 1.6 V_{RHE}, have different optical properties from those formed at potentials above 1.6 V_{RHE}. However, for all upper potential limits, except 1.2 V_{RHE}, the g/mol e^- ratio remains 8. These results has been interpreted as indicating that the oxide formed over the range 1.3 to 1.6 V_{RHE} is PtO, then changing to PtO_2 when the applied potential becomes higher than 1.6 V_{RHE}.

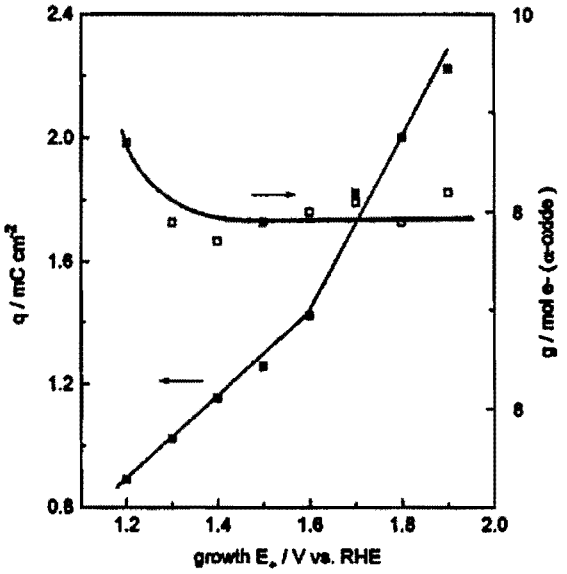

Figure 2.8. α-oxide reduction charge density (solid symbols) at 10 mV/s and its g/mol e^- ratio (open symbols) as a function of applied potential, after 5 minutes of anodisation of Pt-coated quartz crystal in 0.1 M NaOH (Xia and Birss, 2000).

2.5.1.3. Electrochemical behaviour of platinum in acid solutions

Figure 2.9 (solid curve) (Birss et al., 1993) shows a typical cyclic voltammogram of a Pt-coated quartz crystal in 0.1 M H_2SO_4, as well as the associated mass changes (broken curve) measured during the experiment. A mass increase is seen, as expected, during Pt-oxide formation, while oxide reduction is marked by mass loss. From the integrated charge density during α-oxide reduction and the associated change in frequency over the potential range of the cathodic peak, a ratio of ca. 8 g/mol of electrons passed is obtained. This is similar to what was found for the oxide formed in alkaline solutions and suggests again that the α-oxide is anhydrous in nature (either PtO or PtO_2). However, ellipsometric data indicates that the platinum oxide film formed potentiostatically and by multicycling in 0.1 M H_2SO_4 has different optical properties than either of the two α-oxide films formed in base.

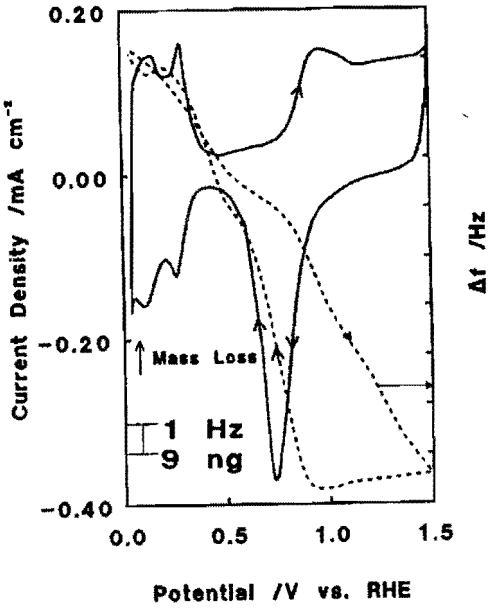

Figure 2.9. Cyclic voltammogram (solid line) and associated frequency change (dotted line) of a Pt coated quartz crystal in 0.1 M H_2SO_4; scanning rate 50 mV/s (Birss et al., 1993)

2.6. Gold-platinum alloys

The gold-platinum system has a miscibility gap (Figure 2.10) in the solid solution field (ASM Handbook, Volume 3: Alloy Phase Diagrams, 1992). The Pt-rich phase is frequently denoted as the α_1 phase and the Au-rich phase as α_2.

There was interest in gold-platinum alloys during the 1950's and 1960's when they were used as spinning jets in the viscose rayon process (Darling, 1962).

2.6.1. Cold rolling of Au-Pt alloys

The whole range of alloys can be cold worked after quenching from temperatures not higher than 1000°C. The most ductile material is achieved by annealing at 1000°C, after which the temperature can be slowly dropped before water-quenching from 850°C (Darling, 1962).

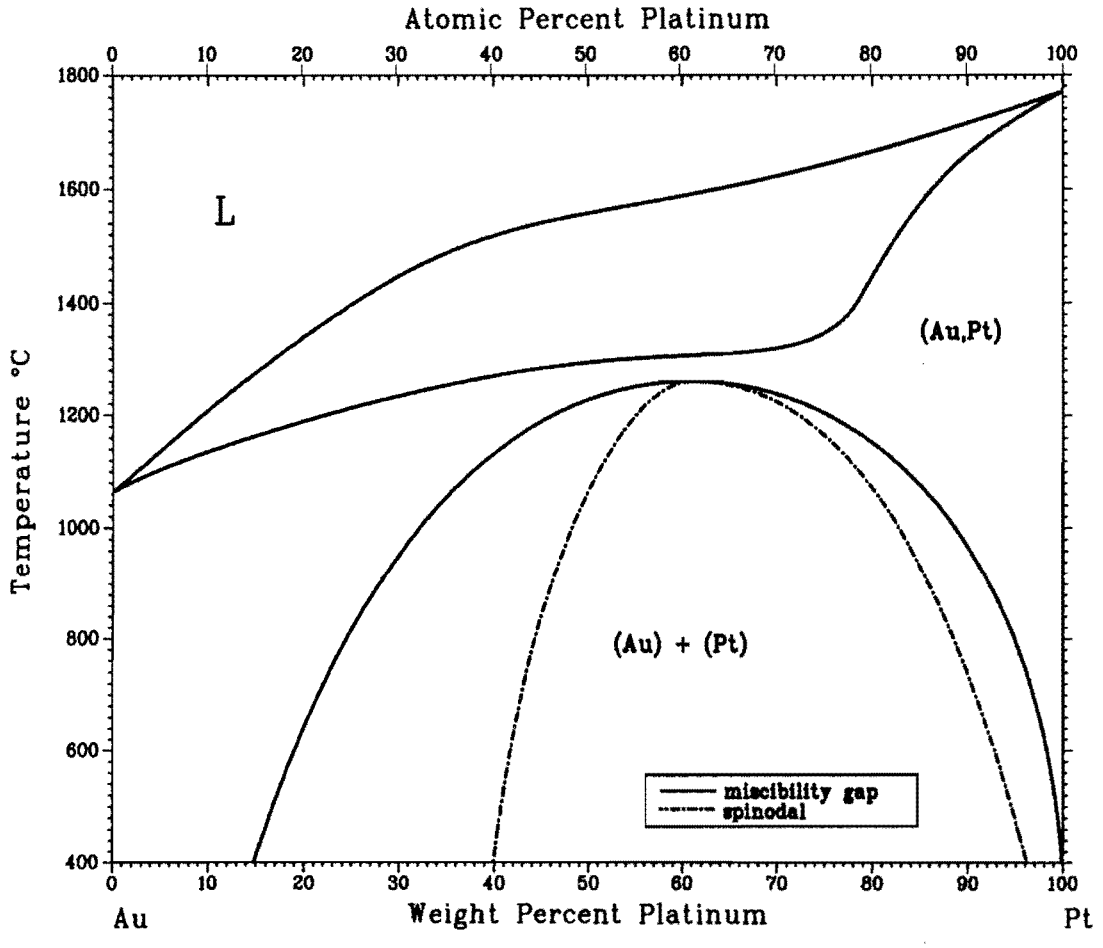

Figure 2.10. The Au-Pt phase diagram (ASM Handbook, Volume 3: Alloy Phase Diagrams, 1992)

2.6.2. Precipitation in Au-Pt alloys

The rate of precipitation depends upon the curvature of the free energy composition curves. The spinodal (Figure 2.10), being the locus of the inflexion points of the isothermal free energy composition curves, forms a lower limit of metastable equilibrium. Between the spinodal and the two-phase field exists a thermodynamic potential barrier that must be overcome before nucleation can occur, with the result that precipitation is retarded in this area (Darling, 1962).

2.6.3. Electrochemical behaviour of Au-Pt alloys

2.6.3.1. Homogeneous alloys

Woods (1971) studied the surface composition of Pt-Au alloys quenched from the region of continuous solid solution. Even though x-ray diffraction indicated that the alloys were homogeneous, the alloy electrodes gave current-potential curves (1 M H_2SO_4) that were equivalent to the sum of a pure platinum and a pure gold surface (Figure 2.11 (Woods. 1971)). It was suggested that this result can be explained if either:

1. Platinum and gold atoms in a homogeneous alloy have hydrogen and oxygen electrosorption properties equal to that of platinum and gold atoms in the pure metals or
2. The surface of platinum/gold alloys always consists of the equilibrium phases even though the bulk is homogeneous.

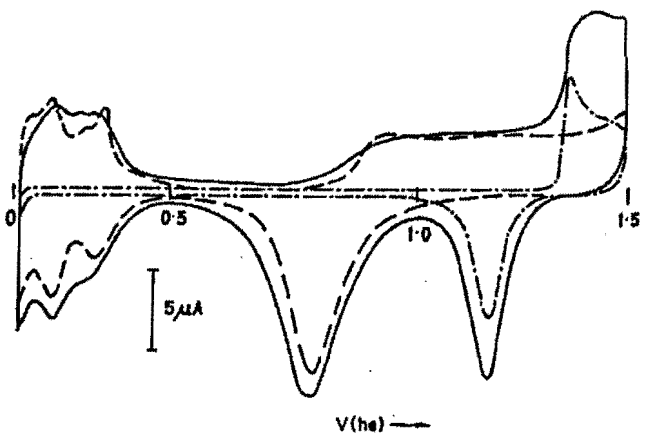

Figure 2.11. Current-potential curves showing hydrogen and oxygen adsorption in 1 M H_2SO_4 for a linear potential sweep of 40 mV/s. (-----) Pt; (-.-.-) Au and (____) homogeneous 65%Pt-35%Au alloy (Woods, 1971).

2.6.3.2. Heterogeneous alloys

Breiter (1965) studied the anodic formation and cathodic reduction of oxygen layers on Au-Pt alloys in acid solutions. Platinum-gold alloys with gold contents ranging from 5 to 70 at% were studied. The alloys had to be annealed at 875°C before wires of 0.3 mm

diameter could be drawn. Heterogeneous (two-phased) Au-Pt alloys were produced with this heat treatment (Fig. 2.10). Current-potential curves were measured in 1 N H_2SO_4 at a sweep rate of 30 mV/s. The current-potential curves of the 20, 40 and 60at% Au alloys are shown in Figure 2.12 (Breiter, 1965). The most notable feature of Figure 2.12 is the fact that the alloys have two reduction waves. The first wave between 1.4 and 1.0 V_{SHE} is attributed to the reduction of the oxygen layer on "gold" and the second one between 1.0 V and 0.6 V_{SHE} to that of the layer on "platinum". "Gold" is designated as being either gold atoms or the gold-rich phase of the heterogeneous alloys, while "platinum" is designated as being either platinum atoms or the platinum-rich phase of the alloys. The first reduction wave increased in height with increasing gold content while the second decreased (Fig. 2.12). The peaks of the two reduction waves appeared at slightly less anodic potentials on the alloys than on the respective pure metals. This indicates that the reduction of the oxygen layer on the two phases occurs with slightly larger hindrance than on the pure metals.

2.6.4. Electro-oxidation of chemical compounds at Au-Pt alloy electrodes

In alkaline media, the electro-oxidation activity of Au-Pt alloy electrodes is enhanced when compared with the respective metals (Stelmach et al., 1994; Beden et al., 1982). There are a few possible explanations for this synergistic effect of gold-platinum alloys.

2.6.5. Possible explanations for synergism on Au-Pt alloys

2.6.5.1. The bifunctional theory

The idea is that surface gold atoms adsorb oxygen-containing species, while surface platinum atoms adsorb the organic compound. The two different species interact leading to a final product. The two sites together give the complete reaction unit (Parsons and VanderNoot, 1988).

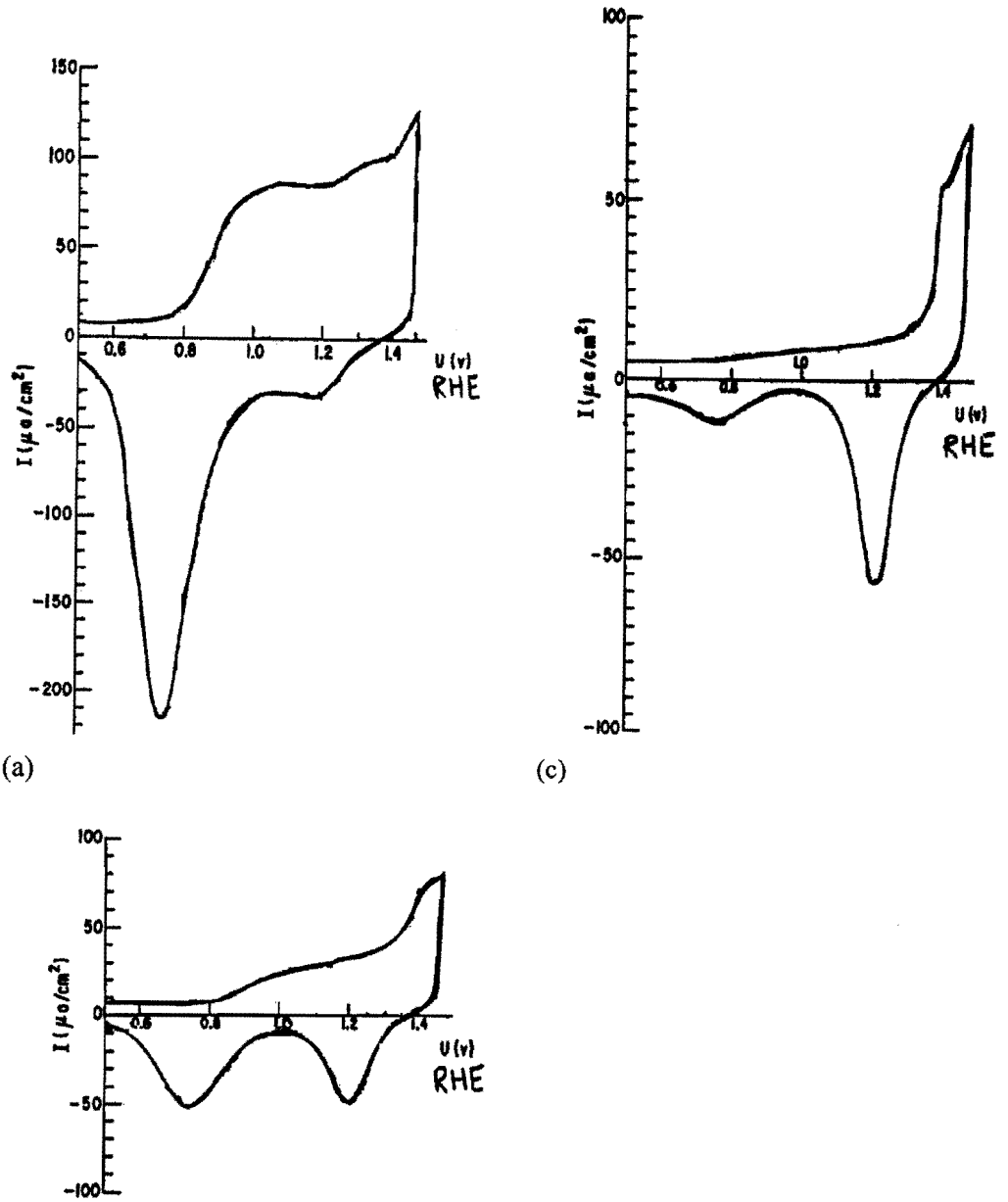

Figure 2.12. Current-potential curves for heterogeneous Au-Pt alloys containing (a) 20%, (b) 40% and (c) 60% Au in 1 N H_2SO_4. Sweep rate 30 mV/s (Breiter, 1965).

2.6.5.2. Changes in adsorption features

Stelmach and co-workers (1994) found an increased rate of electro-oxidation of formaldehyde at alloy electrodes in comparison with the respective pure metals. They proposed that the energy of adsorption for the various forms of the substrate molecule is decreased sufficiently in order to facilitate further oxidative desorption of

intermediates and to suppress the adsorption of strongly bound intermediates. The adsorptivity of the surface remains high enough to support electro-oxidation.

2.6.5.3. The Third-Body effect

The formation of poisonous species adsorbed on more than one surface site is suppressed. For the electro-oxidation of formic acid, it was found that a platinum atom that is surrounded by gold atoms has the highest activity. A single platinum atom cannot be "poisoned" by the strongly bound intermediate since it needs adsorption sites that are only available on larger platinum clusters (Rach and Heitbaum, 1987).

2.6.5.4. The creation of Lewis acid surface sites on alloy electrodes

It is thought that the introduction of an alloying element that has a d-orbital occupancy less than that of the matrix will result in surface states at the alloy that function as Lewis acid sites. Furthermore, it is speculated that these surface sites enable adsorption of reactant species that are Lewis bases because of the existence of non-bonded electron pairs in these compounds e.g. the O-atoms in hydroxyl moieties of alcohols and carbohydrates, and N-atoms in amino acids (Mho and Johnson, 2001). This speculation is supported by successful modelling of the variations in the half-wave potential of the anodic voltammetric wave for dimethyl sulfoxide at β-PbO_2 film electrodes as a function of the variation in the level of doping by Bi (Popovic et al., 1998). The electrocatalytic benefit of reactant adsorption is explained on the basis of increase in residence time for the reactant species within the applied electric field at the electrode/solution interface.

Mho and Johnson (2001) studied the electrocatalytic response of carbohydrates at Cu-Mn alloy electrodes. The occupancy of the outermost d-orbital is lower for Mn ($3d^5$) than that of Cu ($3d^{10}$). The alloy composition of Cu:Mn = 95:5 was chosen to correspond to a homogeneous solid solution. The voltammetric responses observed for carbohydrates in 0.10 M NaOH were significantly larger at the preanodised CuMn electrodes as compared to preanodised pure Cu electrodes. It is speculated that the observed electrocatalytic effect comes as a beneficial consequence of the preadsorption of the carbohydrates at Mn sites (Lewis acid) in the preanodised CuMn surface.

Lewis acid surface sites will also be formed at gold-platinum alloys. The electron configuration of gold is $[Xe]4f^{14}5d^{10}6s^{1}$ and the electron configuration for platinum is $[Xe]4f^{14}5d^{9}6s^{1}$.

2.7. The 60Au-40Pt alloy electrode

The Au-Pt alloy containing 60wt% Au has been identified previously (Stelmach et al., 1994) as the most active for the oxidation of aliphatic alcohols (Beltowska-Brzezinska, 1979), ethylene glycol (Eggert (Stelmach, 1994)) and formaldehyde (Beltowska-Brezezinska and Heitbaum, 1985) in alkaline media.

However, from the Au-Pt phase diagram (Fig. 2.10), it can be seen that different heat treatment temperatures can be used to produce different amounts of the α_1 and α_2 phases. The compositions of the two phases can also be changed by employing different heat treatment temperatures.

For the 60Au-40Pt alloy, annealing at 1100-1260°C will produce a homogeneous solid solution. Heat treatments at temperatures lower than 1100°C will produce a heterogeneous two-phased microstructure (Fig. 2.10). The different weight fractions of α_1 and α_2, and their composition as a function of heat treatment temperature are shown in Table 2.1 for the 60Au-40Pt alloy. The lever rule was applied in order to calculate the various weight fractions.

Table 2.1: Equilibrium weight fractions and composition of phases in a 60wt% Au-40wt% Pt alloy as functions of temperature.

Temp. (°C)	Weight fraction of α_1	Composition of α_1		Weight fraction α_2	Composition of α_2	
		Wt% Au	Wt% Pt		Wt% Au	Wt% Pt
1000	0.13	12	88	0.87	68	32
800	0.21	5	95	0.79	75	25
600	0.26	2	98	0.74	81	19
400	0.30	0	100	0.70	85	15

It will be interesting to study the electrochemical behaviour of the 60Au-40Pt alloy in different heat treatment conditions. The electro-oxidation of an organic compound, such as ethylene glycol, can be used to determine the effect of microstructure on the electrochemical properties of the alloy.

2.8. The electro-oxidation of ethylene glycol at noble metal electrodes

Ethylene glycol, $(CH_2OH)_2$, is a non-toxic diol-alcohol. It has the advantage of involving a large number of electrons per molecule in its oxidation (the oxidation reaction needs 8 electrons per molecule when the final product is oxalate (Hauffe and Heitbaum, 1978)). The electro-oxidation of ethylene glycol at noble metal electrodes has been studied extensively, due to the interest of using it as a fuel for alcohol fuel cells (Christensen and Hamnett, 1989; Kadirgan et al., 1990; Beden et al., 1982, Hahn et al., 1987).

2.8.1. The electro-oxidation of ethylene glycol at gold electrodes in acid

The cyclic voltammogram for the electro-oxidation of ethylene glycol at a gold electrode in acid is show in Figure 2.13 (Beden et al., 1987). It can clearly be seen from Figure 2.13 that nearly no oxidation of ethylene glycol occurs at gold in acid.

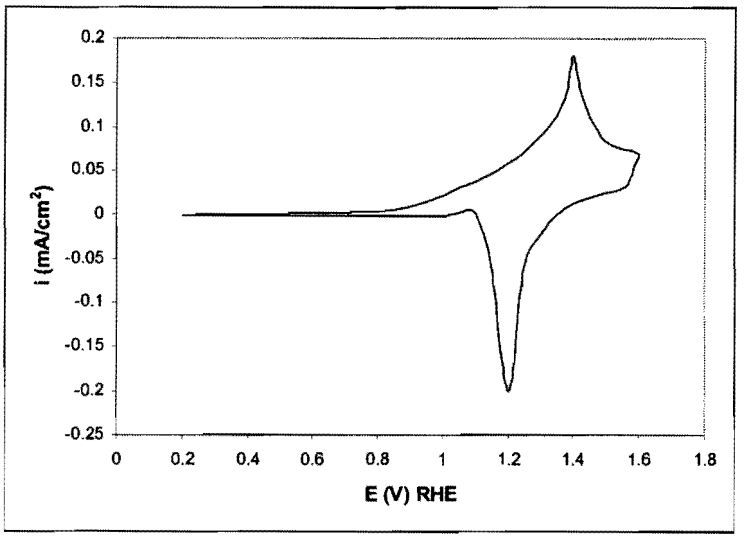

Figure 2.13. Oxidation of ethylene glycol at a gold electrode in acid medium. Conditions: 0.1 M $HClO_4$, 0.1 M ethylene glycol, 25°C, 50 mV/s (After Beden et al., 1987).

2.8.2. The electro-oxidation of ethylene glycol at gold electrodes in base

A cyclic voltammogram for the electro-oxidation of ethylene glycol at a gold electrode in base is show in Figure 2.14, together with the voltammogram of gold in the supporting electrolyte alone (Kadirgan et al., 1990). Ethylene glycol oxidation starts at 0.8 V_{RHE} during the positive sweep, giving a peak of 12 mA/cm^2 at approximately 1.2 V_{RHE} (peak A). The electro-oxidation of ethylene glycol is inhibited by the formation of the surface oxide on the gold electrode. During the negative sweep, oxidation of ethylene glycol commences only after the surface gold oxide has been reduced, reaching a current maximum of about 4 mA/cm^2 at 1 V_{RHE} (peak B). The positive and negative potential scans are almost superimposed in the potential range from 0.8 to 1 V_{RHE}. Hauffe and Heitbaum (1978) found that the peak currents (peaks A and B) are somewhat smaller when the solution is stirred with argon gas. This can be explained by an accelerated transportation of intermediates into the solution.

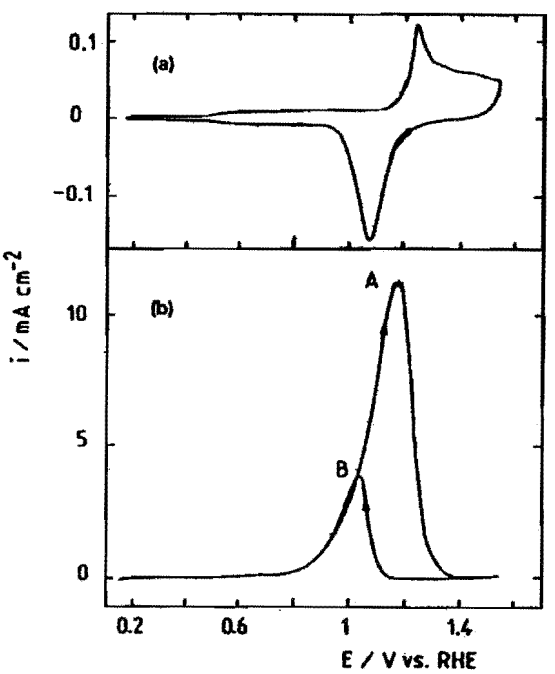

Figure 2.14. Cyclic voltammograms of a gold bead electrode (0.1 M NaOH, 25°C, 50 mV/s. (a) Without ethylene glycol; (b) with 0.1 M ethylene glycol (Kadirgan et al., 1990).

It is not possible to sustain long electrolysis of ethylene glycol at a fixed potential, because of poisoning phenomena that occurs at the electrode surface (Kadirgan et al., 1990). A cleaning procedure has to be used for sustainable electrolysis. The simplest technique is to use potential programs with potential plateaux separated repeatedly by a single cleaning potential sweep. The electrode surface and the poisons are oxidised at the upper potential limit. The surface oxides are reduced at the lower potential limit, before returning to the potential plateaux. The major product of electrolysis at 1.13 V_{RHE} is glycolate. Small quantities of oxalate, carbonate and formate are also formed (Kadirgan et al., 1990).

Kadirgan and co-workers (1990) used electromodulated infrared reflectance spectroscopy (EMIRS) to check for the presence of adsorbed CO-type poisons. These CO poisons would be formed by the rupture of the C-C bond during chemisorption at negative potentials. It was found the CO band is not present initially and that it grows during spectral accumulation performed to improve signal to noise ratio. However, the CO band is far from being the main infrared band observed. This implies that ethylene glycol does not dissociate immediately on gold at low potentials and that the CO poisoning species are formed only progressively. Glycolaldehyde and glyoxalate were found to be the main adsorbed species.

2.8.3. The electro-oxidation of ethylene glycol at platinum electrodes in acid

A cyclic voltammogram for the electro-oxidation of 0.1 M ethylene glycol in 0.1 M $HClO_4$ is shown in Figure 2.15 (Hahn et al., 1987). Several peaks and shoulders, labelled A to D are found.

Inhibition of hydrogen adsorption in the hydrogen region occurs due to adsorption of ethylene glycol. Electrochemically Modulated Infrared Reflectance Spectroscopy (EMIRS) was used by Hahn et al (1987) to study the adsorption of ethylene glycol. It was found that the adsorption is dissociative, leading to the formation of a poisoning linearly bonded CO species. Oxidation of the CO starts at 0.6 V_{RHE}, at the same potential where the overall oxidation process of ethylene glycol begins (Fig. 2.15).

By using in situ FTIR spectroscopy, Christensen and Hamnett (1989) identified the main products of ethylene glycol oxidation in acid as glycolic acid and CO_2.

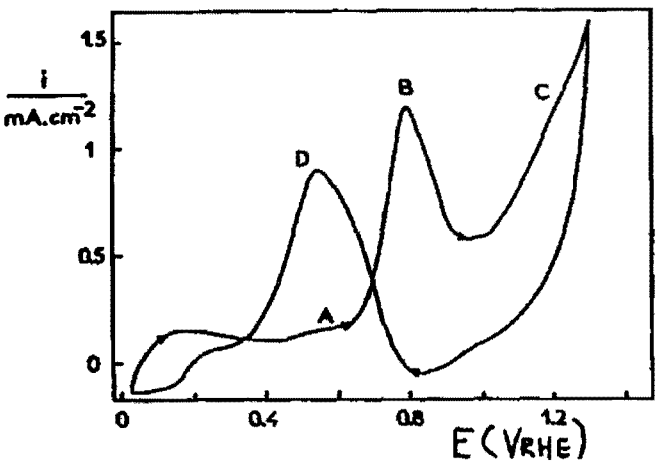

Figure 2.15. Cyclic voltammogram for the oxidation of 0.1 M ethylene glycol in 0.1 M $HClO_4$, on platinum. Conditions: 100 mV/s, 25°C (Hahn et al., 1987).

2.8.4. The electro-oxidation of ethylene glycol at platinum electrodes in base

Cyclic voltammograms of a platinum electrode in 1 M NaOH in the absence and in the presence of 0.1 M ethylene glycol are shown in Figure 2.16 (Kadirgan et al., 1983). Ethylene glycol oxidation begins at 0.35 V_{RHE} during the positive sweep, giving a steep rise A at 0.65 V_{RHE}, then a peak B of 6.6 mA/cm^2 at 0.73 V_{RHE} and a small peak C at 1.05 V_{RHE}. The decrease of current after peak B is related to the formation of surface oxides on the platinum electrode. Ethylene glycol oxidation takes place during the negative sweep after the reduction of the surface oxides, reaching a maximum rate of 2 mA/cm^2 at 0.63 V_{RHE} (peak D). The current densities obtained in alkaline solution are much higher than in acid solution (Figure 2.15). The oxidation process also appears to be less irreversible in alkaline than in acid medium, in which the main oxidation peaks of ethylene glycol are separated by more than 250 mV during the positive and negative sweeps (Fig. 2.15).

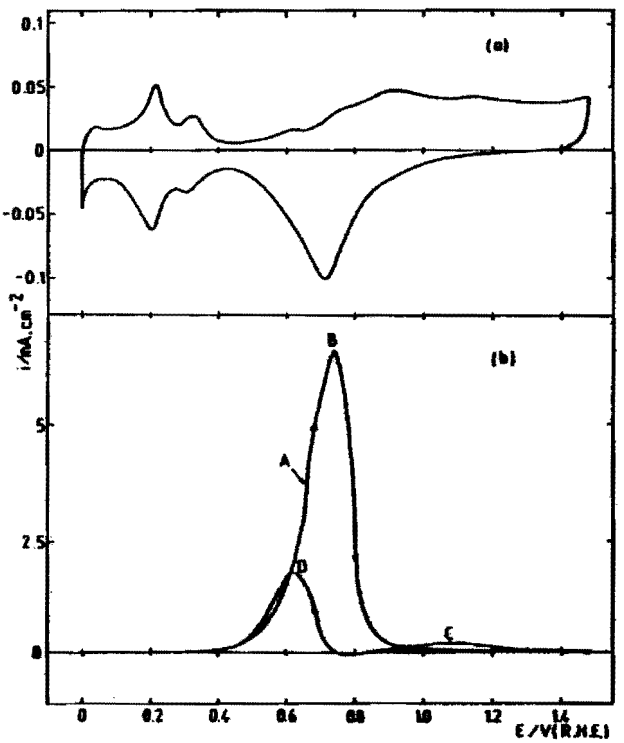

Figure 2.16. Cyclic voltammograms of a Pt bead electrode (1 M NaOH, 25°C, 50 mV/s): (a) without ethylene glycol; (b) with 0.1 M ethylene glycol (Kadirgan et al., 1983).

Electrochemically Modulated Infrared Reflectance Spectroscopy (EMIRS) was used by Hahn et al (1987) to study the adsorption of ethylene glycol at platinum in alkaline solutions. The adsorption was found to be dissociative. However, almost equal amounts of bridge-bonded and linearly bonded CO species were found in alkaline solutions. This is in contrast to acidic solutions, where only linearly bonded CO species were found (Hahn et al., 1987). An important shift towards lower wavenumbers of the linearly-bonded CO band centre was observed when the pH was increased. This might be due to interactions with the solvent or with adsorbed OH species, and a decrease of the CO coverage. The adsorption of molecular ethylene glycol may also play a role. The drastic change in the CO coverage as a function of pH is most probably related to a change in the electrocatalytic activity of platinum towards the oxidation of ethylene glycol when changing from acid to alkaline solutions.

The main products of ethylene glycol oxidation in base at platinum are glycolate, oxalate and CO_3^{2-}, determined by in situ FTIR (Christensen and Hamnett, 1989).

2.8.5. The electro-oxidation of ethylene glycol at Au-Pt electrodes in base

The cyclic voltammograms for ethylene glycol oxidation in base at Au, Pt and a 50Au-50Pt alloy electrode are shown in Figure 2.17 (Beden et al., 1982). The Au-Pt alloy electrode was prepared by electrolytic codeposition of the two metals on a platinum bead. The alloy electrode was then annealed by warming it to red heat in a hydrogen flame. For the alloy electrode it can be seen that during the positive sweep, electro-oxidation of ethylene glycol occurs in two main peaks. The first peak is in the same potential range as pure platinum and the second peak corresponds to oxidation on pure gold. However, the current densities obtained with the alloy electrode are much higher than those on the pure metals. At the Pt-region, the electro-oxidation activity is enhanced eight times and at the Au-region two times.

The 60Au-40Pt alloy electrode has been found to be the most active for ethylene glycol oxidation (Eggert (Stelmach, 1994)). However, the effect of the heat treatment condition of this alloy (Table 3.1) on the electro-oxidation of ethylene glycol needs to be considered.

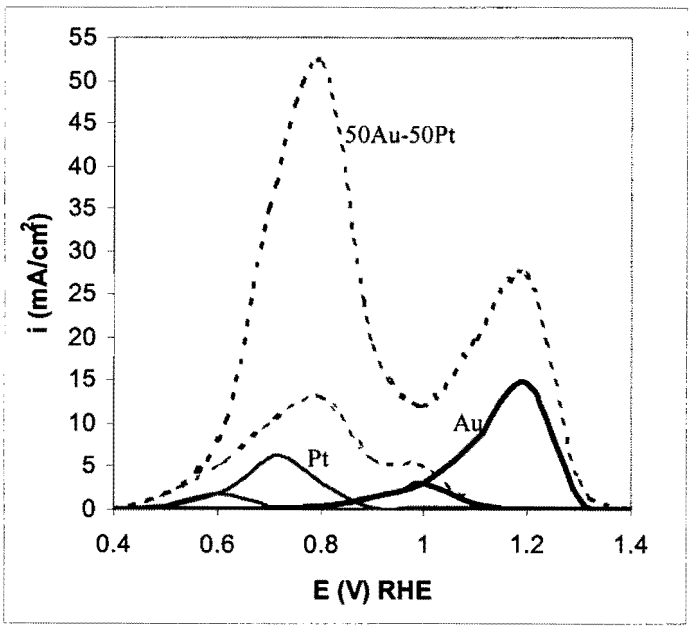

Figure 2.17. Cyclic voltammograms for ethylene glycol electro-oxidation in 1 M NaOH (0.1 M ethylene glycol, 25℃, 50 mV/s) on a platinum bead electrode, a gold bead electrode and a 50Au-50Pt alloy electrode (After Beden et al., 1982).

2.9. The Au-1wt% Ti alloy (Gold 990)

The Au-1wt% Ti alloy was originally developed to produce an alloy with at least 990 fineness, with colour close to that of pure gold and with durability as good as that of standard jewellery alloys (Gafner, 1989).

The addition of 1 wt% (4 at%) of titanium to gold substantially hardens the precious metal and enhances its wear resistance. The enhanced hardening is due to the formation of fine Au_4Ti precipitates under the appropriate thermo-mechanical treatments (The Au-Ti phase diagram (ASM Handbook, Volume 3: Alloy Phase Diagrams, 1992) is shown in Figure. 2.18). The addition of titanium to gold satisfies two important criteria for achieving optimum precipitation hardening:

1) It has a high solubility in gold at elevated temperature, which maximises its dissolution into gold.
2) The gold-titanium system has a shallow solvus curve towards pure gold, which enables a significant proportion of titanium to be retained in supersaturated solid solution on quenching. The Au_4Ti compound, which constitutes the strengthening precipitate, is substantially harder than the gold matrix and so gives rise to a substantial reinforcement.

2.9.1. Preparation of Gold 990

The alloy is prepared (Gafner, 1989) by melting together the constituents in a vacuum induction furnace, and casting the alloy into a suitable ingot. It is then precipitation hardened in two stages by first carrying out a solution heat-treatment, involving a heating stage at 800°C in air, or a vacuum or inert atmosphere, followed by quenching the ingot in water. Tests have shown that no significant loss of titanium occurs when solutionising is in air, because a protective surface layer forms. This brown layer can subsequently be removed mechanically or by dipping the alloy in a 10% $K_2S_2O_7$ solution in water. Precipitation hardening is accomplished by heating the alloy at a lower temperature, typically at 400-500°C, with or without an intermediate cold working stage.

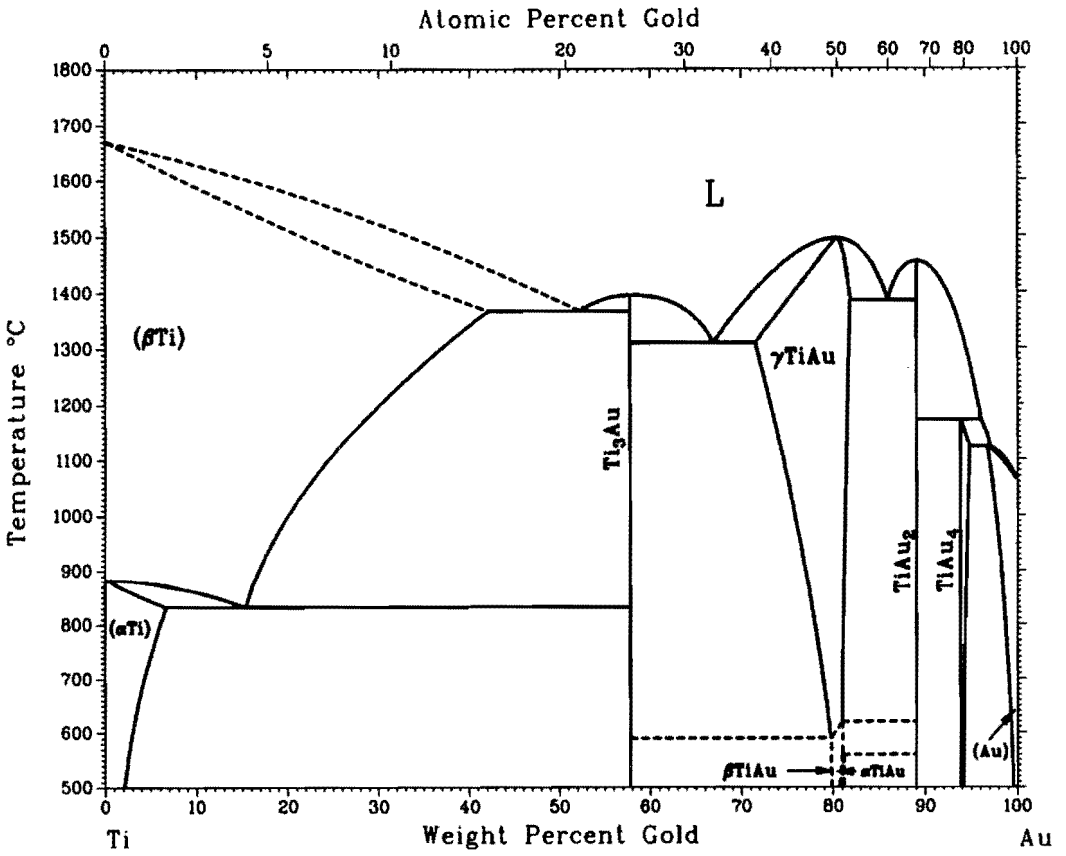

Figure 2.18. The Au-Ti phase diagram (ASM Handbook, Volume 3: Alloy Phase Diagrams, 1992).

It would be of interest to investigate the electrochemical properties of the alloy in two different heat treatment conditions (Fig. 2.18):

1) With titanium in solid solution.
2) In the precipitation-hardened condition (with Au_4Ti precipitates).

2.9.2. The electrochemical behaviour of pure titanium

Potentiodynamic polarisation curves for titanium in 0.5 M H_2SO_4 were measured at 303, 313 and 323 K by Shibata and Zhu (1995) and are shown in Figure 2.19.

An active-passive transition is found at around -0.49 $V_{Ag/AgCl}$. The critical current for passivation and the passive current increase with temperature. It is interesting that a second peak appears around 2.1 $V_{Ag/AgCl}$, which decreases with increase in temperature. The origin of this peak is still uncertain. According to Armstrong (1977) it could be due to a phase transformation of the originally formed oxide. The steady passive current was again reached beyond this second peak. A rapid current increase then

follows due to oxygen evolution. The oxygen evolution potential shifted in the negative direction with increase in temperature.

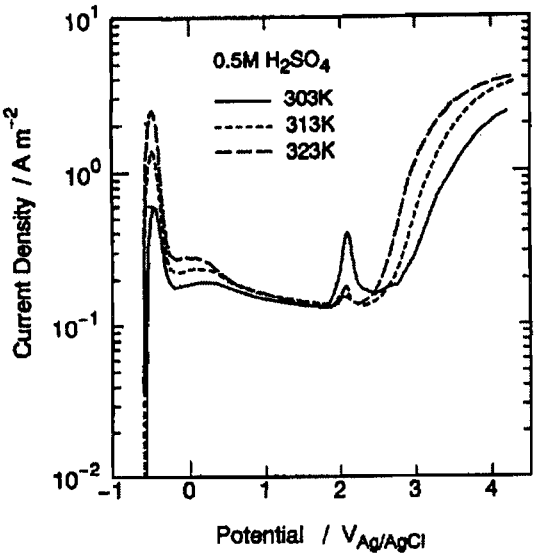

Figure 2.19. Anodic polarisation curves of Ti in 0.5 M H_2SO_4 solution at 303, 313 and 323 K (Shibata and Zhu, 1995).

The frequency and current responses as a function of the potential for titanium in 5 M H_2SO_4 are shown in Figure 2.20 (Herranen and Carlsson, 2001). As expected, the anodic current corresponding to dissolution of titanium is first accompanied by an increase in frequency (this corresponds to a decrease in mass). After reaching the passivation potential at –470 mV_{SCE}, with the corresponding critical current density (i_c), the current decreases as a result of oxide formation. However, the mass continues to decrease in the active-passive region. This indicates that the passive layer is not intact until a passive potential of about –150 mV_{SCE} is reached. An increase in mass is observed in the passive region. A second current density peak at 1.72 V_{SCE} was only found in 0.1 M H_2SO_4 - proposed to be due to a phase transformation of the oxide (Armstrong, 1977).

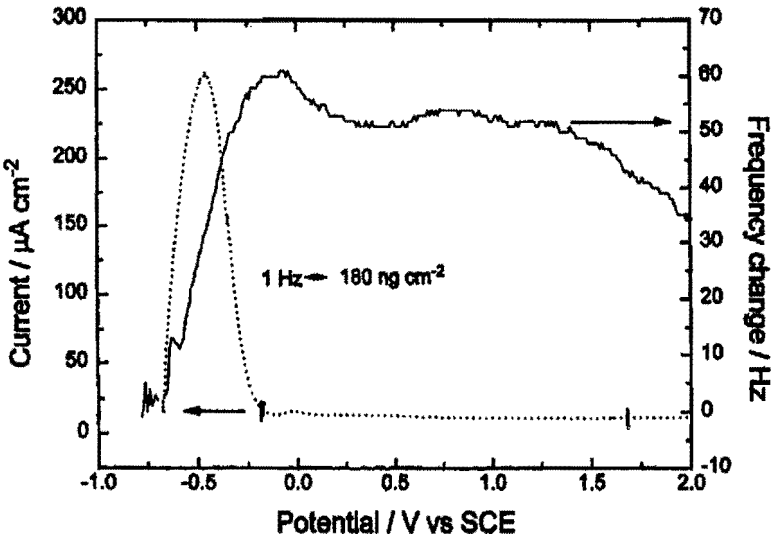

Figure 2.20. Current and frequency changes as functions of the potential of Ti in 5 M H_2SO_4 (Herranen and Carlsson, 2001).

A number of studies of the structure and composition of passive films on titanium have been reported. Armstrong (1977) studied the electrochemical behaviour of titanium films in 1 M $HClO_4$ and 0.5 M H_2SO_4 and characterised the surface oxide by XPS and AES. This indicated a mixture of metal oxides (TiO_2, Ti_2O_3 and TiO). Electrodes prepared at a larger anodic charge (potentials up to 2 V_{SCE}) showed more TiO_2 character.

Pure titanium is expected to be in the passive condition at the potentials applied for cyclic voltammetry of gold electrodes (0 – 1.8 V_{RHE} in acid and 0 – 1.6 V_{RHE} in base, Figures 2.1 and 2.2). This fact is also supported by the Pourbaix diagram for titanium shown in Figure 2.21 (Pourbaix, 1974).

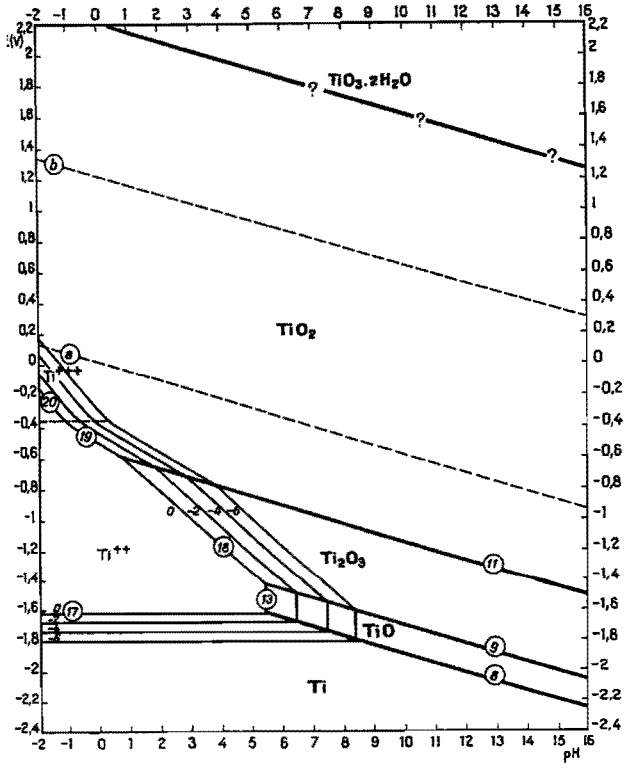

Figure 2.21: Potential – pH equilibrium diagram for the system titanium – water, at 25°C (Pourbaix, 1974).

2.10. Conclusions

- Even though gold is a weak chemisorber, it displays a wide range of electro-oxidation activity, especially in alkaline solutions.
- It is believed that organic compounds are oxidised at gold anodes in the presence of a submonolayer of adsorbed hydroxyl radicals (AuOH) before monolayer oxide formation.
- A bimetallic electrode is usually more active for the electro-oxidation of organics than the respective pure metals.
- The 60Au-40Pt alloy electrode has been identified in the literature as being the most active for the electro-oxidation of various organics in base. However, the effect of the microstructure of the alloy on its electrochemical properties has largely been ignored in the past.
- The electro-oxidation of ethylene glycol at noble metal electrodes has been studied extensively. This organic compound can therefore be used as a model compound to study the effect of heat treatment condition on the electrochemical properties of the gold alloys.

- The Gold 990 alloy was developed originally for the jewellery industry. The electrochemical properties of this alloy have not been studied before.

Chapter 3

THE HEAT TREATMENT OF Au-Pt ALLOYS AND THE GOLD 990 ALLOY

3.1. Introduction

The gold alloy containing 40% platinum has been identified (Stelmach et al., 1994) as being the most active for the oxidation of various organic compounds in alkaline solutions. However, the effect of the microstructure of gold-platinum alloys on their electrochemical properties has largely been ignored in the past. The purpose of this chapter is to discuss the microstructures of the 60Au-40Pt alloy obtained after different heat treatments. The spinodal decomposition reaction in the 50Au-50Pt alloy is also discussed.

The Gold 990 alloy (Au-1wt%Ti) is a precipitation-hardenable alloy. The different heat treatments of the Gold 990 alloy will also be reviewed in this chapter.

3.2. The 60Au-40Pt alloy

Gold and platinum (both 99.99%) were melted together (in the required ratio) in an arc-furnace with a water-cooled copper hearth under a protective argon atmosphere. The sample (approximately 10 g) was turned around after each melt and re-melted three times to ensure homogeneity.

3.2.1. The 60Au-40Pt alloy heat treated at 1300°C

The 1300°C heat treatment of the 60Au-40Pt alloy is shown schematically in Figure 3.1. Partial melting of the sample will occur at 1300°C. The liquid phase will be gold-rich with a composition of approximately 85Au-15Pt. The solid phase will be platinum-rich. The composition of this phase is difficult to estimate, due to the fact that the solidus line is almost horizontal at these temperatures. A small deviation from 1300°C will result in

large deviations in the composition of this phase. For the same reason, the lever rule cannot be used to accurately predict the amount of each phase that will be formed. However, the Pt-rich phase obtained by this heat treatment will have a higher gold content than the Pt-rich phases formed in the miscibility gap (Figure 3.1).

The sample was kept at 1300°C for 1 hour before quenching in water. After quenching, the sample was cold-rolled to a thickness of approximately 2 mm. A disk with a diameter of 6 mm was subsequently punched. The sample was mounted in a resin by using a black phenolic thermosetting powder. It was polished using diamond paste (6, 5 and finally 1 μm). The microstructure was studied by means of optical microscopy and scanning electron microscopy (SEM).

The microstructure of the 60Au-40Pt alloy after the 1300°C heat treatment is shown in Figure 3.2. Etching was not required to produce the microstructure shown in Figure 3.2. It can be seen that the Pt-rich areas formed by this heat treatment are relatively large, with typical diameters of 30 –50 μm (Figure 3.2).

Back-scattered electron imaging cannot be used to study the Au-rich and Pt-rich areas, because the atomic weights of gold and platinum are similar (196.97 and 195.08 g/mol respectively). However, the Au-rich and Pt-rich phases can be distinguished by elemental mapping using energy dispersive X-ray analysis in a scanning electron microscope.

An elemental map (using energy-dispersive X-ray analysis based on the L lines of the two metals) of the 60Au-40Pt alloy heat treated at 1300°C is shown in Figure 3.3. The elemental map confirms that optical microscopy without etching of the sample can be employed to study the microstructures of Au-Pt alloys (Compare Figures 3.2 and 3.3).

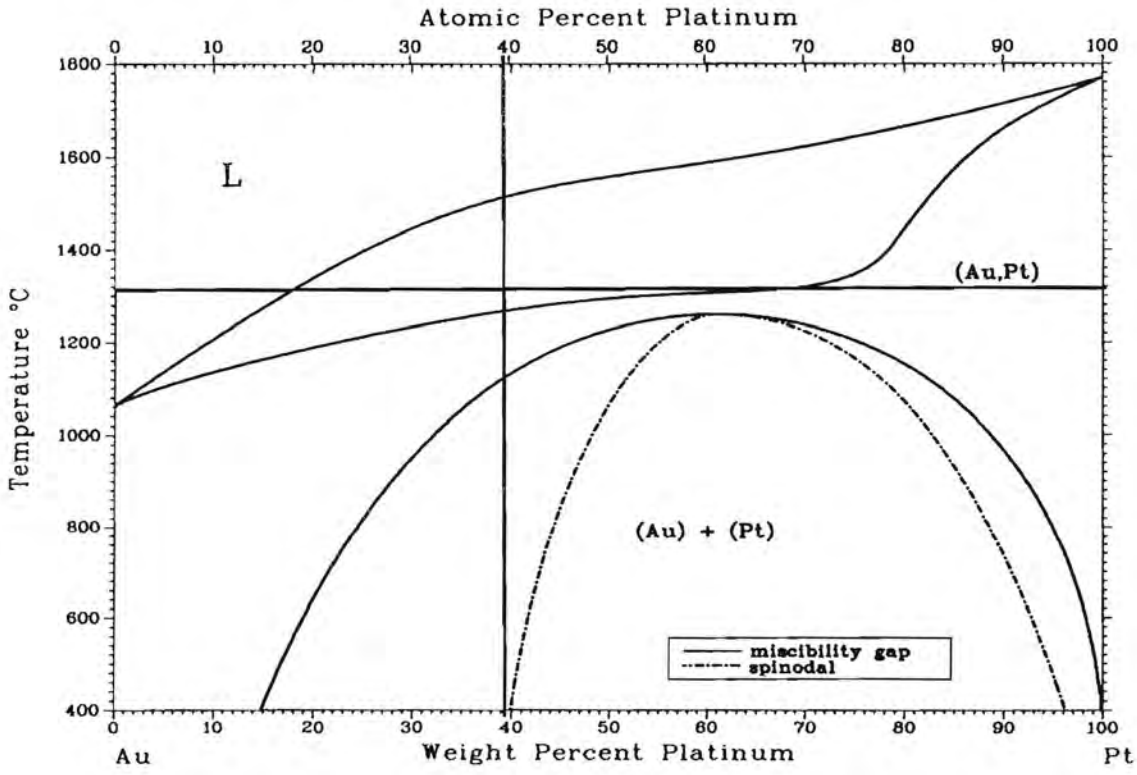

Figure 3.1. The 1300°C heat treatment of the 60Au-40Pt alloy (ASM Handbook, Volume 3: Alloy Phase Diagrams, 1992)

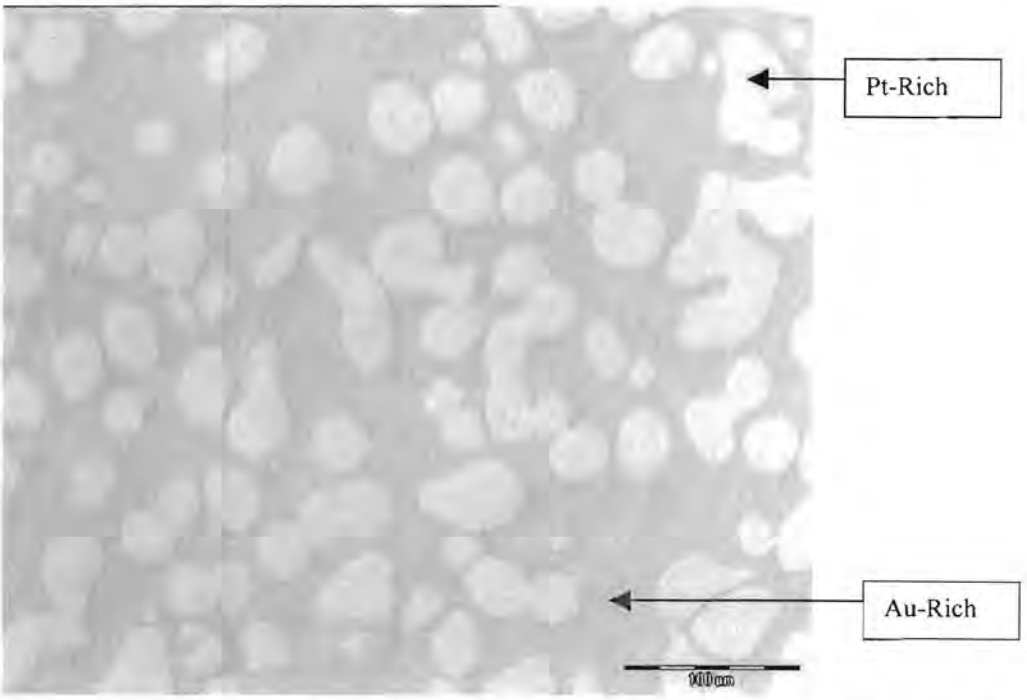

Figure 3.2. Optical photomicrograph of the 60Au-40Pt alloy after heat treatment at 1300°C for 1 hour (No etching).

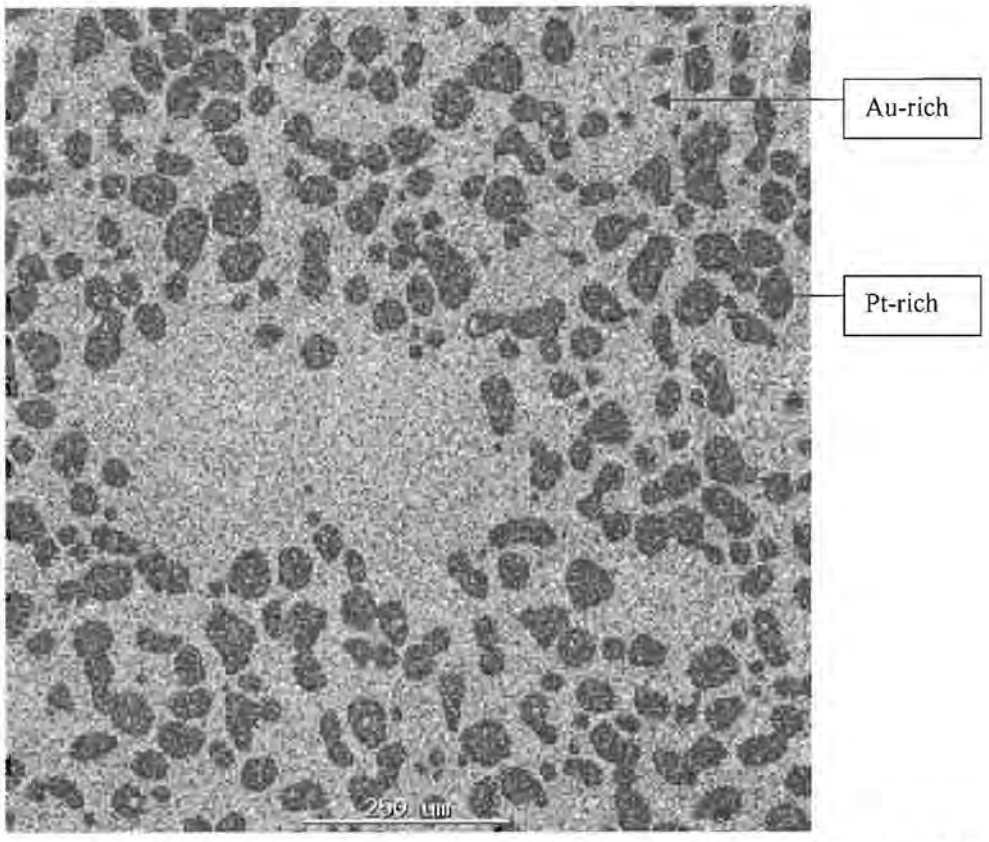

Figure 3.3: Elemental map (based on L lines of energy-dispersive X-ray analysis) of the 60Au-40Pt alloy heat treated at 1300°C.

3.2.2. The 60Au-40Pt alloy heat treated at 1200°C

Samples of the 60Au-40Pt alloy in the 1300°C heat treatment condition were heat treated at 1200°C, followed by water quenching. The 1200°C heat treatment of the 60Au-40Pt alloy is shown schematically in Figure 3.4. This heat treatment is designed to produce a homogeneous solid solution of platinum in gold. Due to the fact that the Pt-rich areas are relatively large in the 1300°C condition (Fig. 3.2), the influence of time at 1200°C was investigated by heat treating two samples for different times. The first sample was treated at 1200°C for 24 hours and the second sample for 168 hours (1 week).

The samples were polished using diamond paste (6, 5 and finally 1 µm). The microstructures were studied by means of optical microscopy and scanning electron microscopy (SEM). X-ray diffraction (XRD) was used to confirm whether a solid solution was produced after the solutionising heat treatment.

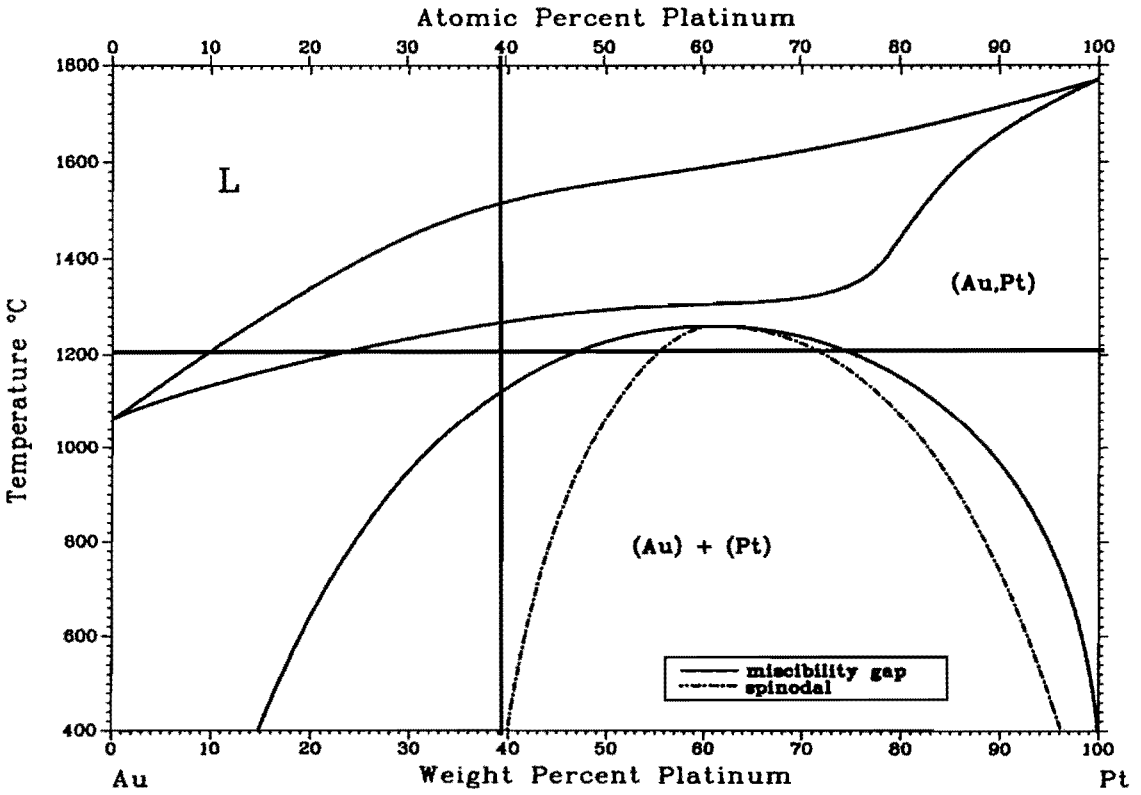

Figure 3.4. The 1200°C heat treatment of the 60Au-40Pt alloy (ASM Handbook, Volume 3: Alloy Phase Diagrams, 1992)

3.2.2.1. The 60Au-40Pt alloy heat treated at 1200°C for 24 hours

The X-ray diffraction patterns for the 1300°C and the 1200°C heat treated samples are shown in Figure 3.5. The 1300°C treated sample has two peaks, corresponding to the Au-rich and Pt-rich phases. Two peaks are observed because of the difference in lattice parameters of the two phases. Both phases are face-centered cubic (fcc). The 1200°C treated sample only has one peak, showing that the solutionising heat treatment was successful. The "prestik" peaks in Figure 3.5 are due to the sample holder that was used during XRD.

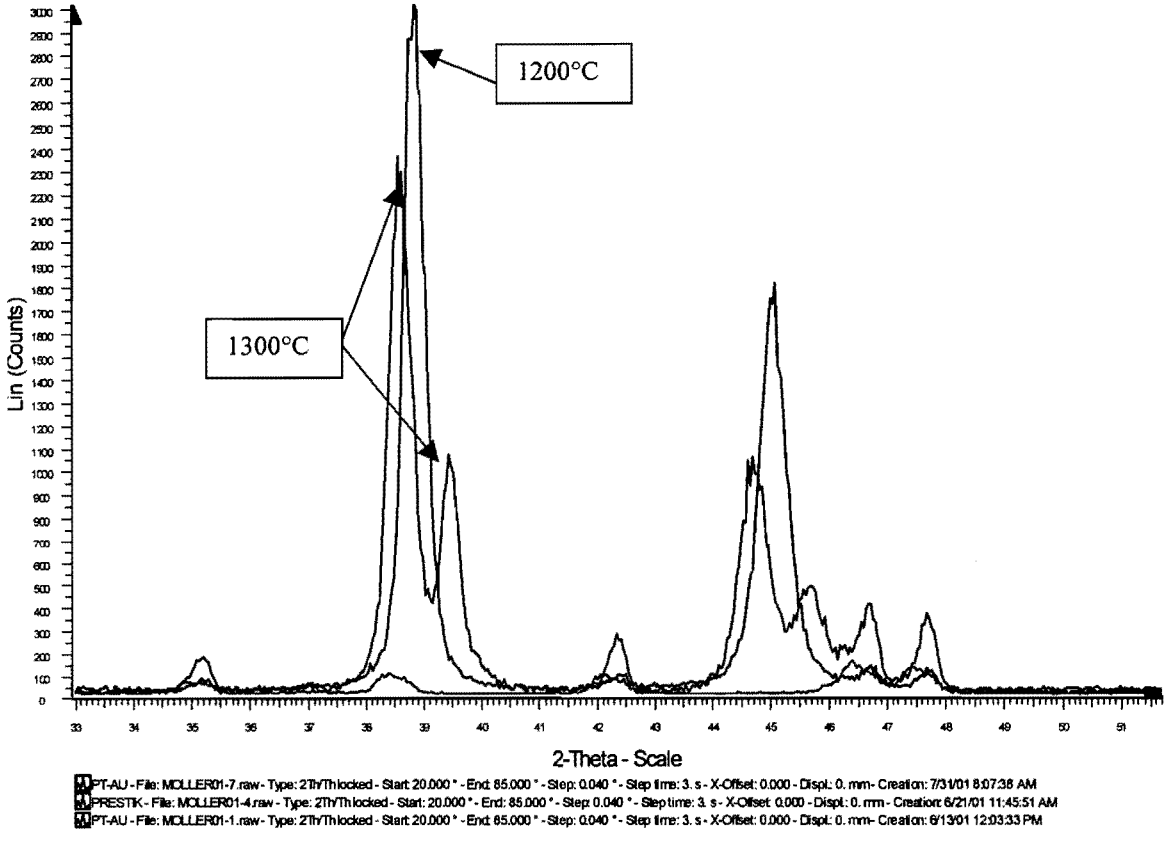

Figure 3.5. X-ray diffraction patterns of the samples heat treated at 1300°C and at 1200°C.

The microstructure of the 60Au-40Pt alloy after heat treatment at 1200°C for 24 hours is shown in Figure 3.6. The microstructure confirms that a single-phase solid solution was produced. However, it can be seen that porosity resulted during this heat treatment.

The porosity is not due to shrinkage during solidification, because at 1200°C no liquid is formed. It can, however, be explained by the Kirkendall effect.

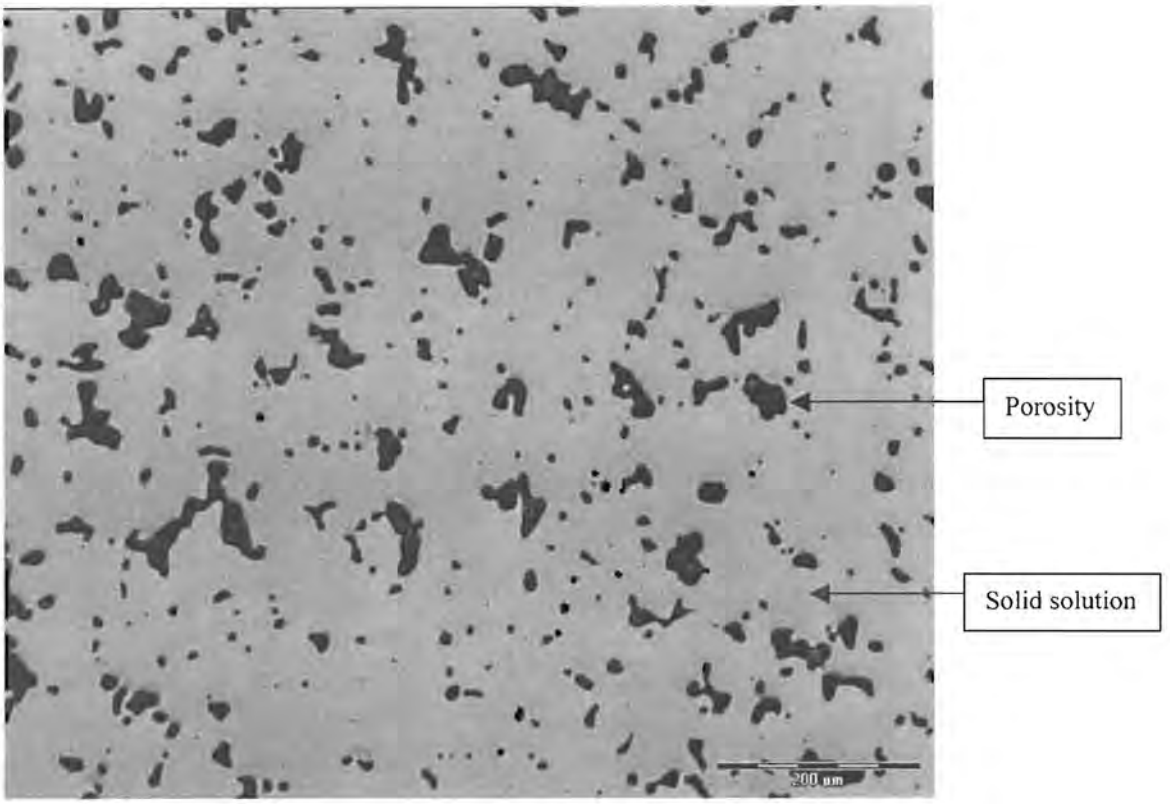

Figure 3.6. Optical photomicrograph of the 60Au-40Pt alloy after heat treatment at 1200°C for 24 hours (No etching).

3.2.2.2. Kirkendall porosity

The rate at which two types of atoms of a binary solution diffuse is not the same. The element with the lower melting point diffuses faster (Reed-Hill and Abbaschian, 1994: 367). The melting points of gold and platinum are 1064°C and 1769°C respectively (Fig. 3.1).

During the homogenising heat treatment (1200°C), the gold atoms diffused faster than the platinum atoms. Since every time an atom makes a jump a vacancy moves in the opposite direction, an unequal flow in the two types of atoms must result in an equivalent flow of vacancies in the reverse direction.

Figure 3.7 shows an optical micrograph of the sample in the 1300°C condition. During the 1200°C heat treatment, more gold atoms left the Au-rich areas than platinum atoms arrived to take their place - resulting in the observed porosity.

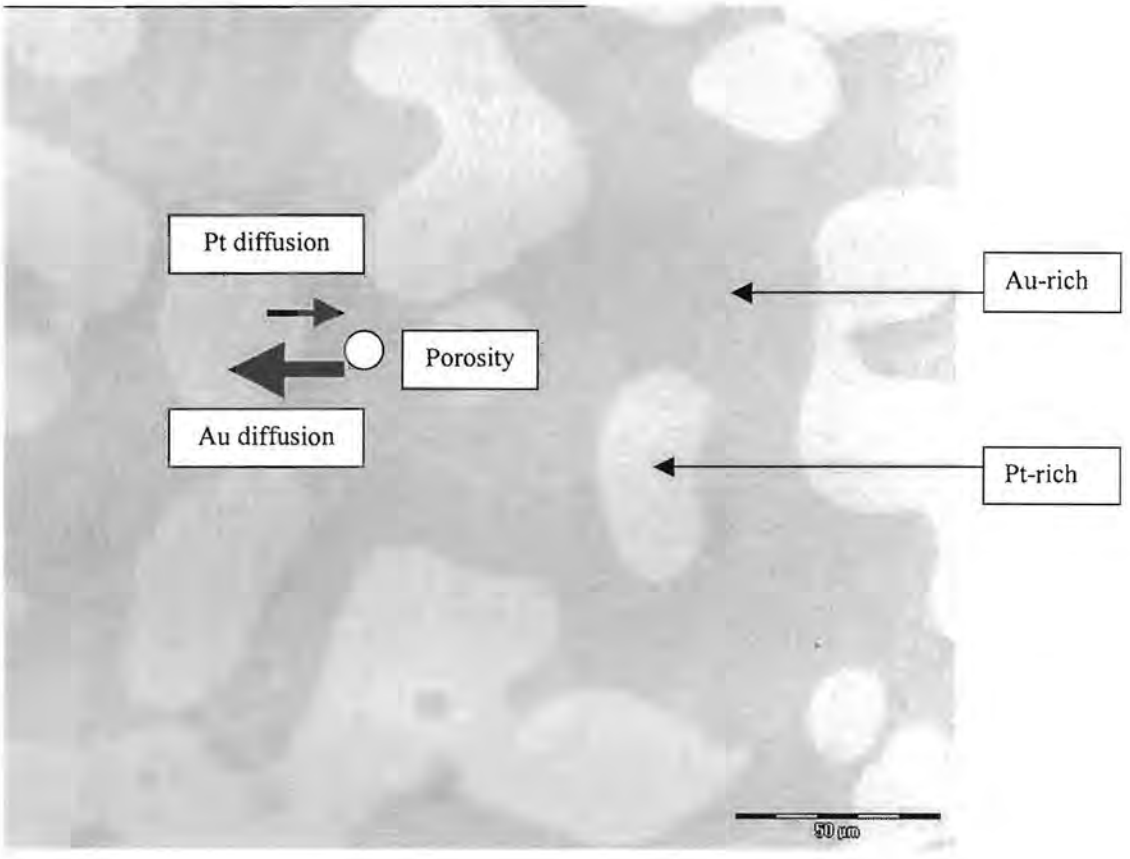

Figure 3.7. Pore formation in the 60Au-40Pt alloy due to the Kirkendall effect.

The Kirkendall effect in Au-Pt alloys has been reported by Bolk (1958). It is also known that failure of aged Cu-Au thin films frequently occurs due to Kirkendall porosity (Feinstein and Bindell, 1979).

3.2.2.3. The 60Au-40Pt alloy heat treated at 1200°C for 168 hours

The microstructure of the 60Au-40Pt alloy after heat treatment at 1200°C for 168 hours is shown in Figure 3.8.

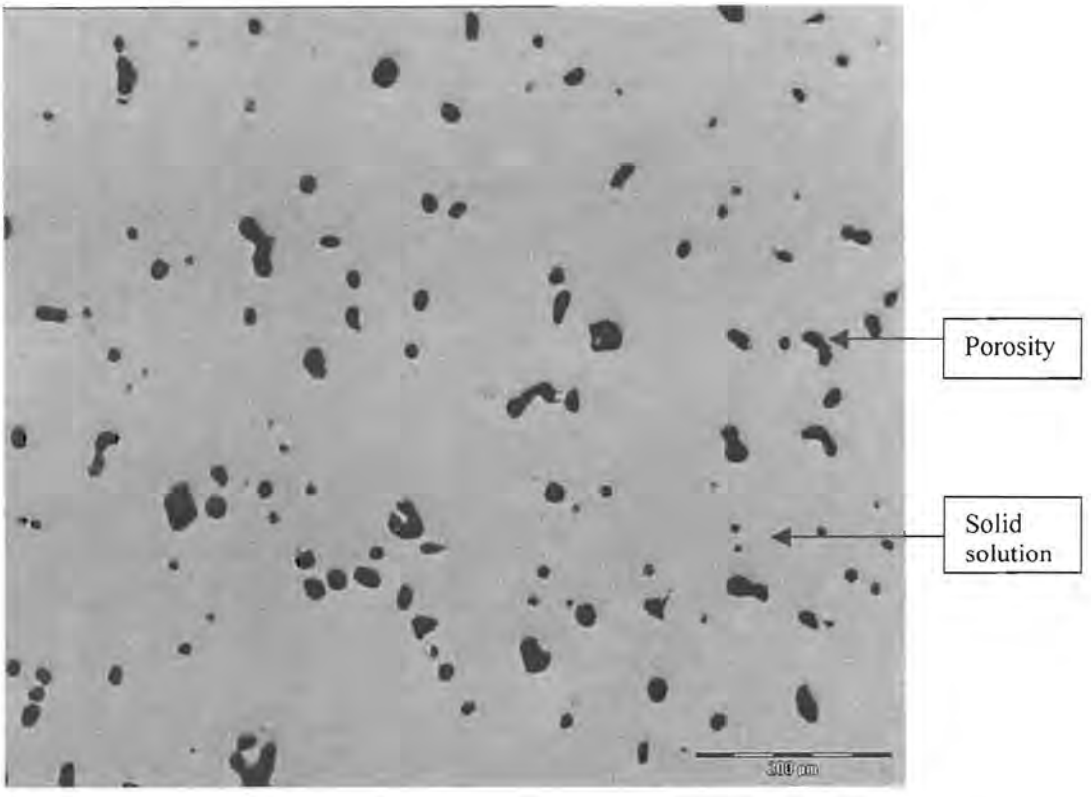

Figure 3.8. Optical photomicrograph of the 60Au-40Pt alloy after heat treatment at 1200°C for 168 hours.

There are fewer pores in the sample heat treated for 168 hours than the sample heat treated for 24 hours (Figures 3.6 en 3.8.). This is probably due to sintering of the pores during the longer heat treatment.

3.2.3. The 60Au-40Pt alloy heat treated directly at 1200°C

In order to produce a 60Au-40Pt sample with less Kirkendall porosity, it was decided to heat treat another sample at 1200°C without the intermediate 1300°C heat treatment step. The 1300°C heat treatment had resulted in large Pt-rich areas (Fig. 3.2) which, in turn, resulted in large pores during the subsequent solutionising heat treatment (Fig. 3.6). A new sample was therefore produced by button-arc melting, and heat treated at 1200°C for 24 hours. The sample was quenched in water after the heat treatment.

From Figure 3.9 it can be seen that diffusion during homogenisation at 1200°C to eliminate solidification segregation resulted in the formation of small pores. No large pores, such as in Figure 3.6, were formed.

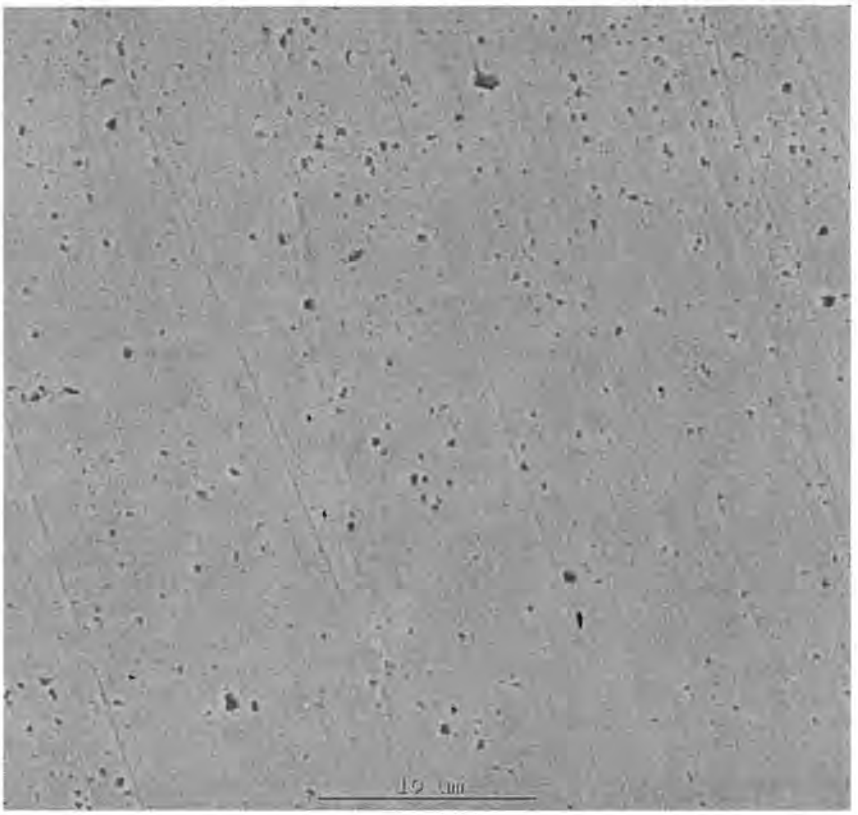

Figure 3.9. Scanning electron micrograph showing small pores in the 60Au-40Pt sample heat treated directly at 1200°C.

It is known that a heat treatment at 1200°C followed by quenching produces brittle material (Darling, 1962). This sample did indeed crack during rolling and discs could not be manufactured for electrochemical testing. A SEM investigation of the crack surface revealed that intergranular cracking occurred during rolling (Fig. 3.10). Intercrystalline cracking in Au-Pt alloys quenched from 1200°C has been attributed to partly suppressed grain boundary precipitation (Darling, 1962).

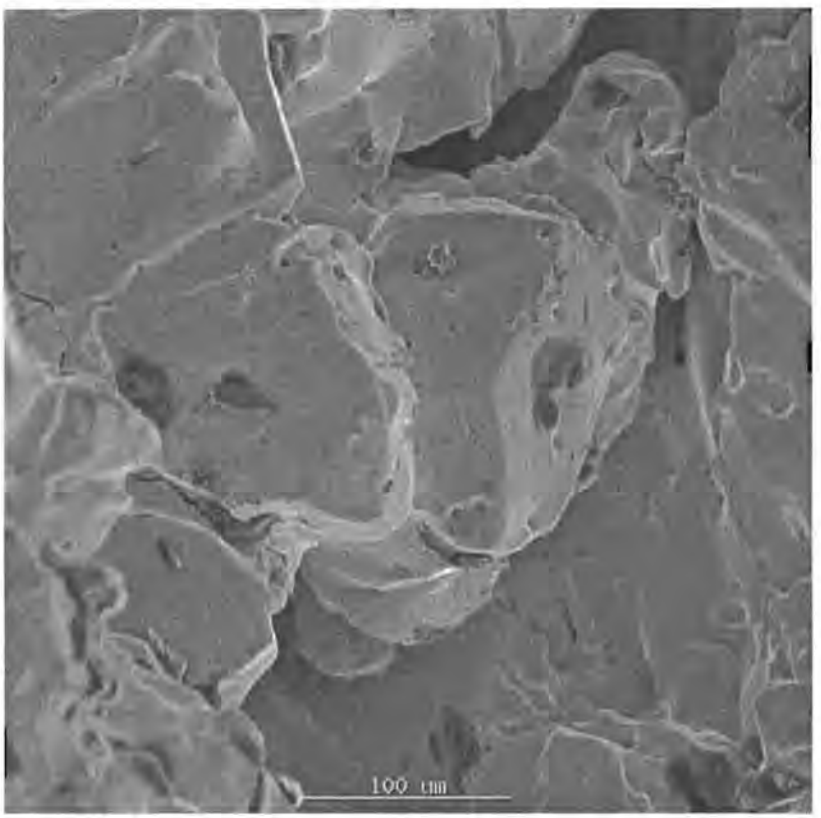

Figure 3.10. Scanning electron micrograph of a crack surface of the 60Au-40Pt sample heat treated directly at 1200°C

3.2.4. The 60Au-40Pt miscibility gap heat treatments

Porous samples in the solid solution condition (1200°C) were heat treated at 800 and 600°C. The predicted equilibrium weight fractions of α_1 (Pt-rich) and α_2 (Au-rich), and their composition as a function of heat treatment temperature, are shown in Table 3.1. The lever rule was applied to calculate the various weight fractions.

3.2.4.1. The 60Au-40Pt alloy heat treated at 800°C for 50 hours

A porous sample in the solid solution condition (1200°C-24h) was heat treated at 800°C for 50 hours, followed by water quenching. The 800°C heat treatment is shown schematically in Figure 3.11.

Table 3.1. Equilibrium weight fractions and composition of phases in a 60wt% Au-40wt% Pt alloy as functions of temperature

Temp. (°C)	Weight fraction of α_1	Composition of α_1		Weight fraction α_2	Composition of α_2	
		Wt% Au	Wt% Pt		Wt% Au	Wt% Pt
800	0.21	5	95	0.79	75	25
600	0.26	2	98	0.74	81	19

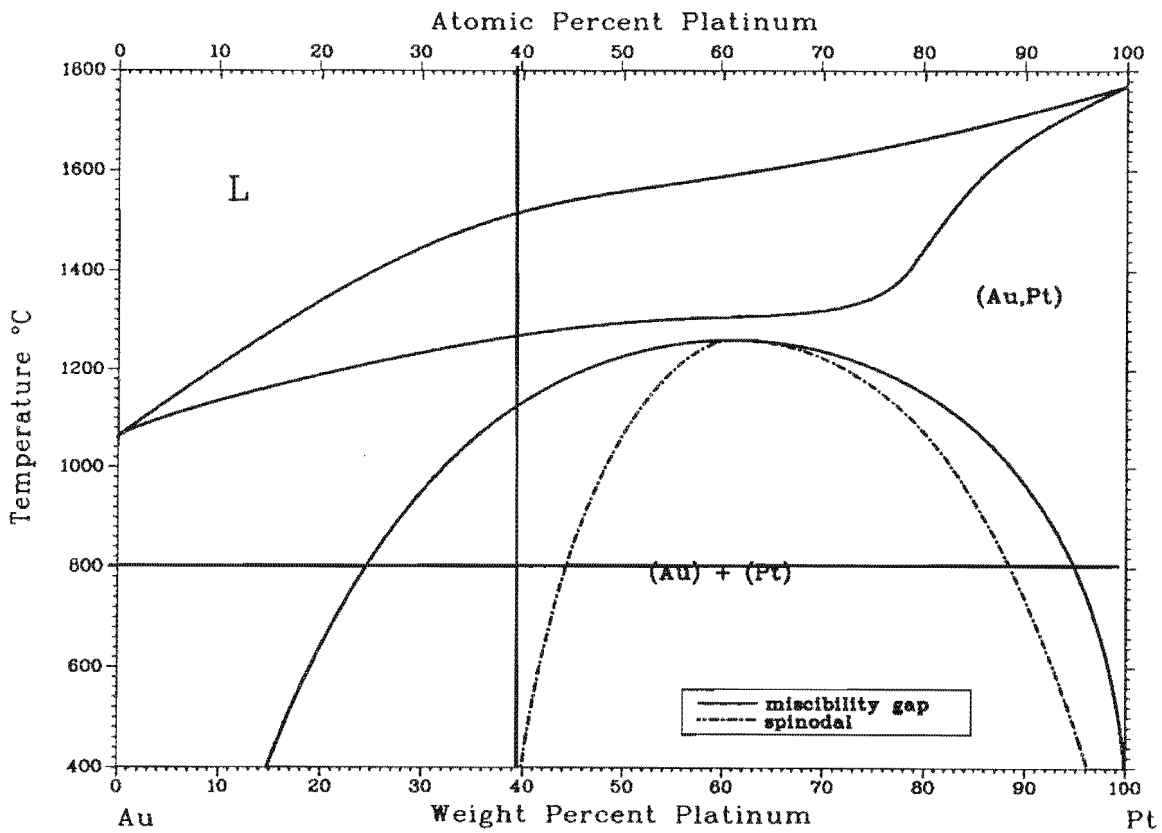

Figure 3.11. The 800°C heat treatment of the 60Au-40Pt alloy (ASM Handbook, Volume 3: Alloy Phase Diagrams, 1992)

The 60Au-40Pt alloy at 800°C lies outside the spinodal phase area (Figure 3.11). Conventional nucleation and growth of the Pt-rich areas is therefore expected.

An elemental map (using energy-dispersive X-ray analysis based on the L lines of the two metals) of the 60Au-40Pt alloy heat treated at 800°C for 50 hours is shown in Figure 3.12. The distribution of phases indicates that heterogeneous nucleation of the Pt-rich areas occurred, probably on grain boundaries. The Pt-rich areas are small, with diameters of only 1 to 3 μm.

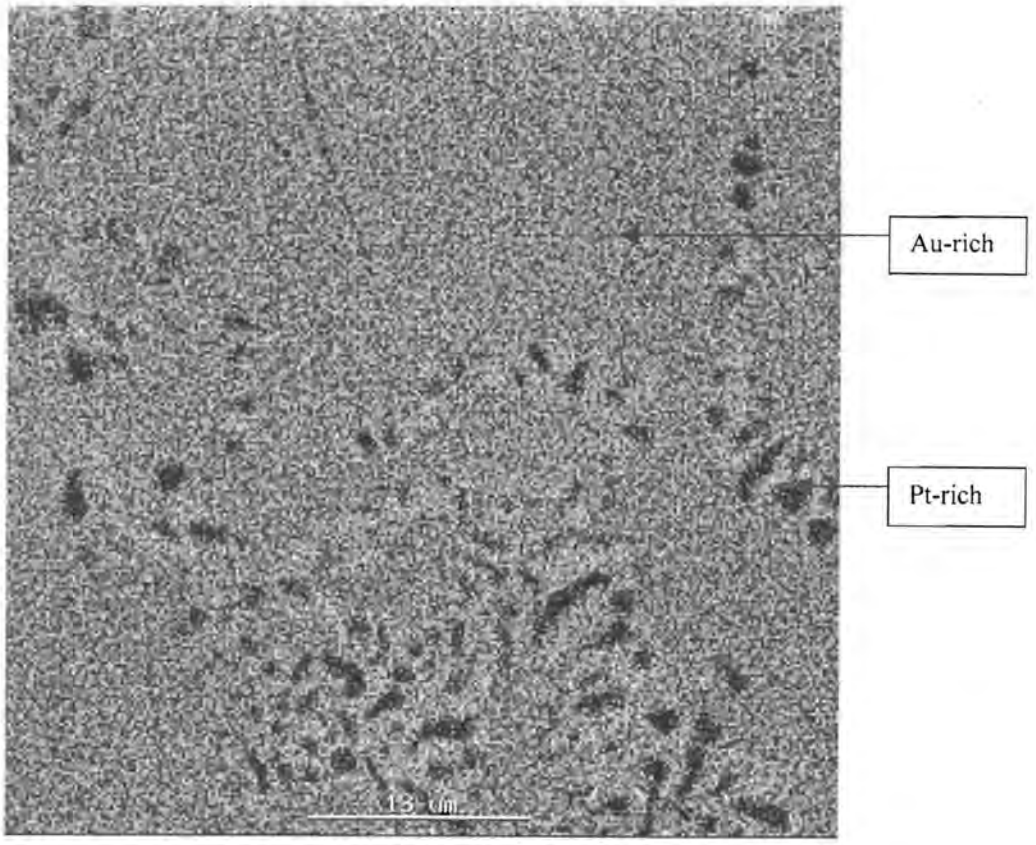

Figure 3.12. Elemental map (based on L lines of energy-dispersive X-ray analysis) of the 60Au-40Pt alloy heat treated at 800°C for 50 h.

The porosity also played an important role during the nucleation of the Pt-rich areas. In Figure 3.13, small Pt-rich areas are seen in close vicinity of a pore.

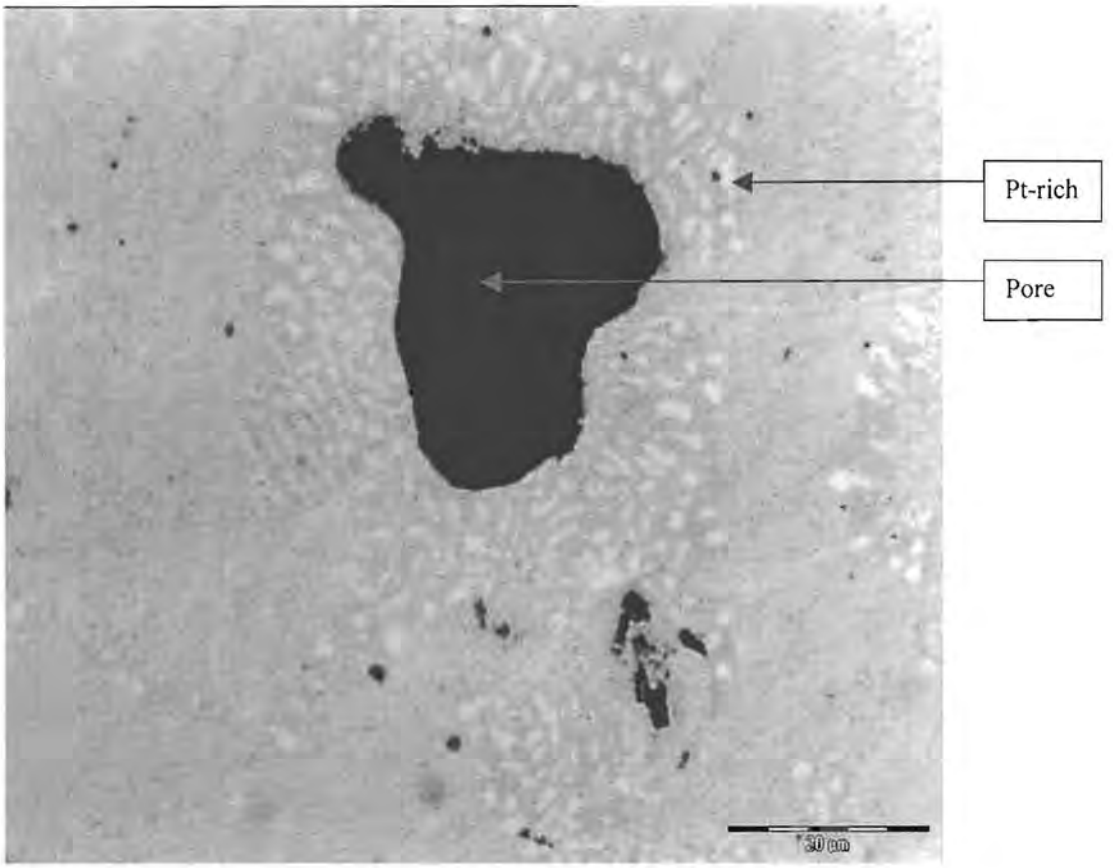

Figure 3.13. Optical photomicrograph of small Pt-rich areas near a pore after a heat treatment at 800°C for 50 h.

3.2.4.2. The 60Au-40Pt alloy heat treated at 600°C for 100 hours

A porous sample in the solid solution condition (1200°C-24h) was heat treated at 600°C for 100 hours, followed by water quenching. The 600°C heat treatment is shown schematically in Figure 3.14.

The 60Au-40Pt alloy at 600°C also lies outside the spinodal phase area (Figure 3.14). Conventional nucleation and growth of the Pt-rich areas is once again expected.

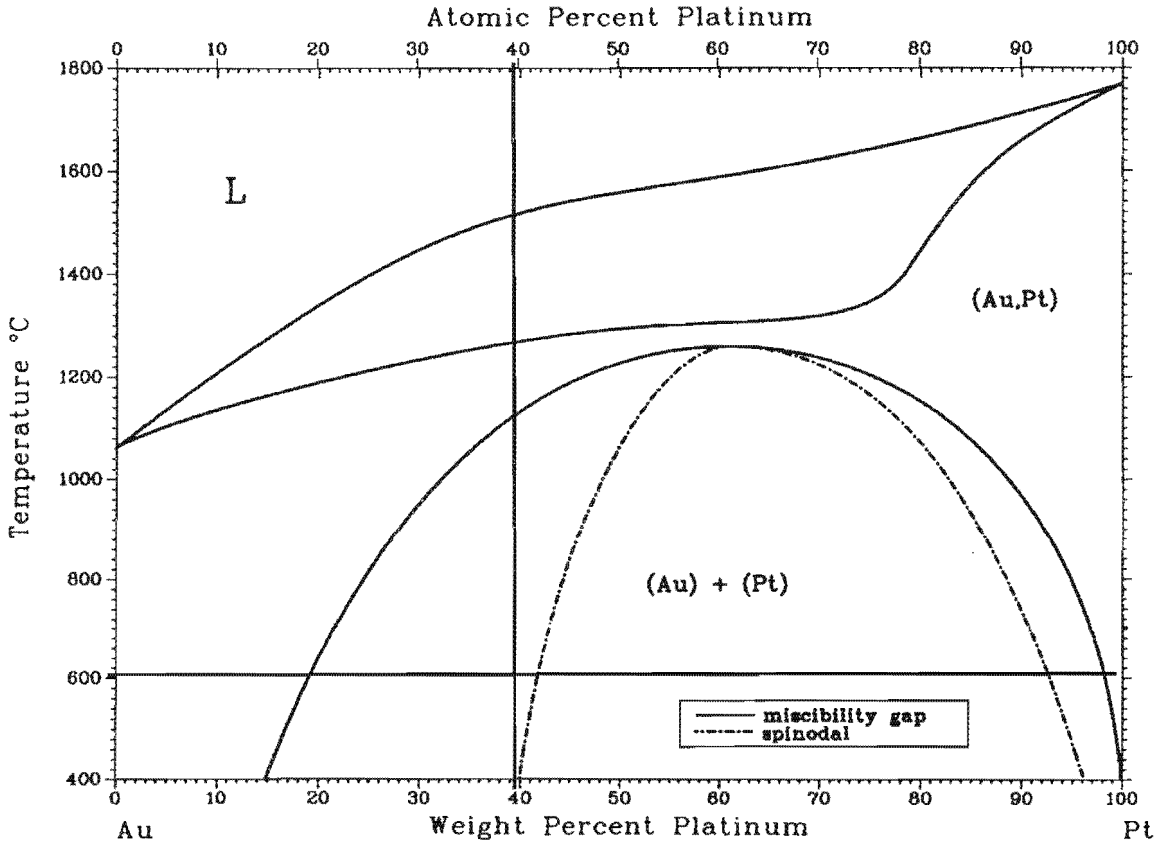

Figure 3.14. The 600°C heat treatment of the 60Au-40Pt alloy (ASM Handbook, Volume 3: Alloy Phase Diagrams, 1992)

An elemental map (using energy-dispersive X-ray analysis based on the L lines of the two metals) of the 60Au-40Pt alloy heat treated at 600°C for 100 hours is shown in Figure 3.15.

Heterogeneous nucleation of the Pt-rich areas is observed for the 60Au-40Pt alloy heat treated at 800°C (Fig. 3.12) and 600°C (Fig. 3.15). For compositions outside the spinodal decomposition area (Fig. 3.14), second-phase formation is by conventional nucleation and growth. In order to study spinodal decomposition in Au-Pt alloys, the 50Au-50Pt alloy was investigated.

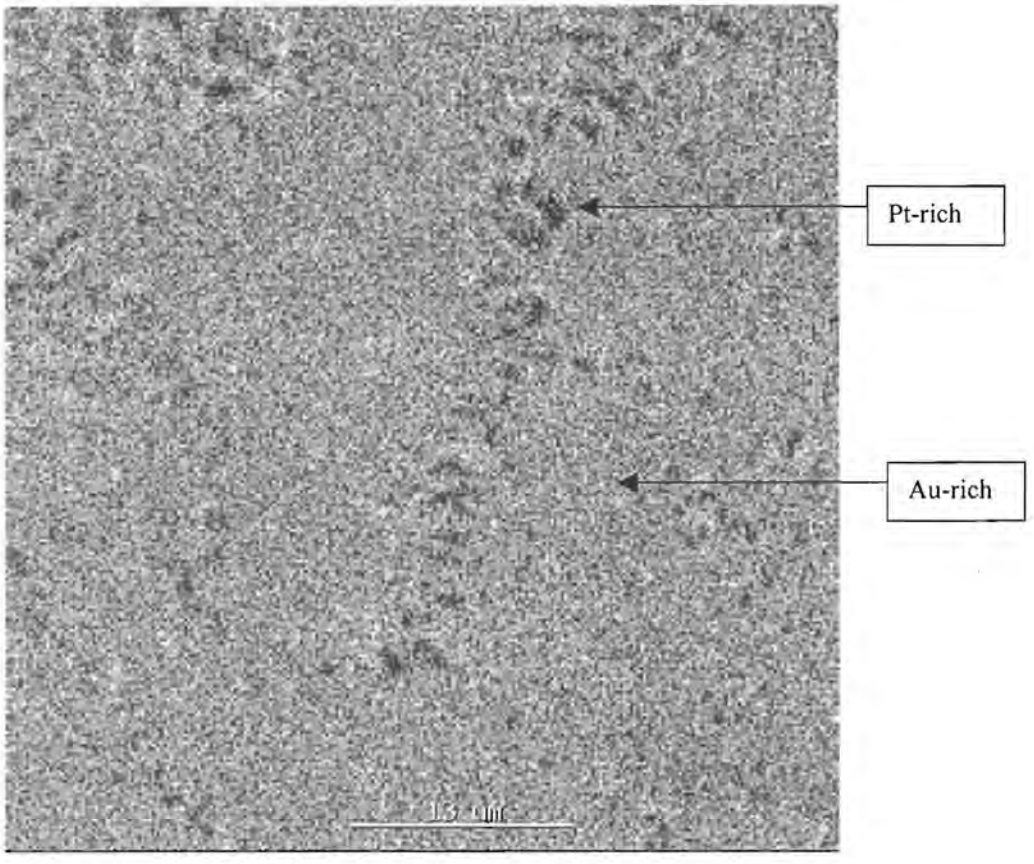

Figure 3.15. Elemental map (based on L lines of energy-dispersive X-ray analysis) of the 60Au-40Pt alloy heat treated at 600°C for 100 h.

3.3. The 50Au-50Pt alloy

Gold and platinum (both 99.99%) were melted together (in the required ratio) in an arc-furnace with a water-cooled copper hearth under a protective argon atmosphere. The sample was turned around after each melt and re-melted three times to ensure homogeneity.

3.3.1 The 50Au-50Pt alloy in the "ductile" condition

A 50Au-50Pt sample was given a heat treatment according to Darling (1962) to produce ductile material. The following procedure was used:

- The sample was placed in the furnace at 1000°C for 2 hours.

- The sample was left in the furnace, and the temperature was reduced to 800°C. The furnace took approximately 1.5 hours (between 85 and 100 minutes) to reach the desired temperature of 800°C.
- Once the temperature reached 800°C, the sample was left in the furnace for a further 2 hours.
- The sample was rapidly cooled by water quenching.

The sample was in the furnace for approximately 5.5 hours. It was then cold rolled. The whole process (heat treatment and cold rolling) was performed three times. The sample therefore spent 16.5 hours (5.5 x 3) in total in the furnace. The two temperature limits of the "ductile" heat treatment are shown in Figure 3.16.

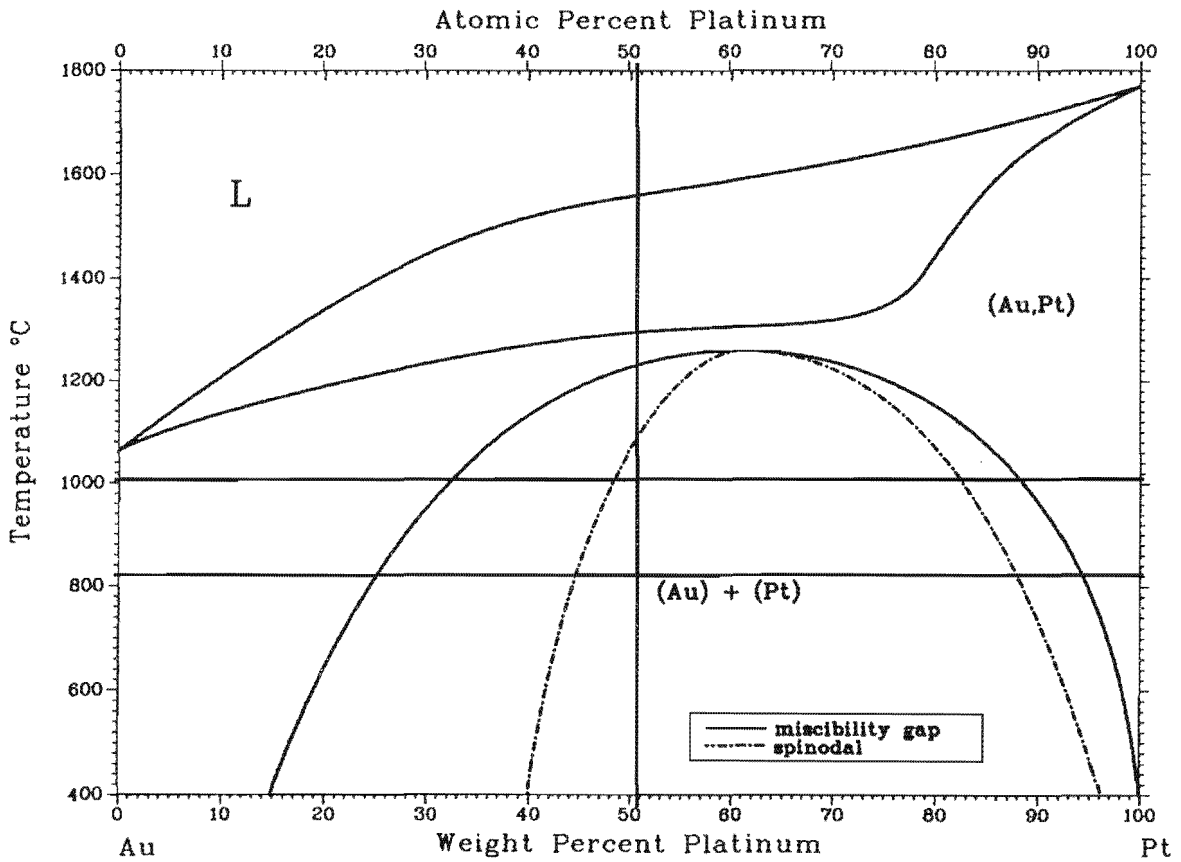

Figure 3.16. The "ductile" heat treatment of the 50Au-50Pt alloy (ASM Handbook, Volume 3: Alloy Phase Diagrams, 1992)

From Figure 3.16, it is seen that this alloy composition lies in the spinodal decomposition area in the temperature range of 800 to 1000°C.

A disc of 6 mm diameter was punched from the cold-rolled material and was mounted in resin by using a black phenolic thermosetting powder. The sample was polished with diamond paste (down to 1 μm) and the microstructures were studied by optical microscopy.

The microstructure of the 50Au-50Pt alloy in the ductile condition is shown in Figure 3.17.

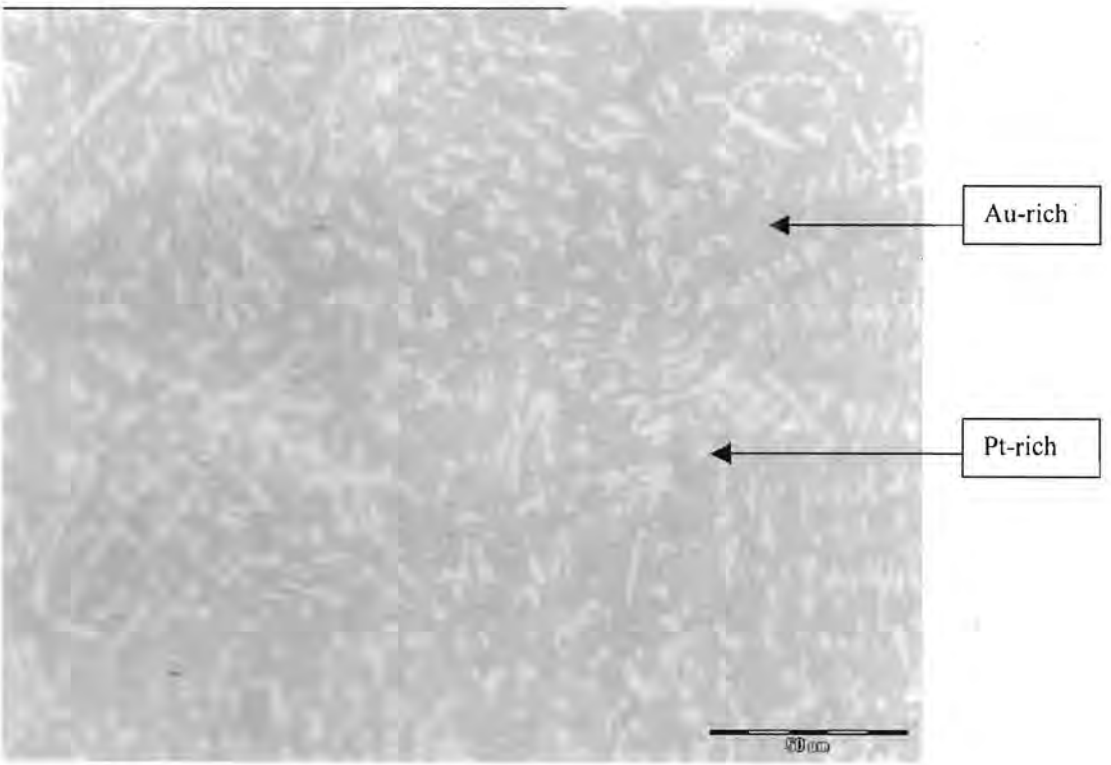

Figure 3.17. Optical photomicrograph of the 50Au-50Pt alloy after the "ductile" heat treatment.

Figure 3.17 shows that nucleation of the Pt-rich areas occurred simultaneously throughout the matrix producing a uniform microstructure. Uniform microstructures are obtained during spinodal decomposition, because there is no thermodynamic barrier to nucleation (Cahn, 1970). In this type of transformation, no definite distinguishable nuclei are formed initially, as the interface between the matrix and the precipitate is diffuse

through a sinusoidal variation in composition throughout the matrix. As time increases, the amplitudes of the composition variation will increase. This requires "uphill" diffusion – solute separation therefore occurs against the concentration gradient.

3.3.2. The 50Au-50Pt alloy in the solid solution condition

A sample in the "ductile" heat treatment condition was solutionised at 1250°C for 24 hours followed by water quenching. This heat treatment is shown in Figure 3.18.

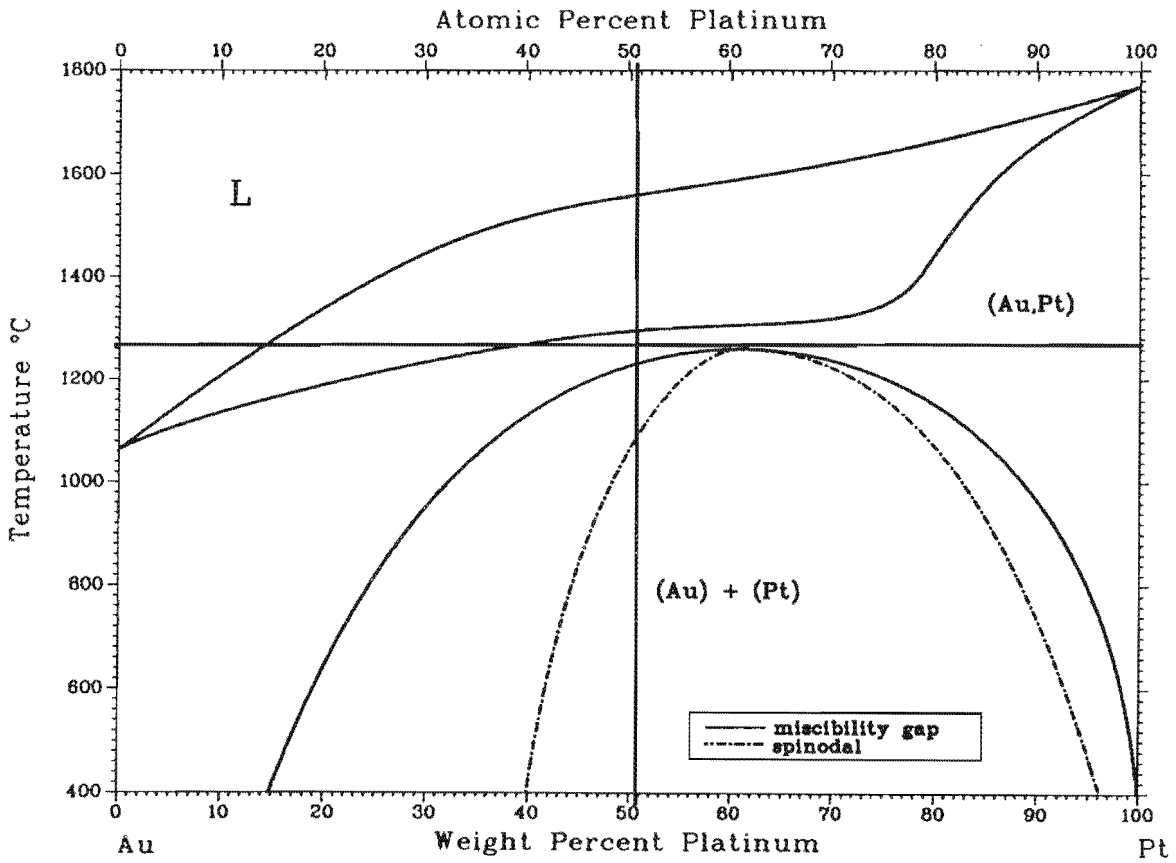

Figure 3.18. The solid solution heat treatment of the 50Au-50Pt alloy (ASM Handbook, Volume 3: Alloy Phase Diagrams, 1992)

The microstructure of the 50Au-50Pt alloy in the solutionised condition is shown in Figure 3.19. Only one phase (solid solution) can be observed and no significant porosity

was formed during solutionising in this case. The reason why spinodal alloys do not form Kirkendall porosity during solutionising is not clear. It may be that the Pt-rich areas were too small prior to solutionising to produce significant porosity (Compare the sizes of the Pt-rich areas in Figures 3.2 and 3.17 before solutionising).

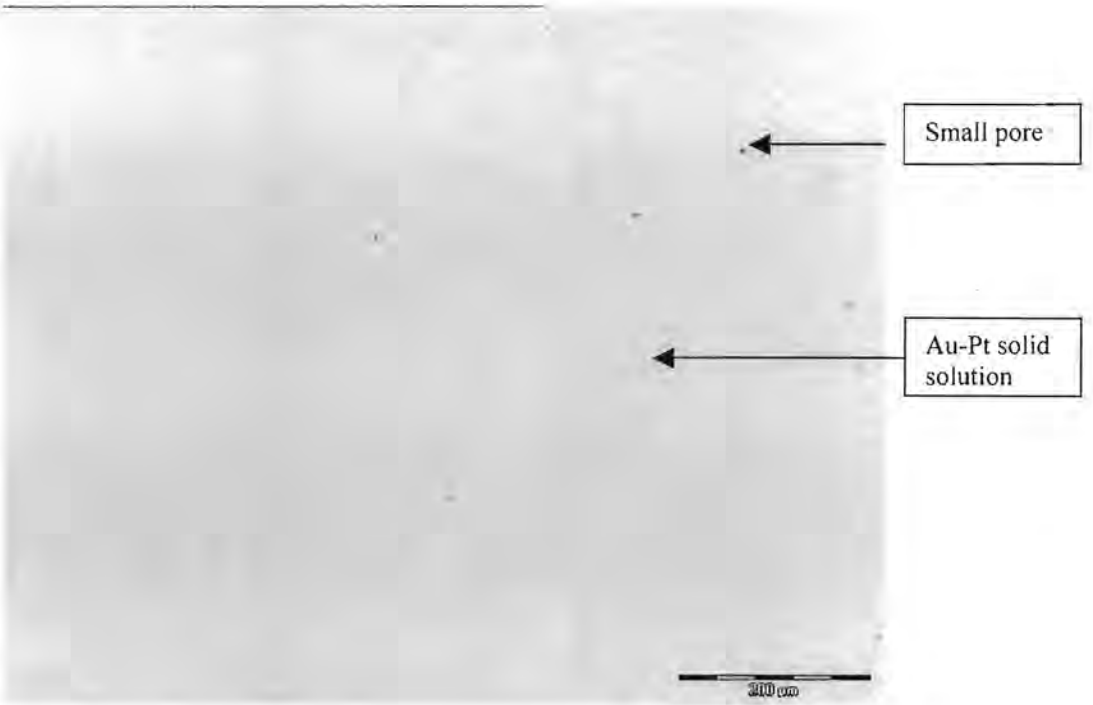

Figure 3.19. Optical photomicrograph of the 50Au-50Pt alloy in the solutionised condition.

3.4. The Gold 990 alloy

The metals were melted together (in the required ratio) in an arc-furnace with a water-cooled copper hearth under an argon protective atmosphere. The sample was turned around after each melt and re-melted three times to ensure homogeneity.

3.4.1. The Gold 990 alloy in the solid solution condition

Gold 990 samples were solutionised in air at 800°C for 1 hour (Figure 3.20). The samples were subsequently quenched in water and the brown tarnish layer removed mechanically.

The Vickers hardness (5kg load) of the material in this condition was found to be approximately 50 kg/mm^2.

3.4.2. The Gold 990 alloy in the precipitation-hardened condition

A solutionised Gold 990 sample was precipitation-hardened by a heat treatment in air at 500°C for 1 hour followed by quenching in water (Figure 3.20). The Vickers hardness value (5kg load) after the heat treatment was found to be 150 kg/mm^2. The increase in the hardness is due to the formation of nanosized Au_4Ti precipitates (Gafner, 1989).

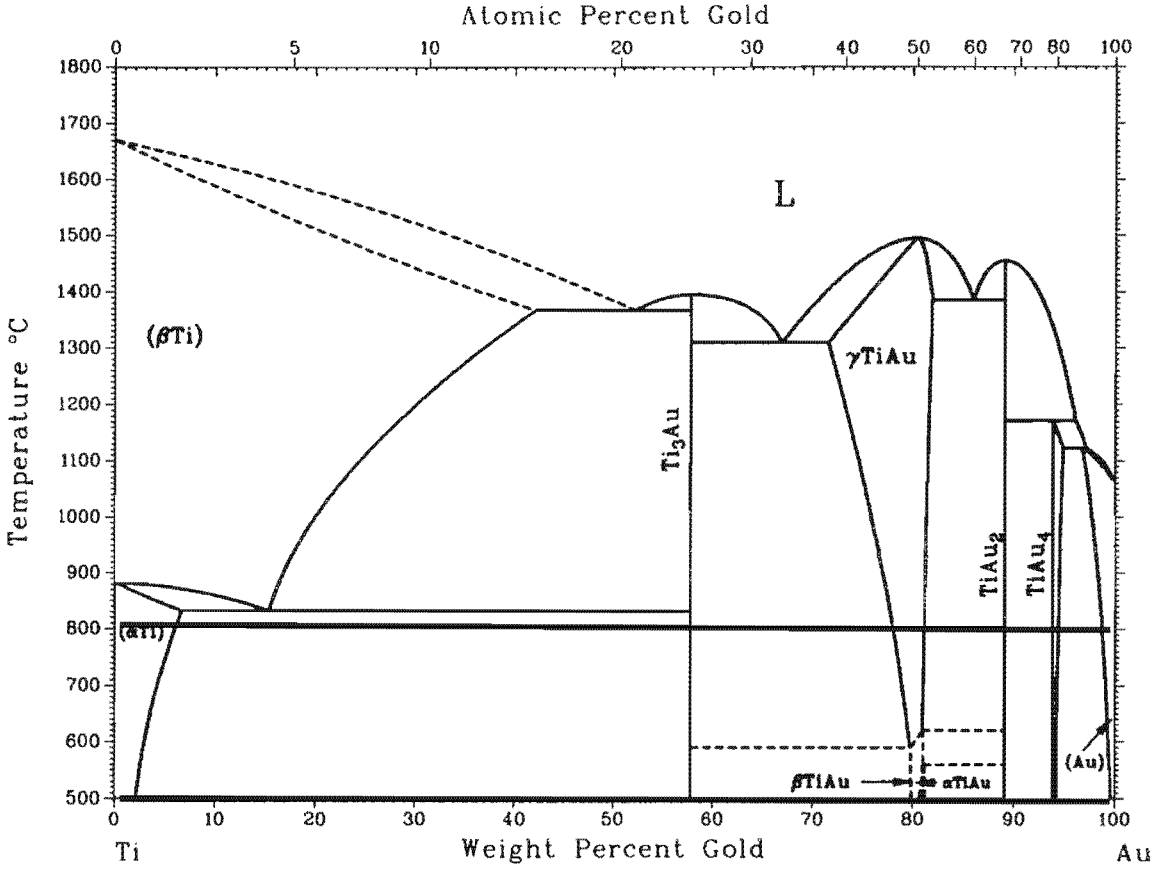

Figure 3.20. The Gold 990 alloy heat treatments (ASM Handbook, Volume 3: Alloy Phase Diagrams, 1992).

3.5. Conclusions

- The 60Au-40Pt alloy heat treated at 1300°C followed by water quenching has large Pt-rich areas in a Au-rich matrix.
- Solutionising of the 1300°C treated sample leads to the formation of Kirkendall porosity.
- The 60Au-40Pt alloy heat treated directly at 1200°C (without the intermediate 1300°C heat treatment) is brittle and cracked during cold rolling. A disc of this sample could therefore not be manufactured for electrochemical testing.
- Heterogeneous nucleation of Pt-rich areas occurs during the miscibility gap heat treatments of the 60Au-40Pt alloy.
- Spinodal decomposition occurs when a 50Au-50Pt alloy is heat treated in the miscibility gap. No significant Kirkendall porosity is found when this sample is solutionised.
- The Gold 990 alloy was heat treated to produce two different conditions: a solid solution and a precipitation-hardened condition.

This chapter indicated that different microstructures can be obtained in the Au-Pt alloys by varying the heat treatments of the samples. The Gold 990 alloy was heat treated to produce samples in the solid solution condition and the precipitation-hardened condition. The influence of the heat treatment condition of the samples on their electrochemical behaviour will be discussed in the following chapters.